Improved Efficacy of Localized Brain Tumor Therapy Using Photosensitive Nanoparticles

by

Kristen Anastasia Simmer

A dissertation submitted in partial fulfillment
of the requirements for the degree of
Doctor of Philosophy
(Biophysics)
in the University of Michigan
2014

Doctoral Committee:

Professor Raoul Kopelman, Chair
Assistant Professor Julie Suzanne Biteen
Professor Ari Gafni
Professor Martin A. Philbert
Professor Michal R. Zochowski

To my nieces and nephews, for your youthful spirit
and innocent outlook of the world – I thank you.
May each of you appreciate your potential
and flourish beyond your dreams.

To my husband – Always and forever.

Acknowledgements

I would like to begin by thanking my mentor, Dr. Raoul Kopelman, for his guidance and expertise. From the start of my career he was always supportive of my ideas and has provided me the opportunity to explore new ideas of research both under his supervision and under the direction of collaborators. He provided a truly challenging and enlightening educational experience.

Special thanks to Dr. Martin Philbert, whose vast expanse of knowledge has been a constant source of information. I have learned so much from him, especially after having him as an instructor of pathology. Now that I am finishing the program, I can look back at the immense value of his lecture style and one-on-one discussions. His guidance has changed my perspective on the biological and clinical relevance of science.

I am very thankful to Dr. Ari Gafni for his mentorship at the start of my career. He set the standard as my first graduate lab mentor, and also gave me direction as the Biophysics graduate chair.I would like to express my deepest gratitude to the other distinguished members of my graduate committee, Dr. Julie Biteen and Dr. Michael Zochowski for their valuable critiques of my research. I would also like to thank my collaborators on these projects, Dr. Oren Sagher, Dr. Daniel Orringer, Dr. Martin Philbert, and Mr. Dah-Luen Huang. It was a pleasure to work with such an elite group of experts from whom I gained a rich clinical acumen.

Thank you to Dr. Yong-Eun Lee Koo for always making time to review my experimental objectives and conclusions, as well as her excellent critique and guidance for future works. Her vast knowledge of cancer research was an inspiration for my graduate career and future endeavors.

Thank you to the past members of the Kopelman group, who have contributed to my research as well as my graduate experience. To Dr. Hoe Sin Hah, Dr. Gwangseong Kim, Dr. Shouyan Wang, and Dr. Qinghong Yao for sharing their knowledge of nanoparticle synthesis and application.

To my lab mates, Remy Elbez and Ariel Hecht for being such wonderful friends and helping to ease the stress of graduate life with an eclectic array of movie nights. A huge thank you to Dr. Aniruddha Ray for being one of my closest friends. I will forever remember the untraceable walks around Ann Arbor, and your enthusiasm while helping to celebrate my biggest achievements. Also thank you to the current members of the Kopelman group, Leshern Karamchand for his constant concern of my happiness; Hyung Ki Yoon, Teppei Shirakura, and Ming Qin for their hilarious banter and always lending a helping hand for nanoparticle synthesis.

My deepest appreciation to Dr. Andrei Kogan, my professor and supervisor during my undergraduate career at the University of Cincinnati. He always had great enthusiasm in the classroom and extended our relationship personally by encouraging me to further my physics career. He instilled in me a curiosity in the experimental sciences and was instrumental in my pursuit of graduate studies. I would also like to thank Dr. Richard Gass and Dr. Cenalo Vaz for their early mentorship in my studies at the University of Cincinnati and initiating me into the pursuit of a degree in physics. A special thank you to the University of Cincinnati physics, graduate class of 2008. I often think of our never-ending nights of studying and perfecting theories of great scientists.

I would like to acknowledge the funding from the National Institute of Health, Rackham Travel Grant, and Rackham Merit Fellowship.

I would like to thank all of my friends from all walks of life for their support and love throughout the years. Special gratitude to D.C., G.A., A.R., P.M., and A.V. for their uncompromising friendship and frequent words of advice. To the parish of the Greek Orthodox Church of Cincinnati for their constant praise and reassurance.

Most important, I would like to dedicate my thesis to my loving family. Thank you to my parents, Dennis and Anastasia Herrmann, and to my siblings Melissa, AnnaMarie, and Nick and their families for their endless love, faith, and encouragement to pursue my educational dreams. To my grandparents, Betsy Pascal and Jean Herrmann-Heisler, who do not measure my success by my achievements but rather my happiness. To my husband's family for their great generosity and willingness to always help me achieve my goals. And an exceptional thank you to my husband, Stephen Simmer, for always being by my side. I thank him for his constant encouragement and perpetual love. Finally to my puppy Jill, for her enthusiastic puppy kisses and continuously reminding Stephen and I to keep exploring world.

Table of Contents

Dedication……...ii

Acknowledgements……iii

List of Figures……...viii

Abstract……..xii

Chapter

1. Introduction……..1
   References……..14

2. Delayed Brain Tumor Growth Using Methylene Blue Mediated Photodynamic Therapy……..19
   Introduction……19
   Experimental……..23
   Results and Discussion……..32
   Conclusions……50
   Acknowledgement…….51
   References……..51

3. Evaluating the Effect of HPPH Mediated Photodynamic Therapy for Arresting Glioma.56
   Introduction……....56
   Experimental……..59
   Results and Discussion……..68
   Conclusions……86
   Acknowledgement…….87
   References……..88

4. Efficacy of Reactive Oxygen Species Production for Methylene Blue and Coomassie Blue Mixture: For Possible Combined Tumor Delineation and Therapy……..…..93
   Introduction……93
   Experimental……..96
   Results and Discussion……...97
   Conclusions……..102
   Acknowledgement……...103
   References……103

5. Future Directions……………………………………………………………………..106
References……………………………………………………………………113

List of Figures

Figure 1.1: Reaction kinetics of photosensitization leading to PDT……...5

Figure 2.1: Surface modification and conjugation of MB-loaded PAA nanoparticles…….25

Figure 2.2: (A) Size distribution of polyacrylamide nanoparticles in solution using dynamic light scattering measurments. ROS production measurement of (B) Methylene Blue free dye in DI water and (C) Methylene Blue polyacrylamide nanoparticles. Peak excitation for Methylene Blue was found at 678 nm: linear fitted plot of fluorescence change in ADPA as a function of irradiation time……...34

Figure 2.3: Examination of cytotoxicity using the MTT assay. Cell viability of 9L gliosarcoma, evaluated after 24 hours incubation with varying concentrations of F3-targeted and non-targeted Methylene Blue nanoparticles. Cell survival rates indicated no measurable variance between nanoparticle concentrations (0.1, 0.2, 0.5, and 1.0 mg/mL), including the cell only control group (no NPs)…….....35

Figure 2.4: Confocal images of 9L cell lines treated with Methylene Blue-conjugated PAA nanoparticles. Intensity dependent cytotoxicity, induced by F3-targted Methylene Blue PAA nanoparticles and laser irradiation. The 9L gliosarcoma cells were incubated with Methylene Blue nanoparticles and irradiated with fluencies of 100 mW/cm^2 and 222 mW/cm^2. Images were taken (a) before light exposure; (b-e) over 30 min of light exposure at a dose of 100 mW/cm^2. Images were taken (f) before light exposure; (g-j) over 30 min light exposure at a dose of 222 mW/cm^2. Cytotoxicity was monitored by labeling the cells with Calcein-AM (green, for viable cells) and propidium iodide (red, for dead cells). Measurements taken on a confocal microscope…….37

Figure 2.5: Cell viability assessment for the phototoxic effects of F3-targeted Methylene Blue polyacrylamide nanoparticles on a 9L cell line. Fluency dependent PDT efficiency at light doses of 100 mW/cm^2 and 222 mW/cm^2, over the course of 30 minutes of illumination. Cells exposed to a higher fluency responded with a more rapid cellular death than for a lower fluency…….38

Figure 2.6: Confocal images of 9L cell lines treated with Methylene Blue-conjugated PAA nanoparticles, before and after laser illumination. Cell viability was monitored by labeling cells with Calcein-AM (green, viable cells) and propidium iodide (red, dead cells). Images were taken before illumination at 60X magnification. Post-illumination images were taken at a lower magnification to illustrate that cellular death merely occurred in the area exposed to laser irradiation……...39

Figure 2.7: A series of cranial window pictures of a rat with an implanted 9L glioma, before and after the PDT, using F3-Methylene Blue polyacrylamide nanoparticles and a time interval of 105min between nanoparticle injection and light illumination. The dotted circle encloses the tumor area in each picture……...……..42

Figure 2.8: (A) Photograph displaying therapy setup. Rats with BTW are positioned in sterotactic frames with distance between cranial window and laser collimator fixed at 1 inch. Photographs of a tumor as seen through the BTW (B) before therapy and (C) during irradiation with a 671nm laser……...….43

Figure 2.9: Incubation time dependent effects of photodynamic therapy treatment. F3-targeted Methylene Blue polyacrylamide nanoparticles were intravenously injected, and once completing 105 minutes or 24 hours of systemic incubation, the tumors were irradiated at 180 J/cm^2 through the BTW and observed daily……..44

Figure 2.10: Daily photographs of the cortical surface depict tumor growth, images taken through brain tumor windows on rat models. Animals groups receiving irradiation experienced a fluence dose of 180 J/cm^2 using 671 nm laser…….……...45

Figure 2.11: Effect of PDT treatment delivered 105 minutes after injection of Methylene Blue F3-targeted nanoparticles, Methylene Blue PEGylated nanoparticles and Methylene Blue free dye. The control animal was not administered with photosensitizer or exposed to the laser illumination. Another control animal group treated with light illumination showed the same tumor growth trend as the "no treatment" control animal group……...47

Figure 2.12: Post-PDT treatment necrotic tissue measurements for tumors treated with F3-targeted Methylene Blue polyacrylamide nanoparticles verses non-targeted (PEGylated) Methylene Blue nanoparticles. Both treatment groups express similar necrotic formation and regression patterns with a greater formation of necrotic tissue for non-targeted Methylene Blue nanoparticles……..48

Figure 2.13: Gross specimen from animal model, excised 10 days post-PDT therapy. Representation of brain tumor for animal groups (A,B) without photosensitizer or laser illumination, and (C,D) animals receiving non-targeted Methylene Blue nanoparticles (105 minute incubation time) with irradiation fluence dose of 180 J/cm^2 using a 671 nm laser……...49

Figure 3.1: Surface modification and conjugation of HPPH post-loaded PAA nanoparticles….61

Figure 3.2: Cytotoxicity test using the MTT assay. Cell viability of 9L gliosarcoma, evaluated after 24 hours incubation, with varying concentrations of F3-targted and non-targeted HPPH polyacrylamide nanoparticles. Cell survival rates indicated no measurable differences among nanoparticle concentrations (0.1, 0.2, 0.5, and 1.0 mg/mL), including the cell only control group (not treated with nanoparticles)…….70

Figure 3.3: (A) Size distribution of polyacrylamide nanoparticles in solution as measured by DLS. (B) ROS production measurement of HPPH post-loaded polyacrylamide nanoparticles in DI water,

with excitation peak for HPPH at 665nm: Linear fitted plot of fluorescence change of ADPA as a function of irradiation time, irradiation performed at 378nm…….……71

Figure 3.4: Confocal images of 9L cell lines treated with F3-targeted HPPH post-loaded PAA nanoparticles. Intensity dependent cytotoxicity, induced by F3-targted HPPH PAA nanoparticles and laser irradiation at 671 nm. The 9L gliosarcoma cells were incubated with HPPH nanoparticles and irradiated with fluencies of 100 J/cm^2 and 144 J/cm^2. Images were taken (A) before light exposure; (B-E) over 30 min of light exposure at a dose of 100 mW/cm^2. Images were taken (F) before light exposure; (G-J) over 30 min light exposure at a dose of 144 mW/cm^2. Cytotoxicity was monitored by labeling the cells with Calcein-AM (green, for viable cells) and propidium iodide (red, for dead cells). Measurements taken on a confocal microscope…… ….....…72

Figure 3.5: Cell viability assessment for the phototoxic effects of F3-targeted HPPH post-loaded polyacrylamide nanoparticles on a 9L cell line. Fluency dependent PDT efficiency at light doses of 100 mW/cm^2 and 144 mW/cm^2, over the course of 20 minutes of illumination. Cells exposed to a higher fluency responded with a more rapid cellular death than for a lower fluency. .....…73

Figure 3.6: (A) Photograph displaying photodynamic therapy setup. Rats with BTW are placed in sterotactic frames with distance between cranial window and laser collimator fixed at 1 inch. Photographs of a tumor as seen through the BTW (B) before laser therapy and (C) during irradiation with a 671nm laser…….……...74

Figure 3.7: A series of cranial window pictures of an implanted 9L glioma, before and after the PDT, using non-targeted HPPH polyacrylamide nanoparticles and a time interval of 6 hours between nanoparticle injection and light illumination. The dotted circle encloses the tumor area in each picture……..……..……75

Figure 3.8: BTW view of the brain on the day of photodynamic therapy (Day 0), showing tumor growth of approximate size of 3mm. Days following PDT treatment, extensive necrosis was seen in the treatment area for those animals administered HPPH nanoparticles and irradiated with the laser light……77

Figure 3.9: Tumor response as a result of delivery dependent photodynamic therapy. HPPH in the form of free dye and post-loaded in nanoparticles, F3-targeted or non-targeted polyacrylamide nanoparticles, were intravenously injected. Following nanoparticle incubation time of 105 minutes tumors were irradiated at 180 J/cm^2 using 671 nm laser light through the BTW and observed daily…….……...79

Figure 3.10: Tumor necrosis measurements. Following nanoparticle incubation time of 105 minutes tumors were irradiated at 180 J/cm^2, for 30 minutes, using 671 nm laser light. Measurements were taken for animal groups treated with non-targeted HPPH PEGylated polyacrylamide nanoparticles and F3-targted HPPH polyacrylamide nanoparticles. Both treatment groups demonstrate irradiation induced tumor necrosis…….……79

Figure 3.11: Tumor response for variations in incubation times of non-targeted HPPH PEGylated polyacrylamide nanoparticles. Following nanoparticle incubation time of 105 minutes, , 6 hours,

and 10 hours tumors were irradiated at 180 J/cm^2 using 671 nm laser light through the BTW and observed daily……81

Figure 3.12: Tumor necrosis measurements for variations in incubation times of non-targeted HPPH PEGylated polyacrylamide nanoparticles. Following nanoparticle incubation time of 105 minutes, 6 hours, and 10 hours tumors were irradiated at 180 J/cm^2 using 671 nm laser light. Prolonged duration of tumor necrosis found in treatment groups receiving irradiation following 6 hour incubation……..81

Figure 3.13: Representation of animal groups receiving PEGylated HPPH polyacrylamide nanoparticles with systemic incubation time of 6 hours between nanoparticle administration and laser illumination. Photographs depict the brain as seen through the BTW on the day of photodynamic therapy (Day 0), showing tumor growth of approximate size of 3mm, and the days post-treatment. Days following PDT treatment, significant necrosis was seen in the treatment area for all animal groups following PDT treatment……82

Figure 3.14: Response of glioma treated with HPPH post-loaded PEGylated polyacrylamide sensitized at 671 nm using varying irradiation regimens. Following nanoparticle incubation time of 6 hours tumors were irradiated at 180 J/cm^2 (100 mW/cm^2) – 30 minute illumination, 260 J/cm^2 (100 W/cm^2) – 45 minute illumination, and 260 J/cm^2 (144 mW/cm^2) – 30 minute illumination……..84

Figure 3.15: Tumor necrosis measurements for variations in fluence rates of exposed non-targeted HPPH PEGylated polyacrylamide nanoparticles. Following nanoparticle incubation time of 6 hours tumors were irradiated at 180 J/cm^2 (100 mW/cm^2) – 30 minute illumination, 260 J/cm^2 (100 W/cm^2) – 45 minute illumination, and 260 J/cm^2 (144 mW/cm^2) – 30 minute illumination, using 671 nm laser light. Tumor necrosis as seen through the BTW, observed daily……84

Figure 3.16: Gross specimen from animal model, excised 10 days post-PDT therapy. Representation of brain tumor for animal groups (A,B) without photosensitizer or laser illumination, and (C,D) animals receiving non-targeted HPPH nanoparticles (6 hour incubation time) with irradiation fluence dose of 260 J/cm^2 (144 mW/cm^2) using a 671 nm laser……85

Figure 4.1: Fluorescence spectra of ADPA over time course of 30 minutes……98

Figure 4.2: ADPA was used to detect the ROS production from Methylene Blue when combined with Coomassie Blue dye. The logarithm of the ratio of ADPA fluorescence intensity at 431nm provides the first order decay rate constant, or k-value. A) Calculation of the rate of ROS production from MB free dye using ADPA. (B-J) ROS production of various MB:CB mixtures……..99

Figure 4.3: Comparison of ROS generation from the various compositions of Methylene Blue and Coomassie Blue mixtures……...……..100

Abstract

Currently, surgical resection serves as the leading management for the treatment of brain tumors. Performing a maximal resection must be balanced with the need to preserve adjacent non-cancerous brain tissue, and even with the best microsurgical technique, resection may leave behind residual tumor tissue. In order to provide a better approach to treat cancer patients, a minimally invasive localized treatment, photodynamic therapy (PDT), has been utilized to specifically treat localized and superficial tumors. PDT uses exogenously administered photosensitizers, such as Methylene Blue and HPPH, which are activated by a specific wavelength of light. The sensitizer, in its excited state, transfers its energy to molecular oxygen, forming reactive oxygen species which irreversibly oxidize essential cellular components, resulting in injury and necrosis of nearby tumor tissue.

Photosensitizer-conjugated polyacrylamide nanoparticles were prepared for *in vivo* characterization of the minimally invasive and localized treatment of photodynamic therapy on brain tumors. PDT efficiency was improved by incorporating a variety of nanoparticle matrixes, photosensitizers, and targeting methods as well as exploring the systemic incubation of nanoparticles and fluence dependence on tumor response. Advancements and considerable attention to nanoparticle characteristics, incubation time, and photosensitizer delivery are proving allowance for further PDT quantification. Tumor growth patterns and tumorigenic response to various treatments were determined via visual observation by the use of an animal cranial window model. PDT treatments with photosensitizer loaded polyacrylamide nanoparticles, both with F3-

targeting and PEG, displayed worthy homing and passive targeting efficiency towards the implanted 9L glioma, as shown by the significant phototoxic effect, killing the tumor cells in the treatment area of the cranial window. These photoreactive nanoparticles produced significant adjournment of tumor growth over control groups, clearly demonstrating the advantages of nanoparticle-based PDT agents. The advancements in therapy efficacy described in this thesis, has the potential to be utilized as an aid to neurosurgery for the eradication of local tumors, leading to the potential palliation of the advancing disease. This form of treatment can be extended to many other types of tumors to complement surgery or even by itself for small tumors.

CHAPTER 1

INTRODUCTION

Cancer is one of the most common causes of death in the US, only second to heart disease, accounting for nearly a half a million deaths each year. The National Cancer Institute approximated in 2012 that 13.7 million people in the United States have either survived or have evidence of cancer and may be undergoing treatment [1].

Glioma

Approximately 13,700 deaths and 24,600 new cases of primary malignant brain and central nervous system (CNS) tumors occur annually in the US [2]. Of the various types of cancer, primary tumors of the CNS account for 2% of human malignancies, with malignant glioma being the most common CNS cancer in adults. In general, malignant gliomas are not curable tumors, making it one of the deadliest forms of cancer. Patients diagnosed have a mean survival of a little over a year, and only 20 weeks for those with recurring brain cancer [3-5].

Primary brain (intracerebral) tumors, also referred to as gliomas, encompass all tumors that are thought to be of glial cell origin. Comprising 50-60% of all adult brain tumors, gliomas include astrocytic tumors, oligodendrogliomas, ependymomas, and mixed gliomas [2,6]. The World Health Organization (WHO) divides gliomas into four grades, based on differentiation and histopathologic characteristics of the tumor, with glioblastoma being classified as the highest grade tumor (grade IV) [6].

Glioma therapy & treatment

Treatment of tumors of glial origin, gliomas, remains challenging due to considerable molecular and cellular heterogeneity. Numerous treatment modalities have been applied, surgical resectioning, radiation, and chemotherapy, and have helped improve the quality of life and survival for patients [7]. Surgical resection serves as the leading mode of management for the treatment of brain tumors. Mounting evidence suggests that maximal surgical resection correlates with an improvement in survival in patients with glioma [7-8]. Performing a maximal resection must be balanced with the need to preserve adjacent non-cancerous brain tissue. Even with the best microsurgical technique, resection may leave behind residual tumor tissue. In order to provide a better approach to treat cancer patients, an adjuvant therapy, secondary to surgery, may be applied, in attempt to kill any remaining tumor cells. Radiation therapy and chemotherapy can be the means of treatment to combat residual tumor cells post-surgery.

Radiotherapy employs high-energy ionizing radiation to kill cells by directly damaging their DNA, or by the creation of free radicals within cells that will ultimately damage the cell's DNA [1]. Although this additional treatment may be essential for potential palliation of the tumor, the therapy is not localized and can damage healthy cells, as well as the cancer cells, leading to partial loss of brain function, causing memory loss, personality inconsistency, and difficulty concentrating [1].

Another treatment method readily used in addition to surgical resectioning of tumors, is chemotherapy. Chemo drugs can be administered to the patient intravenously or taken orally. Some of these drugs include, but are not limited to: cisplatin, carboplatin, etoposide, paclitaxel, and temozolomide (TMZ) [9]. The most widely used chemo treatment method for patients with glioblastoma utilizes the orally administered temozolomide [10]. However this alkylating drug can

lead to systemic toxicity and long-term side effects, associated with most conventionally used chemotherapy drugs: hair loss, lethargy, increased susceptibility to infection, fatigue, etc. [1]. In addition, glioblastoma can develop multi-drug resistant (MDR) proteins, limiting the delivery, and thus, the effectiveness of chemotherapy drugs [11]. This inability of chemo drugs to be delivered with a full payload could cause further tumor growth and a high frequency of tumor recurrence post-therapy.

The major challenge associated with brain tumor therapies is the preferential destruction of malignant tissue while sparing eloquent tissue. Although surgical resection remains to be the primary method of treatment, gliomas are well known for diffusely infiltrating adjacent cerebral parenchyma, making clear tumor margins differentiation difficult [12]. A minimally invasive and localized treatment, photodynamic therapy (PDT), has been utilized to specifically treat superficial tumors reaming after surgical resectioning [13-15]. PDT uses exogenously administered photosensitizers that become activated by a specific wavelength of light. After excitation, the sensitizer, in its excited state, transfers its energy to molecular oxygen, forming reactive oxygen species. The cytotoxic products irreversibly oxidize essential cellular components, resulting in injury and necrosis of nearby tumor tissue [16-20]. Having an accessible treatment field in which to illuminate, this treatment method can selectively kill tumor cells within the treatment area without resulting in permanent damage to adjacent tissue. Thus eliminating the side effects throughout the body which are often associated with radiotherapy and chemotherapy.

Photodynamic Therapy

Mechanism

Photodynamic therapy is a minimally invasive localized treatment modality based on three key components: photosensitizer, light and molecular oxygen [21]. The PDT treatment involves 1) the delivery of photosensitizers (PS) to tumors; 2) local excitation of tumor containing photosensitizer with a specific wavelength of light; 3) a photodynamic reaction between an optically excited photosensitizer and surrounding oxygen molecules, so as to produce reactive oxygen species (ROS). This complex interplay between the photosensitizer and light can efficiently eradicate local tumors.

The PDT action is described by two well defined mechanisms. Type I reactions produce free radicals or superoxide ions by the direct transfer of an electron from the photosensitizer to the substrate (cell membrane or other molecules), forming free radicals which interact with oxygen creating ROS [21]. Type II reactions generate singlet oxygen ($^1O_2$) and ROS by the means of energy transfer via collisions of the excited sensitizer with the surrounding oxygen molecules. The relative contribution from type I and II reactions depends on the type of photosensitizer used, the available tissue oxygen and the type of substrate (e.g., a cell membrane or a biomolecule), as well as the binding affinity of the sensitizer for the substrate [21]. The mutual consensus has been that singlet oxygen created by Type II reactions has been the primary method of destruction of nearby biomolecules [22-23].

A free radical is an electrically neutral atom or molecule with an unpaired electron. These, having one lone electron, become unstable and acquire electrons from neighboring molecules. Thus, the photodynamic reactions causing free radicals are known to cause structural damage to several key

biomolecules in cellular membranes and nucleic acids: carbohydrates, proteins, and lipids. Specifically, phototoxicity induced by the activation of photosensitizers can damage plasmatic or organelle membranes, causing membrane lysis and a disruption in cell homeostasis, leading to the destruction of treated cells [24].

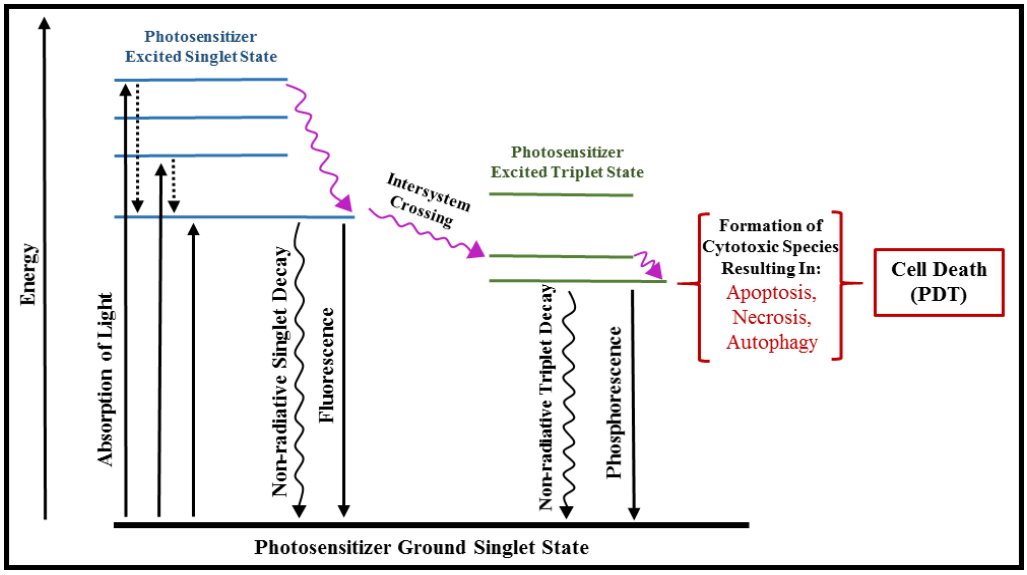

Figure 1.1: Reaction kinetics of photosensitization leading to PDT.

Reactive oxygen species

ROS is a collective term that includes a set of different high energy molecules and radicals derived from the oxygen molecule. The set of ROS include singlet oxygen ($^1O_2$), superoxide ($\bullet O_2^-$), Hydrogen peroxide (H_2O_2), Hydroxyl Radical (HO•), etc. These highly energetic molecules or radicals, created by transfer of energy from the photosensitizers during illumination, has the potential to damage cells by oxidation of biomolecules such as lipids, proteins, nucleic acids and enzymes. The specific damage to the cell is governed by the localization of these drugs in the

specific type of cells (tumor vs vasculature) as well as the specific subcellular compartments, such as the mitochrondia, cell membrane, nuclear membrane, lysozomes etc. [25-26] The damage caused by each individual species is also governed by its lifetime, which determines its diffusion length. For example, singlet oxygen has a lifetime of 4.4 μsec in water, as compared to 2.0 nsec for hydroxyl radicals, rendering it the freedom to move for a longer distance and increasing its potency [27-28**].** Thus determination of the type and amount of each ROS produced is quite essential towards the success of this therapeautic modality. Optical methods based on fluorescence and absorbance have been regularly used for this purpose. Several fluorescencent dyes, like Anthracene dipropionic acid, 2'-7'dichlorfluorescein diacetate, Di-hydrorhodamine 123, Singlet Oxygen Sensor Green, etc., have been used for monitoring the changes in local concentration of the ROS, based on changes in fluorescence intensities due to oxidation by the ROS [28-29]. Although most of these dyes display a lack of absolute specificity towards a particular species, they do have different sensitivity towards each of these ROS, allowing for a fairly good estimation of the contribution from each of the ROS [30].

Photosensitizers

Photosensitizers are drugs that are activated by light whose wavelength is specific to its absorption. As mentioned before, upon irradiation, these molecules become excited and this results in the production of ROS, through non-radiative energy transfer to oxygen. An ideal photosensitizer should exhibit the following properties: [31-32]

1. Strong absorption cross-section at longer wavelength, to increase the penetration depth.
2. High quantum yield of ROS production.
3. Good photostability: low photobleaching and degradation.

4. Minimal dark toxicity.

5. High selectively towards tumor tissues.

6. Fast clearance from the body.

Several different photosensitizers have been used for various tumor therapies such as skin, head and neck, brain, gastroenterological, pulmonary, cervical, etc. [33]. The first generation photosensitizers mainly consisted of photofrin, which is a porphyrene derivative. The porphyrene based photosensitizers are the first and historically the most extensively used. Other kinds of non-porphyrene based photosensitizers are broadly categorized as either chlorophyll derivative or dye [33].

Photofrin was the first photosensitizer to gain FDA approval for several types of tumors. Since then numerous other photosensitizers such as temoporfin (Foscan), 5-aminolevulinic acid (5-ALA, Levulan), verteporfin (Visudyne), Methylene Blue, etc. as have been approved by the FDA. Some of the other photosensitizers such as HPPH, Chlorine e6, etc. have undergone clinical trials as well. The second generation photosensitizers are more promising, with improved properties, making them quite effective for clinical applications. However some of the drawbacks most commonly associated with photosensitizers are dark toxicity, low selectivity and specificity towards the target tissue, photo-degradation, slow clearance from the body, and pain associated with injecting some of the more hydrophobic drugs [34]. Currently, third generation photosensitizers that include modifications to previous drugs, such as conjugating antibodies, lipids, etc., are being explored [35]. Another area of interest is the utilization of nanocarriers of photosensitizers with the aim of improving their performance and delivery [36].

Nanotechnology of drug carriers

Nanotechnology facilitates the design of novel and effective drug delivery platforms that have the ability to overcome some of the potential drawbacks associated with the free drugs, be it for PDT or Chemotherapy [37]. Utilizing a nanoparticle design can limit the non-specific interaction between the free drug and plasma proteins, enzymes, immune system cells, etc. This can help reduce the changes in chemical or physical properties of the small molecule drugs, caused by degradation/breakdown, before its delivery to the intended location. Additionally, it offers the following advantages over free drugs [36-38]:

1. Ability to simultaneously load multiple drugs and small molecule sensitizers into the nanoparticle.
2. Capacity to control the drug release based on various stimuli such as pH, temperature, reducing agents such as glutathione, etc.
3. Potential reduction in cytotoxicity.
4. Enhanced plasma lifetime.
5. Specific targeting to the particular cell line, and to its subcellular location.
6. Synergistic loading withy image contrast agents.

Over the past decade there has been significant progress in the design and development of various nanoparticles for the purpose of drug delivery. The attractiveness of the nanoparticle as a drug delivery vehicle lies in the flexibility offered by them in terms of its bulk and surface, which can be easily tuned during synthesis, as well as its toxicity properties. The most important considerations for the nanoparticle formulation is the material for the matrix and the functional groups. The nanoparticles can be engineered to load a specific drug for a particular application, by modifying its bulk and surface properties. The bulk properties such as density, elasticity,

hydrophobicity, etc., can be modified by choosing the appropriate materials for the matrix. The surface properties can be changed by modifying the surface and attachment of peptides, antibodies, or smaller targeting molecules, such as aptamers. The most commonly used matrixes for drug delivery are based on polymers, particularly hydrogels, due to their biocompatability and ease of engineerability [38].

Several types of, polymer and non-polymer, hydrogel based drug nanocarriers, such as silica, ormosil, PLGA, polystyrene, polymerized liposomes, pluronic co-polymers, polyacrylamide, polyacrylic acid, etc., have been utilized for therapeutic applications [36-38]. In this thesis, we will focus on polyacrylamide based nanoparticles as drug delivery vehicles. The polyacrylamide based nanoparticle has gained a lot of attention recently because of the ease in controlling the different chemical and physical properties, as well as its excellent biocompatibility and nontoxic properties. [39]. Polyacrylamide as a material has been frequently used in humans for different biomedical applications, the most prominent being its utilization as permanent filler for soft tissue augmentation during aesthetic facial surgery [40]. It has also been used for developing soft contact lenses. The polyacrylamide based matrix is inert and does not chemically interact with cells or tissues to cause any interference with their proper functioning, and neither does it lead to any perturbation in its vicinity. Polyacrylamide nanoparticles also act as an excellent choice for encapsulating different types of drugs and small molecules [41].

Up to now, the polyacrylamide based nanoparticles have already been used for drug delivery applications for both PDT and Chemotherapy [42-44]. Additionally this matrix has also been utilized for other applications, such as chemical sensing of ions and small molecules, tumor imaging etc. [41, 44-45]. They have also been applied as a visual contrast agent for delineating brain tumors [46].

Nanoparticle and tissue interaction

Tumor cells, like healthy cells, need blood supply to grow. Without constant blood supply, solid tumor growth is limited to 2 mm in diameter. Such tumors may remain benign. However, in order to grow in size, tumors must develop their own blood vessel supply, to deliver nutrients and replenish oxygen [47]. Angiogenesis is the act of forming new capillary blood vessels. The tumor's recruitment of new vasculature is initiated by angiogenic factors, such as *endothelial growth factor* (VEGF), *platelet-derived growth factors* (PDGF), and *basic fibroblast growth factor* (bFGF), which activate the proliferation of neighboring vessels [48]. This newly formed vasculature has little smooth muscle support and its vessels are more permeable than normal blood vessels. A solid tumor's growth relies on the production of angiogenic vasculature; thus effective use of the leaky vasculature could facilitate tumor therapy. Angiogenic vasculature permeability and lack of lymphatic drainage allows for the accumulation of photosensitizer containing nanoparticles.

Coating nanoparticles with the hydrophilic, water-soluble, polymer, polyethylene glycol (PEG), allows for longer plasma circulation times after nanoparticle administration [49]. PEG has been readily applied in different commercial, uses including incorporation into foods, cosmetics, ointments, pharmaceutics, etc. [50-51]. Long systemic circulation through tumor vasculature, having considerable fissures between endothelial cells in tumor blood vessels and tumor tissue, permits nanoparticle delivery and retention in tumors through "passive targeting" due to the "enhanced permeability and retention effect" (EPR) [52]. This unique quality, derived as a result of the angiogenesis process, allows for the selective extravasation into, and retention by, the tumor, of macromolecular/nanoparticle drugs used for tumor therapy.

Potential enhancement of tumor drug delivery has been realized with the use of targeted cancer therapy, utilizing targeting molecules specific to tumor cell development and growth [53].

Numerous targeted cancer therapies have been approved by the U.S. Food and Drug Administration (FDA), while others are undergoing clinical and pre-clinical tests show promise of success [54]. These therapies are designed using targeting molecules – antibodies and small molecule peptides - having distinct delivery methods.

Most targeted cancer therapies have been developed with the intent of capitalizing on targets that play a key role in cancer cell growth and survival. Antibodies are used as delivery vehicles, engineered for the interaction with specific cell surface receptors [54]. Although being a very effective method, the large size and non-specific uptake of antibodies may prevent drugs from crossing cell membranes, limiting drug delivery to the outside of cells. Alleviating this problem associated with antibody targeting, small targeting molecule delivery of drugs can traverse cellular membranes, making this delivery method better suited for greater interaction with molecules located on the exterior and interior of cells [54]. Such therapy can be directed for the interference of gene expression, cellular function, signaling pathways, etc. "Small molecules" used for the delivery of therapeutic drugs include peptides. The 31-amino acid derived from the NH_2-terminal fragment of the human high-mobility group protein 2 (HMGN2) [55], F3-peptide, selectively targets tumor blood vessels and tumor cells, due to their significant expression of nucleolin. This made the F3-peptide a desirable candidate for the delivery of photosensitizers in the work described in this thesis.

The F3-tumor homing peptide binds to angiogenic vasculature and particular tumor cells expressing the cell surface receptor nucleolin [56-57]. Nucleolin is a multifunctional phosphoprotein ubiquitously dispersed throughout the nucleolus. Upon accumulation on the cell membrane surface, nucleolin can act as a shuttle protein, allowing for the internalization of drugs into the nucleus of tumor [58].

Targeted therapies are designed to interact with specific molecules associated with tumor development, resulting in a reduced systemic toxicity, compared to standard chemotherapy and radiation treatments [56]. Using molecular targets reduces or eliminates collateral damage to healthy cells. This can contribute to improved patient comfort while undergoing treatment and better quality of life post-treatment.

In Chapter two the development, characterization, and therapeutic application of Methylene Blue loaded nanoparticles on a rat glioma model *in vivo* is presented. The photosensitizer Methylene Blue was covalently conjugated to the nanoparticle matrix to prevent any leaching and non-specific staining. *In vitro* experiments demonstrated its high efficiency in producing reactive oxygen species as well as its cell killing ability. Further *in vivo* experiments were performed by first optimizing the different parameters of the therapy such as nanoparticle dose, effect of surface modification by attachment of targeting moieties such as F3-peptide, incubation time and the light fluence. The quantitative growth patterns of the glioma were determined through visual observation of the tumorigenic response to various treatments by the use of an animal cranial window model. The cranial window model was prepared by replacing a part of the rat skull with a glass window above the tumor. PDT treatments with Methylene Blue loaded nanoparticles produced significant adjournment of tumor growth over control groups, clearly demonstrating the advantages of nanoparticle-based PDT agents for the eradication of local tumors, leading to the potential palliation of the advancing disease.

In chapter three we successfully demonstrate the application of another photosensitizer, (2-[1-hexyloxyethyl]-2-devinyl pyropheophorbide-a) (HPPH), loaded nanoparticle towards an optimal treatment conditions for PDT. HPPH is a photosensitizer that has effective photodynamic efficiency and has been used for human clinical trials. The HPPH dye was incorporated into the

nanoparticle by post-loading. The hydrophobicity of the dye helps retain it inside the matrix, which is designed accordingly. Experiments on live cells show that these nanoparticles have minimal dark toxicity yet has excellent cell killing abilities when irradiated with light of appropriate wavelength. Both F3-targeted and non-targeted nanoparticles were used as well as different incubation times and light irradiation doses were applied to optimize the treatment parameters. *In vivo* PDT treatment on rat glioma, with windows, led to significant arrest of tumor growth over control groups. The results presented here demonstrate that PDT creates significant amount of necrosis and damages the vasculature that halts the tumor growth significantly.

In chapter four we explore the possibility of combining multiple dyes such as, Methylene blue and Coomassie Blue, inside a nanoparticle, and predict its efficiency towards PDT by monitoring the ROS production from the mixture at different ratio. The rationale of using multiple dyes is to extend the application of the nanoparticles in guiding surgery in addition to PDT. We observe a significant decrease in the generation of ROS from the mixture with increasing concentration of Coomassie Blue dye. This can be attributed to the quenching of ROS production as well as its interaction with the dye, reducing its lifetime. These results show that such a selection of dye would not be optimal for combining PDT and visual delineation and highlights the need for an alternate strategy to achieve this goal.

In chapter five we discuss some of the possible future direction. Following PDT we observe a significant arrest in tumor growth, however tumor re-growth is observed again at a later stage. This is attributed to the superficial nature of this treatment. Discussed in this chapter are the methods for improving this technique such as enhancing the ROS production using special NP design involving metal core. Additionally we also describe methods to monitor the *in vivo* dynamics of changes in oxygen concentration and ROS production as well as the cell killing and onset of

necrosis at the cellular level. Here we also propose the combination of surgery and PDT towards the treatment of glioma. That would involve development of multifunctional NP that can be used for visual tumor delineation and therapy as well, without compromising the efficiency of ROS production. The proposed treatment method of nanoparticle aided PDT would be most effective if used as an adjuvant therapy to surgery for treatment of glioma.

REFERENCES

[1] "American Cancer Society | Information and Resources for Cancer: Breast, Colon, Lung, Prostate, Skin | Cancer Facts and Figures 2012." *American Cancer Society | Information and Resources for Cancer: Breast, Colon, Lung, Prostate, Skin*. N.p., n.d. Web, <http://www.cancer.org>. 2 Jan. 2014.

[2] "2012 Fact Sheet." *Central Brain Tumor Registry of the United States*. N.p., n.d. Web, <http://www.CBTRUS.org>. 20 Dec. 2013.

[3] Sampson, John H., et al. "Tumor-specific immunotherapy targeting the EGFRvIII mutation in patients with malignant glioma." *Seminars in immunology*. Vol. 20. No. 5. Academic Press, 2008.

[4] Kiwit, J. C., F. W. Floeth, and W. J. Bock. "Survival in malignant glioma: analysis of prognostic factors with special regard to cytoreductive surgery."*Zentralblatt fur Neurochirurgie* 57.2 (1995): 76-88.

[5] Kopelman, Raoul, et al. "Multifunctional nanoparticle platforms for in vivo MRI enhancement and photodynamic therapy of a rat brain cancer." *Journal of Magnetism and Magnetic Materials* 293.1 (2005): 404-410.

[6] Gilman, Sid. *Neurobiology of disease*. Academic Press, 2011.

[7] Gilbertson, Richard J. "Medulloblastoma: signalling a change in treatment." *The lancet oncology* 5.4 (2004): 209-218.

[8] Bailey, Percival, and Harvey Cushing. "A classification of the tumors of the glioma group on a histogenic basis with a correlated study of prognosis." (1928).

[9] Liu, Gentao, et al. "Cytotoxic T cell targeting of TRP-2 sensitizes human malignant glioma to chemotherapy." *Oncogene* 24.33 (2005): 5226-5234.

[10] Hegi, Monika E., et al. "MGMT gene silencing and benefit from temozolomide in glioblastoma." *New England Journal of Medicine* 352.10 (2005): 997-1003.

[11] de Faria, Giselle Pinto, et al. "Differences in the expression pattern of P-glycoprotein and MRP1 in low-grade and high-grade gliomas." *Cancer investigation* 26.9 (2008): 883-889.

[12] Schwartzbaum, Judith A., et al. "Epidemiology and molecular pathology of glioma." *Nature Clinical Practice Neurology* 2.9 (2006): 494-503.

[13] Eljamel, M. Sam. "Brain photodiagnosis (PD), fluorescence guided resection (FGR) and photodynamic therapy (PDT): past, present and future."*Photodiagnosis and photodynamic Therapy* 5.1 (2008): 29-35.

[14] Fayter, D., et al. "A systematic review of photodynamic therapy in the treatment of pre-cancerous skin conditions, Barrett's oesophagus and cancers of the biliary tract, brain, head and neck, lung, oesophagus and skin." (2010).

[15] O'Connor, Aisling E., William M. Gallagher, and Annette T. Byrne. "Porphyrin and nonporphyrin photosensitizers in oncology: preclinical and clinical advances in photodynamic therapy." *Photochemistry and photobiology* 85.5 (2009): 1053-1074.

[16] Fayter, D., et al. "A systematic review of photodynamic therapy in the treatment of pre-cancerous skin conditions, Barrett's oesophagus and cancers of the biliary tract, brain, head and neck, lung, oesophagus and skin." (2010).

[17] O'Connor, Aisling E., William M. Gallagher, and Annette T. Byrne. "Porphyrin and nonporphyrin photosensitizers in oncology: preclinical and clinical advances in photodynamic therapy." *Photochemistry and photobiology* 85.5 (2009): 1053-1074.

[18] Henderson, Barbara W., et al. "Choice of oxygen-conserving treatment regimen determines the inflammatory response and outcome of photodynamic therapy of tumors." *Cancer research* 64.6 (2004): 2120-2126.

[19] Konan, Yvette Niamien, Robert Gurny, and Eric Allémann. "State of the art in the delivery of photosensitizers for photodynamic therapy." *Journal of Photochemistry and Photobiology B: Biology* 66.2 (2002): 89-106.

[20] Wiedmann, Marcus W., and Karel Caca. "General principles of photodynamic therapy (PDT) and gastrointestinal applications." *Current pharmaceutical biotechnology* 5.4 (2004): 397-408.

[21] Dolmans, Dennis EJGJ, Dai Fukumura, and Rakesh K. Jain. "Photodynamic therapy for cancer." *Nature Reviews Cancer* 3.5 (2003): 380-387.

[22] Foote, Christopher S. "Definition of type I and type II photosensitized oxidation."*Photochemistry and photobiology* 54.5 (1991): 659-659.

[23] Niedre, Mark, Michael S. Patterson, and Brian C. Wilson. "Direct Near-infrared Luminescence Detection of Singlet Oxygen Generated by Photodynamic Therapy in Cells In Vitro and Tissues In Vivo." *Photochemistry and photobiology* 75.4 (2002): 382-391.

[24] Valenzeno, Dennis Paul. "Photomodification of biological membranes with emphasis on singlet oxygen mechanisms." *Photochemistry and photobiology*46.1 (1987): 147-160.

[25] Ochsner, M. "Photophysical and photobiological processes in the photodynamic therapy of tumours." *Journal of Photochemistry and Photobiology B: Biology* 39.1 (1997): 1-18.

[26] Chen, Bin, et al. "Vascular and cellular targeting for photodynamic therapy. "*Critical Reviews™ in Eukaryotic Gene Expression* 16.4 (2006).

[27] Rodgers, Michael AJ, and Paul T. Snowden. "Lifetime of oxygen (O2 (1. DELTA. g)) in liquid water as determined by time-resolved infrared luminescence measurements." *Journal of the American Chemical Society* 104.20 (1982): 5541-5543.

[28] Spence, Michelle T. Z., and Iain D. Johnson. *The Molecular Probes Handbook: A Guide to Fluorescent Probes and Labeling Technologies*. Carlsbad, CA: Life Technologies Corporation, 2010.

[29] Wardman, Peter. "Fluorescent and luminescent probes for measurement of oxidative and nitrosative species in cells and tissues: progress, pitfalls, and prospects." *Free radical biology and medicine* 43.7 (2007): 995-1022.

[30] Price, Michael, and David Kessel. "On the use of fluorescence probes for detecting reactive oxygen and nitrogen species associated with photodynamic therapy." *Journal of biomedical optics* 15.5 (2010): 051605-051605.

[31] Allison, Ron R., et al. "Photosensitizers in clinical PDT." *Photodiagnosis and photodynamic therapy* 1.1 (2004): 27-42.

[32] Detty, Michael R., Scott L. Gibson, and Stephen J. Wagner. "Current clinical and preclinical photosensitizers for use in photodynamic therapy." *Journal of medicinal chemistry* 47.16 (2004): 3897-3915.

[33] Huang, Zheng. "A review of progress in clinical photodynamic therapy."*Technology in cancer research & treatment* 4.3 (2005): 283.

[34] Garland, Martin J., et al. "Designing photosensitizers for photodynamic therapy: strategies, challenges and promising developments." *Future medicinal chemistry* 1.4 (2009): 667-691.

[35] Moser, Joerg G. "1.1. DEFINITIONS AND GENERAL PROPERTIES OF 2nd AND 3rd GENERATION PHOTOSENSITIZERS." *Photodynamic Tumor Therapy* (1998): 1.

[36] Chatterjee, Dev Kumar, Li Shan Fong, and Yong Zhang. "Nanoparticles in photodynamic therapy: an emerging paradigm." *Advanced drug delivery reviews*60.15 (2008): 1627-1637.

[37] Farokhzad, Omid C., and Robert Langer. "Impact of nanotechnology on drug delivery." *ACS nano* 3.1 (2009): 16-20.

[38] Lee, Yong-Eun Koo, and Raoul Kopelman. "Polymeric nanoparticles for photodynamic therapy." *Biomedical nanotechnology*. Humana Press, 2011. 151-178.

[39] Yang, Tsung-Hua. "Recent applications of polyacrylamide as biomaterials."*Recent Patents Mater. Sci* 1.1 (2008): 29-40.

[40] Pallua, Norbert, and Timm P. Wolter. "A 5-year assessment of safety and aesthetic results after facial soft-tissue augmentation with polyacrylamide hydrogel (Aquamid): a prospective multicenter study of 251 patients." *Plastic and reconstructive surgery* 125.6 (2010): 1797-1804.

[41] Lee, Yong-Eun Koo, Raoul Kopelman, and Ron Smith. "Nanoparticle PEBBLE sensors in live cells and in vivo." *Annual review of analytical chemistry (Palo Alto, Calif.)* 2 (2009): 57.

[42] Hah, Hoe Jin, et al. "Methylene Blue-Conjugated Hydrogel Nanoparticles and Tumor-Cell Targeted Photodynamic Therapy." *Macromolecular bioscience* 11.1 (2011): 90-99.

[43] Winer, Ira, et al. "F3-targeted cisplatin-hydrogel nanoparticles as an effective therapeutic that targets both murine and human ovarian tumor endothelial cells in vivo." *Cancer research* 70.21 (2010): 8674-8683.

[44] Reddy, G. Ramachandra, et al. "Vascular targeted nanoparticles for imaging and treatment of brain tumors." *Clinical Cancer Research* 12.22 (2006): 6677-6686.

[45] Ray, Aniruddha, and Raoul Kopelman. "Hydrogel nanosensors for biophotonic imaging of chemical analytes." *Nanomedicine* 8.11 (2013): 1829-1838.

[46] Nie, Guochao, et al. "Hydrogel nanoparticles with covalently linked coomassie blue for brain tumor delineation visible to the surgeon." *Small* 8.6 (2012): 884-891.

[47] Makrilia, Nektaria, et al. "The role of angiogenesis in solid tumours: an overview." *European journal of internal medicine* 20.7 (2009): 663-671.

[48] Folkman, Judah. "Angiogenesis." *Annu. Rev. Med.* 57 (2006): 1-18.

[49] Moffat, Bradford A., et al. "A novel polyacrylamide magnetic nanoparticle contrast agent for molecular imaging using MRI." *Molecular imaging* 2.4 (2003).

[50] Sheftel, Victor O. *Indirect food additives and polymers: migration and toxicology*. CRC Press, 2000.

[51] Nalam, Prathima C., et al. "Macrotribological studies of poly (L-lysine)-graft-poly (ethylene glycol) in aqueous glycerol mixtures." *Tribology letters* 37.3 (2010): 541-552.

[52] Matsumura, Yasuhiro, and Hiroshi Maeda. "A new concept for macromolecular therapeutics in cancer chemotherapy: mechanism of tumoritropic accumulation of proteins and the antitumor agent smancs." *Cancer research* 46.12 Part 1 (1986): 6387-6392.

[53] Ruoslahti, Erkki, Sangeeta N. Bhatia, and Michael J. Sailor. "Targeting of drugs and nanoparticles to tumors." *The Journal of cell biology* 188.6 (2010): 759-768.

[54] "Targeted Cancer Therapies - National Cancer Institute." *Targeted Cancer Therapies - National Cancer Institute*. N.p., n.d. Web, <http://www.cancer.gov/cancertopics/factsheet/Therapy/targeted>. 8 Jan. 2014.

[55] Moan, Johan, and Kristian Berg. "The photodegradation of porphyrins in cells can be used to estimate the lifetime of singlet oxygen." *Photochemistry and photobiology* 53.4 (1991): 549-553.

[56] Orringer, Daniel A., et al. "The brain tumor window model: a combined cranial window and implanted glioma model for evaluating intraoperative contrast agents." *Neurosurgery* 66.4 (2010): 736-743.

[57] Vinogradov, Serguei V., Tatiana K. Bronich, and Alexander V. Kabanov. "Nanosized cationic hydrogels for drug delivery: preparation, properties and interactions with cells." *Advanced drug delivery reviews* 54.1 (2002): 135-147.

[58] Gollnick, S. O., et al. "Role of cytokines in photodynamic therapy-induced local and systemic inflammation." *British journal of cancer* 88.11 (2003): 1772-1779.

CHAPTER 2

Delayed Brain Tumor Growth Using Methylene Blue Mediated Photodynamic Therapy

INTRODUCTION

Choosing an appropriate and suitable photosensitizer is of upmost importance when designing a PDT agent. The ideal agent should exhibit chemical purity, nominal dark toxicity for the photosensitizer and its metabolites, high efficiency of tumor selectivity, high photochemical ability, activation at high absorbance wavelengths which achieve sufficient tissue penetration and are within the therapeutic window (600-900nm), and rapid system clearance to diminish photosensitivity [1-5].

The above requirements, and especially the consequences of skin phototoxicity, led to second generation photosensitizers. Second-generation synthetic photosensitizers are recognized for having known chemical composition, a greater affinity for tumor selectivity, shorter periods of photosensitivity, higher yields of singlet oxygen, and an increase in penetration depth due to longer activation wavelengths in the range of 650-800nm [6].

Methylene Blue (MB), a second generation photosensitizer, is of particular interest with well-established photochemical properties. This dye has a high quantum yield of singlet oxygen generation (Φ_{Δ}~0.5) and is a highly efficient sensitizer for PDT [7]. Methylene Blue belongs to

the phenothiazinium family, allowing for increased efficacies of singlet oxygen production and a high molar absorption coefficient (ε_{max}) ~ 82,000 M^{-1} cm^{-1}. Furthermore, this dye has excitation within the therapeutic window (600-900nm) allowing for greater penetration depths [3, 8-13].

Methylene Blue has been utilized for a number of medical applications and therapies [14]. 2013, over 13,000 entries for "Methylene Blue" have been accepted by the biomedical library PubMed, not including studies which were not covered by PubMed. Methylene Blue has made history as a histochemical stain, a biochemical reagent and a chief compound in the development of therapeutic agents for diseases ranging from microbial disease to cyanide poisoning [15-16]. In 1891, Paul Ehrlich used the dye as an anti-malarial drug during the Pacific War; later it was rejected for the staining side effects: turning the urine green and the sclera (whites of the eyes) blue [17-18]. This staining response of Methylene Blue provided the foundation of modern chemotherapy [15]. During the past decade, there has been considerable attention to the use of Methylene Blue as a potential drug for Alzheimer's disease. Having the ability to inhibit the aggregation of the tau protein and the dissociation of amyloids, Methylene Blue shows promising results in halting the progression of Alzheimer's dementia [19-20].

Expanding the use of this therapeutic modality, there have been extensive experimental studies considering the application of Methylene Blue for photodynamic therapy *in vitro* [3,21], *in vivo* [22] and in clinical studies[4, 23-26], and it has been identified for having a promising potential for the treatment of cancer. Clinical PDT treatments and trials using Methylene Blue include basal cell carcinoma, melanoma, Kaposi's sarcoma [27], and chronic periodontitis [28]. However the widespread use of Methylene Blue as a photosensitizer for clinical PDT has been limited due to its susceptibility to enzymatic degradation when delivered intravenously.

Methylene Blue can easily cross the cell membrane and anchor in the mitochondria [29-30], lysosomes [31] and double-stranded DNA [32]. It has been found that when Methylene Blue binds to the mitochondria it can traverse the matrix by the mitochondrial matrix proton potential [29]. Additionally increase in local concentrations of Methylene Blue induces the formation of Methylene Blue dimers, previously shown to be less effective in production of reactive oxygen species. [8-9]. This accumulation of Methylene Blue in the mitochondria reduces the compound - induced by oxidation of the dye by NAD(P)H - to the colorless Leuko-Methylene Blue (LMB), a molecule with no photodynamic ability [12,22-23]. The physical uptake and reducing agent of Methylene Blue can be attributed to both the thiazine dye reductase found on the surface of endothelial cells and NADH/NADPH within the cells [33-35].

The ability to maintain the photosensitizing capability of Methylene Blue in a biological environment is critical for its application to PDT of cancer. Its incorporation into nanoparticle matrix composed of polymers such as polyacrylamide (PAA), silica, poly(lactic-co-glycolic acid), etc. can serve to embed the active form of the Methylene Blue photosensitizer, protecting it against enzymatic degradation [36]. Furthermore, nanoparticle surface modification can allow for enhanced and active targeting by attachment of a tumor specific homing moiety, e.g. the F3-peptide, and coating it with polyethylene glycol (PEG) for longer plasma circulation [37].

Loading of the Methylene Blue photosensitizer is achieved by physical encapsulation during synthesis or post loading after synthesis or even covalently linking the dye to the PAA nanoparticle matrix. The complex process of covalently linking the dye prevents any leaching related problems during *in vivo* studies. This loading method has been designed and tested, in serum solution, cells, and *in vivo* and has exhibited potential for future clinical applications [36].

There are many advantages to the use of NPs for PDT due to its ability to reduce systemic toxicity of the drugs, improve the local delivery and specificity of drugs as well as enhance its plasma circulation time [38-43]. Engineering nanoparticles to lie within the desired diameter of 10-100 nm avoid renal elimination and recognition by phagocytes [38-40]. Nanoparticle accumulation in brain tumor tissue and vasculature is achieved through "enhanced permeability and retention effect" (EPR), allowing macromolecules retention within tissue by way of leaky microvasculature and poor lymphatic drainage [41-44]. Nanoparticle matrix surface engineering can improve retention within tumor tissue with the attachment of a tumor specific homing moiety, e.g. the F3-peptide and enhance plasma circulation (~24 hours) by coating the matrix with polyethylene glycol (PEG) [40].These novel delivery methods minimize side effects as well as enhances therapeutic efficiency. To avoid possible side effects caused by the accumulation of nanoparticles post-treatment, biodegradable cross-linkers are incorporated into the nanoparticle matrix, allowing for slow biodegradation and bioelimination *in vivo* [45].

Polyacrylamide nanoparticles containing Photofrin and surface-modified with F3-peptide have been utilized for specific targeting of the gliosarcoma cells. Nanoparticle targeting has also displayed high intratumoral NP uptake thereby increasing the phototoxicity – resulting in complete remission of tumor for 40% of the animals treated with F3-targeted Photofrin nanoparticles. While all control rats, including those treated with non-targeted NPs or free Photofrin, died within 2 weeks [46].

In this chapter, the photosensitizer Methylene Blue was covalently conjugated to the nanoparticle matrix and used in *in vitro* and *in vivo* experiments to demonstrate its high proficiency in producing reactive oxygen species as well as its cell killing ability. *In vivo* experiments utilized glioma bearing rats adorning cranial windows allowing for direct serial inspection of various therapy

parameters of the such as nanoparticle dose, effect of surface modification by attachment of targeting moieties such as F3-peptide, incubation time and the light fluence.

EXPERIMENTAL

Nanoparticle synthesis

Materials

Methylene Blue succinimidylesther (MB-SE) was purchased from Emp. Biotech. Acrylamide (AA), 3-(acryloyoxy))-2-hydroxypropyl methacrylate (AHM), ammonium persulfate (APS), N,N,N',N'-tetramethylethylenediamine (TEMED), sodium dioctylsulfosuccinate (AOT), Brij 30, were all acquired from Sigma-Aldrich (St Louis, MO). 3-(aminopropyl) methacrylamide hydrochloride salt (APMA) was purchased from Polysciences Inc. (Warrington, PA). Ethanol (95%) and hexane were purchased from Fisher Scientific. Phosphate-buffered solution (PBS) was made using a phosphate-buffered saline tablet from Sigma-Aldrich. F3-Cys peptide (KDEPQRRSARLSAKPAPPKPEPKPKKAPAKKC) was purchased from SynBioSci. The heterobifunctional PEG (MAL-PEG-NHS, 2k) was purchased from Creative PEG Works. All chemicals were used as purchased without further purification.

Preparation of Methylene Blue nanoparticles

Methylene Blue-conjugated polyacrylamide nanoparticles were prepared by a reverse microemulsion polymerization method [18]. A monomer solution was prepared by dissolving monomers, acrylamide and APMA, in PBS. A dye solution consisting of MB-SE and biodegradable cross-linker, AHM, was prepared and gently stirred for 2 hours at room temperature.

The monomer solution and the dye solution were sonicated and added to a deoxygenated hexane solution containing two surfactants, AOT and Brij 30. The two mixtures were emulsified by stirring for 20 min, followed by the initiation of polymerization by addition of a freshly prepared APS solution (10% w/v) and TEMED. The solution was then stirred under inert atmosphere, at room temperature, for 2 hours. After completing the polymerization, hexane was removed using a Rotavapor-P (Brinkmann Instruments) and the residue was suspended in ethanol. Excess surfactant and dye from the remnant mixture were removed by washing the particles with ethanol and distilled water through an Amicon ultra-filtration cell (Millipore Corp., Bedford, MA), with a 300 kDa filter membrane under pressure (10–20 psi). The resultant nanoparticles were then freeze-dried using a 5L ModulyoD freeze dryer (ThermoFisher Scientific).

F3-peptide conjugation to polyacrylamide nanoparticles

F3-peptides were conjugated to the surface of the nanoparticles for specific targeting to nucleolin expressed on the glioma cells. The freeze-dried PAA nanopartciles (50 mg) were dissolved in PBS (2.5 mL, pH 7.4) and bifunctional PEG (4 mg) was conjugated to the nanoparticle surface by amine-succinimidyl ester. This mixture was allowed to react under stirring condition for 30 min at room temperature before undergoing thorough washings using an Amicon centrifugal filter (Millipore, 100 kDa) thereby removing any unreacted ligands, and the final solution concentrated to ~20 mg/mL. Cystein tagged F3-peptide, F3-Cys peptides (0.06 μmol), were added to the concentrated nanosensor solution and gently stirred overnight (>6 hours), at room temperature. L-Cysteine aqueous solution was added to the mixture and stirred for 2 hours in order to deactivate the terminal site of unreacted PEG. The resultant F3-targeted MB-conjugated PAA nanoparticle solution was thoroughly washed with PBS and distilled water in an Amicon ultra-filtration cell

(Millipore Corp., Bedford, MA), and then freeze-dried with a 5L ModulyoD freeze dryer (ThermoFisher Scientific) until re-hydrated for experimental use.

Surface modification of non-targeted nanoparticles

Dye-conjugated PAA nanopartciles (50 mg) were dissolved in PBS (2.5 mL, pH 7.4). Bifunctional PEG (4 mg), was added to the nanoparticles solution and then the mixture was stirred for 30 min at room temperature. A rinsing procedure was carried out, using an Amicon centrifugal filter (Millipore, 100 kDa), removing any unreacted ligands, and concentrated to ~20 mg/mL. Following the addition of PEG, an aqueous solution of L-Cysteine was added to the mixture and stirred for 2 hours in order to deactivate the terminal site of PEG. The resultant non-targeted MB-conjugated polyacrylamide nanoparticle solution was thoroughly washed with PBS and distilled water in an Amicon ultra-filtration cell (Millipore Corp., Bedford, MA), and then freeze-dried with a 5L ModulyoD freeze dryer (ThermoFisher Scientific) until re-hydrated for experimental use.

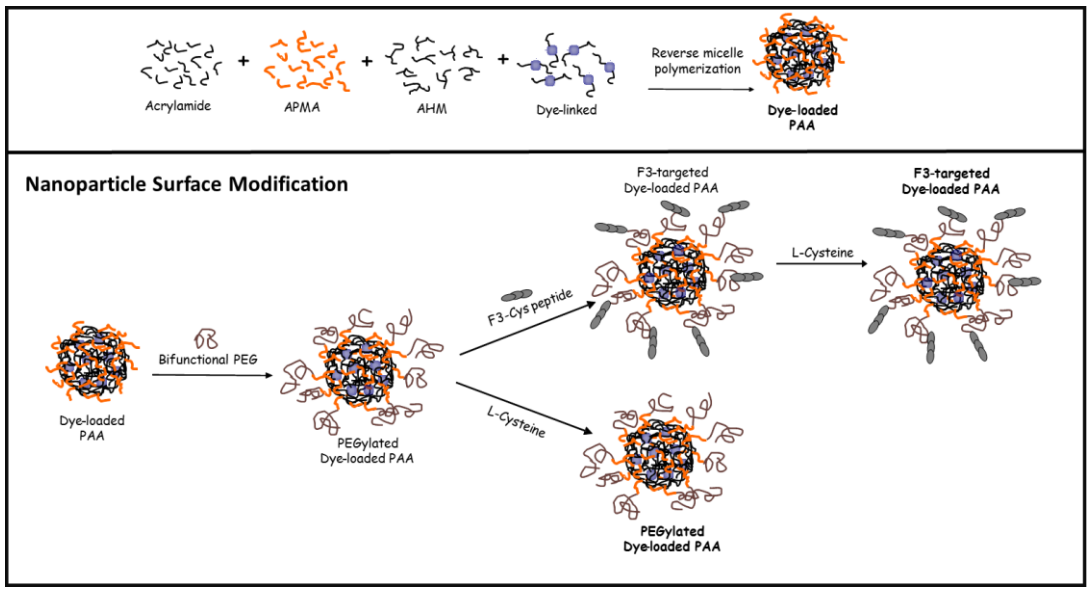

Figure 2.1: Surface modification and conjugation of MB-loaded PAA nanoparticles.

Nanoparticle characterization

Dynamic light scattering measurements

The size distribution of the MB-conjugated PAA nanoparticles in an aqueous solution was measured by dynamic light scattering (DLS, DelsaNano, Beckman Coulter, Inc., Brea, CA, USA). The surface charge of the MB-conjugated PAA nanoparticles in water was measured as a zeta potential value, using the above instrument.

Quantification of dye loading

The amount of dye in the nanoparticles was evaluated by absorption measurements, using a UV-Vis spectrometer (UV-1601, Shimadzu, Scientific Instruments Inc., Columbia, MD, USA). The amount of photosensitizer loaded was calculated using the Beer-Lambert law.

Reactive oxygen species detection

ROS (reactive oxygen species) production from MB-PAA NPs was measured using Anthracene-9,10-dipropionic acid disodium salt (ADPA) as a ROS ($^1O_2$) detection probe [47-48]. MB-conjugated nanoparticles were suspended in PBS and mixed with ADPA in a cuvette and while under constant stirring the solution was irradiated at the excitation wavelength to determine $^1O_2$ generation using fluorescence spectroscopy (FluoroMax-3, JobinYvon/SPEX Division, Instruments S.A. Inc., Edison, NJ, USA).

Toxicity analysis

MTT assay

For cytotoxicity studies, 9L glioma cells were plated on 96-well plates, at a density of 5000 cells per well, and incubated at 37^{o}C overnight. For comparison, the cells were incubated with blank PAA, PEGylated PAA, and F3-targeted PAA nanoparticles at various concentrations (0.1, 0.2, 0.5, and 1.0 mg/ml) and left for 2 hours at 37^{o}C with slow intermittent rocking. After incubation, to remove any unbound nanoparticles, the treated cells were carefully washed 3 times with fresh cell medium. The cells were further prepared using the MTT assay kit; 25 μl of 5.0 mg/ml 3-(4,5-dimethylthiazol-2-yl)-2,5-diphenyltetrazolium bromide (MTT) in PBS was added to each well and left to incubate for 4 hours while slowly rocking. After 4 hours the solution was removed and 200 μl of DMSO was added to each well, so as to solubilize the water-insoluble formazan crystals produced by the MTT cellular dehydrogenase activity in viable cells. The 96-well plate was covered with foil and left to steadily rock on a 55S single platform shaker (Reliable Scientific, Inc) overnight. To quantify cell viability of the treated cells, the absorbance spectra was analyzed using a microplate reader (SpectraMAXPlus 384, Molecular Devices LLC, Sunnyvale, CA) at 550nm and compared to untreated cells. Each condition was performed using 12 wells so as to assure dependable results.

Endotoxin detection

Enodotoxin levels were measured using an Endosafe-PTS (Charles River) and following the LAL Assay [49]. A portable endotoxin meter has sterile cartridges for detecting endotoxin in aqueous samples. Within the device, a reaction between horseshoe crab blood extract, limulus amebocyte

lysate (LAL), and bacterial endotoxin, or with a membrane component of Gram negative bacteria can quantify bacterial endotoxins. All nanoparticle batches and samples were tested one hour prior to injecting the nanoparticle solution into the animal model during PDT treatment.

Based on our experience with testing endotoxin levels for the nanoparticle samples, bacteria growth rates are highly sensitive to both time and temperature – longer exposure to solutions after hydration and warm temperatures can exacerbate bacteria growth. To avoid growth and contamination, the nanoparticle samples were rehydrated with minimal time intervals between hydration and injection; in addition, the sample was refrigerated at all times post rehydration, with the exception of when the sample was warmed to physiological temperature prior to injection.

Cell culture

Cell culture

Rat 9L gliosarcoma cells (Brain Tumor Research Center, University of California, San Francisco, CA) were routinely maintained in Rosewell Park Memorial Institute medium (RPMI) with 400mg/L $_{D}$-glucose and 292 mg/ml $_{L}$-gluamine supplemented with 10% fetal bovine serum, 100U/ml (3%) penicillin, 1mM sodium pyruvate, and 100 μg/ml streptomycin sulfate. Cells were grown at 37^{o}C, 5% CO_2 , 95% air, and 100 % humidity environment.

Cells were plated on the 96 well plates for the MTT assay and on 35mm culture dishes with coverslip bottom, for *in vitro* PDT.

In vitro set-up

Fluence dependent PDT

To investigate the effects of PDT phototoxicity, a series of *in vitro* experiments were performed on rat 9L gliosarcoma cells. Glass cover slips were incubated with 1 mg/mL MB-loaded polyacrylamide nanoparticles (containing F3-peptide) for 1 hour, rinsed with appropriate cell media and placed in a temperature-controlled sample chamber at 37^{o}C. Methylene Blue-mediated cytotoxicity was then monitored before and after illumination by labeling the cells with 5 μL Calcein-AM and 10 μL propidium iodide (PI) fluorescent stains. Fluorescent observations of Calcein-AM (excitation: 490nm, emission: 515nm) and PI (excitation: 536nm, emission: 617nm) were monitored for 30 minutes using a Perkin Elmer Ultra View Confocal microscope system equipped with an argon-krypton laser. Irradiation with the microscope laser, illumination was performed at 671 nm, for 1 minute intervals and stopped. The live/dead assay allows for obvious distinctions of viable/cytotoxic cells. In living cells, intracellular esterase converts the non-fluorescent Calcein-AM into a green fluorescent Calcein, indicating viable cell. PI is barred by viable cells but can invade cells with damaged membranes. Upon irradiation, in a time-dependent manner, compromised cells release the green fluorescence of the Calcein-AM through damaged membranes and permit the binding of PI to their nucleic acids - emitting red fluorescence. A series of images of the cells were sequentially taken for 30 minutes, in minute intervals, using an Olympus IX-70 confocal microscope. Upon completion of treatment, the objective was switched to a lower magnification so as to show that the treatment was localized to the illumination area – showing red stained, dead cells, which are surrounded by viable, green stained cells, just outside the illuminated area. At each time interval, the survival rate was presented as a percentage of the number of viable cells divided by the total number of cells (viable and non-viable).

Furthermore separate, fluency-dependent PDT studies were performed at illumination power density of 100 mW/cm^2 and 222 mW/cm^2. Pre-exposure images were taken using a 60X objective. The cells were exposed, for a total of 30 minutes, to a 671nm red diode laser (model 671RLMH1W, Changchun Dragon Lasers Co., Ltd) with light intensity of 100 mW/cm^2 and 222 mW/cm^2. Post-exposure images were taken using a 20X objective, to observe the localized cellular damage.

In vivo set-up

Cranial window model

The animal research protocol was reviewed and approved by the University Committee on Use and Care of Animals (UCUCA) at the University of Michigan, Ann Arbor. Biparietalcraniectomies were performed on 8-week old Sprague-Dawley male rats (Charles River Laboratory, Wilmington, MA). Rats weighing between 250 to 350 g were anesthetized and placed into a stereotactic frame. Rat 9L gliosarcoma cells were harvested in monolayers and following a full craniectomy suspended in media and the cells (10^5) were injected using a syringe micro-injector (Medfusion 3500 syringe pump). The 9L cells were implanted in the forebrain at a depth of 1.5mm through a burr hole extending 1mm below the injection location to create a pocket for growth. To allow for serial inspection, a thin, round microscope cover slip was bonded to the cranial opening with cyanoacrylate glue creating a brain tumor window (BTW) model [50].

Methylene Blue nanoparticle administration

Nanoparticles were synthesized and formulated according to the previously described methods. The nanoparticles had a dye loading of 0.27% wt/(NP wt) and the dose administered is equivalent to 0.86 mg of MB/(kg of rat)..The stock solution was determined to have nominal endotoxin levels as determined by the LAL assay. Once the tumor radius reached 2-3 mm in diameter, photosensitizers in the form of free dye, or embedded within polyacrylamide nanoparticles, were administered intravenously through the right femoral vein using a programmable micro-injector (Medfusion 3500 syringe pump). After injection, rats were kept in the dark until undergoing irradiation therapy.

Laser set-up

Tumors in the BTW model were irradiated in a cross sectional manner, via the exposed tumor surface immediately beneath the window. *In vivo* light illumination was performed using a 671nm red diode laser (model 671RLMH1W, Changchun Dragon Lasers Co., Ltd) with tunable output power (0 – 1 W),to precisely expose at various fluency rates.

The size of the laser beam was controlled by using a collimator (CSMA-8-B collimator, Newport Corp) so as to accurately control the light fluence for PDT. For all experiments, a constant beam diameter of 4 mm was used, while the distance between the cranial window and the collimator was fixed at 1 inch.

Calibration of the laser was performed; it was tuned to the desired power, set to warm for 30 minutes, and then checked again using a power meter to assure stability. After observing a complete hour of consistent power the laser was cleared for PDT illumination. It was not typical

to find fluctuations in power, and it was important to assure that the laser was working at the desired standard before treatment.

Tumor size measurement

Damage to sensitized tumor and brain parenchyma by photoirradiation was observed using a Sony digital camera. Daily photographs of the cortical surface through the BTW provided an evident depiction of the tumor growth patterns prior and post PDT treatments. Tumor growth patterns were then evaluated by delineating the tumor boundaries, based on the variations of pixelated coloration and measuring the total pixelated surface area of the tumor. The *in vivo* PDT efficiency was determined by measuring tumor surface area as seen through the BTW and comparing tumor growth patterns of individual animals and animal groups.

RESULTS AND DISCUSSION

The size of the surface-modified Methylene Blue-conjugated polyacrylamide nanoparticles was measured using a particle size analyzer. The DLS data indicated that the mean diameter of the modified nanoparticles in solution was 55.0 (± 5.0) nm, Figure 1, similar to that of the unmodified nanoparticles. Thus modification of the surface by the attachment of PEG or targeting ligands had no significant effect on the size of particles in solution. These nanoparticles fall within the optimal range of 10-100nm which has proved to be very effective for *in vivo* applications. This is because nanoparticles greater than 10nm have the ability to avoid clearance by the kidney, allowing for prolonged and elevated circulatory levels, and nanoparticles smaller than 100nm avoid entrapment

by phagocytes [51-52]. Furthermore, leaky angiogenic vasculatures have fenestrations that improves the penetration phenomenon of enhanced penetration and retention (EPR) effect, allowing nanoparticles to be delivered and to accumulate in tumor tissue more readily than in the surrounding healthy tissue [41-44, 53].

The F3-modified nanoparticles have a surface charge of +12 (±1) mV, whereas the non-targeted (surface PEGylated) nanoparticles have a charge of +2 (±1) mV, in comparison to the unmodified nanoparticles that have free amine groups on the surface, having a charge of +14 (±3) mV. The non-targeted nanoparticles have a near neutral surface charge due to the presence of the neutral PEG molecules on the particle surface. However the F3-targeted Methylene Blue-conjugated polyacrylamide nanoparticles display a positive surface charge because the cationic F3-peptide on the surface of the nanoparticle has high positive charge.

The amount of dye encapsulated in the nanoparticle was determined by comparing the fluorescence and absorbance spectra of a data set of known concentrations of nanoparticles in water with precise amounts of dye in addition to nanoparticles in water. It was determined from the absorbance spectra of the covalently linked Methylene Blue polyacrylamide nanoparticles that the dye concentration in these nanoparticles was 0.27% by weight.

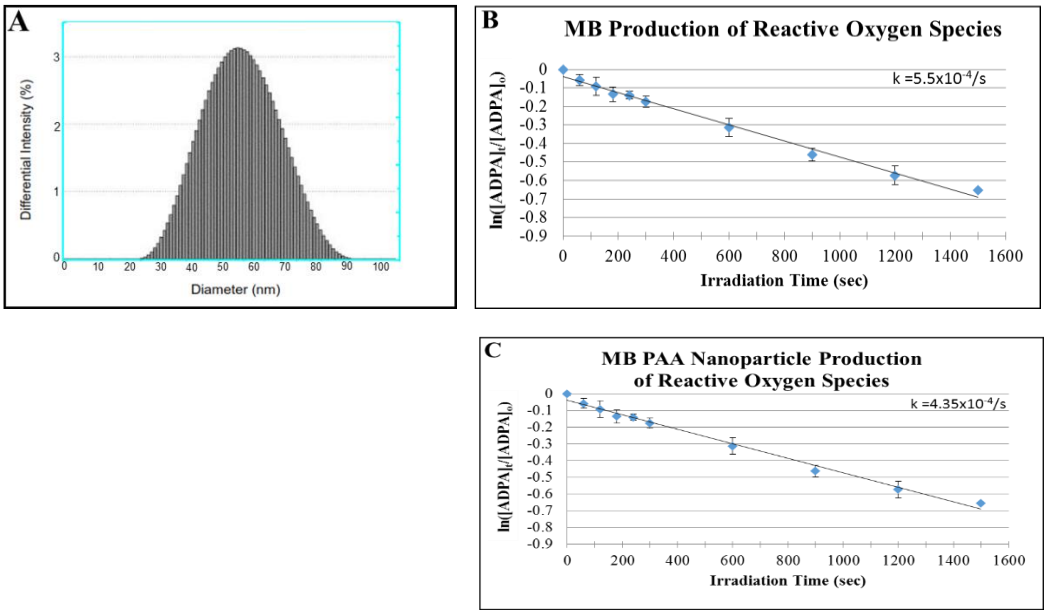

Figure 2.2: (A) Size distribution of polyacrylamide nanoparticles in solution using dynamic light scattering measurments. ROS production measurement of (B) Methylene Blue free dye in DI water and (C) Methylene Blue polyacrylamide nanoparticles. Peak excitation for Methylene Blue was found at 678 nm: linear fitted plot of fluorescence change in ADPA as a function of irradiation time.

The efficiency of photodynamic therapy depends directly on the photosensitizer's ability to produce reactive oxygen species (ROS), on the availability of molecular oxygen, on the light fluency (intensity and duration), as well as on the photosensitizer concentration at the treatment area. Figure 2.2 shows the generation of ROS of Methylene Blue dye and Methylene Blue encapsulated in nanoparticles. The ROS production rate constant was measured by the fluorescence decay of ADPA and was found to be $5.5x10^{-4}$/s for 1.0 µM free Methylene Blue dye in PBS. For Methylene Blue 0.37% wt/(NP wt) encapsulated in nanoparticles the rate constant was $4.35x10^{-4}$/s. The capability of the targeted nanoparticles to produce reactive oxygen species and kill cells was optimized through *in vitro* experiments [36]. Experiments performed *in vitro* provided a foundation of preliminary studies for the *in vivo* PDT protocols: nanoparticle delivery conditions, dose and optimal light fluence, and rudimentary glioma growth rates [36, 50].

To investigate the PDT efficiency of Methylene Blue-conjugated polyacrylamide nanoparticles in *in vitro* experiments, MTT assays were carried out under conditions of various doses of nanoparticles. F3-targeted and non-targeted nanoparticles were added with increasing concentrations for survival assessment as determined by the MTT assay. The cytotoxicity of the nanoparticles was determined by the conversion of MTT to formazan via mitochondrial oxidation. Cell survival rates showed no significant differences among cells treated with Methylene Blue polyacrylamide nanoparticles (in the dark) and the control (cells only). The average cell survival rates exhibited a higher than 97% viability, up to 1mg/ml nanoparticle concentration (Figure 2.3). Overall, the treated cells endured no detectable cytotoxicity as a result of being treated with the Methylene Blue polyacrylamide nanoparticle solution (in the dark), ensuring that viability variances in PDT experiments will not be compromised by dark toxicity produced by the nanoparticles.

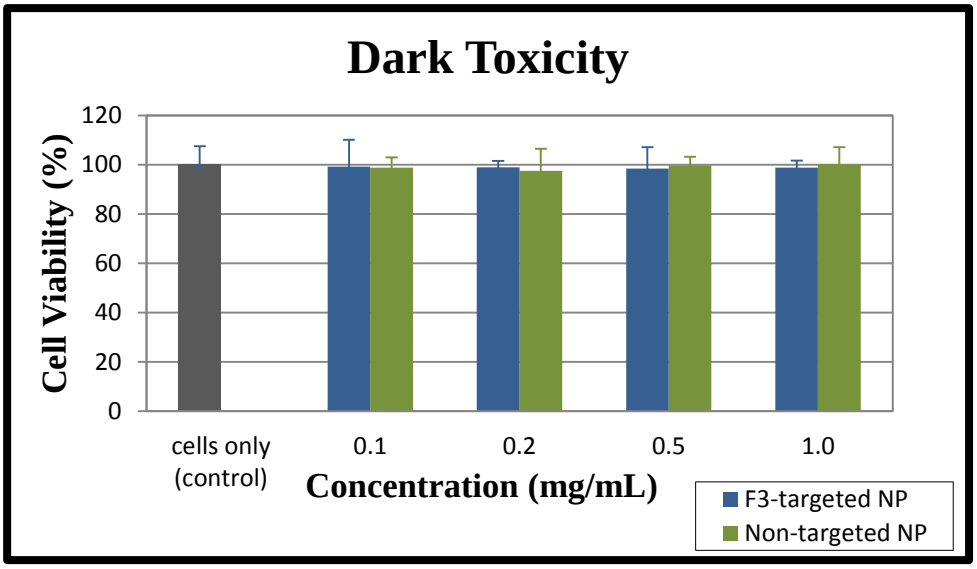

Figure 2.3: Examination of cytotoxicity using the MTT assay. Cell viability of 9L gliosarcoma, evaluated after 24 hours incubation with varying concentrations of F3-targeted and non-targeted Methylene Blue nanoparticles. Cell survival rates indicated no measurable variance between nanoparticle concentrations (0.1, 0.2, 0.5, and 1.0 mg/mL), including the cell only control group (no NPs).

To ensure that the ROS was generated as a response to light activating the dye encapsulated in the nanoparticle matrix, dye leaching needed to be examined. It is imperative to test dye leaching because photosensitizers outside the nanoparticle can interact with cellular surface proteins and organelles *in vitro*; furthermore, enzymatic degradation of the leached out Methylene Blue dye might alter the optical properties of the dye during intraoperative *in vivo* applications. In order to survey the dye leaching, the Methylene Blue content in the filtrate separated from the nanoparticles by centrifugation filtration was measured, using UV-Vis absorbance spectra. There was no detectable absorbance at 668nm, verifying negligible dye leaching of Methylene Blue out of the Methylene Blue polyacrylamide nanoparticles. This verifies that the detected reaction between the Methylene Blue dye and the ROS must occur within the nanoparticle. It also verified that covalently linking the Methylene Blue dye to the nanoparticle matrix completely eliminates dye leaching, thus ensuring the delivery of the full pay-load of photosensitizer to cells *in vitro* or to tumor sites *in vivo*.

To investigate the fluence rate dependence of PDT phototoxicity, a series of *in vitro* experiments were performed on rat 9L gliosarcoma cells. Using the optimized protocols for the live/dead assay, 9L cells were irradiated at two separate light intensities, 100 mW/cm^2 and 222 mW/cm^2, using an excitation wavelength of 671 nm. A series of images of the cells were sequentially taken over 30 minutes, in 1 minute intervals, using an Ultra-View confocal microscope (Figure 2.4).

Two experiments were carried out with the intention of examining cytotoxicity rates at different laser fluencies; their images are displayed side-by-side (100 mW/cm^2: Figure 2.4a-e; 222 mW/cm^2: Figure 2.4f-j). Before light irradiation, all cells were stained by Calcein-AM, showing green fluorescence, verifying cell viability for both experiments (Figures 2.4a, 2.4f). After 5 minutes of irradiation, the cells exposed to the greater fluence rate show the earliest indication of cell death,

by the presence of PI-stained red nuclei (Figure 2.4g) while the lesser fluence rate shows no sign of cellular death (Figure 2.4b). After completing 10 minutes of illumination, the cells exposed to the higher illumination fluence show a convincing display of cellular death (Figure 2.4h) and continuously improve in displaying cytotoxic effects throughout the 30 minute experiment (Figure 2.4j). Similarly, the lower fluence rate displayed primary signs of cell death at 10 minutes and the cellular cytotoxicity intensified between 20 and 30 minutes of illumination (Figures 2.4d, 2.4e).

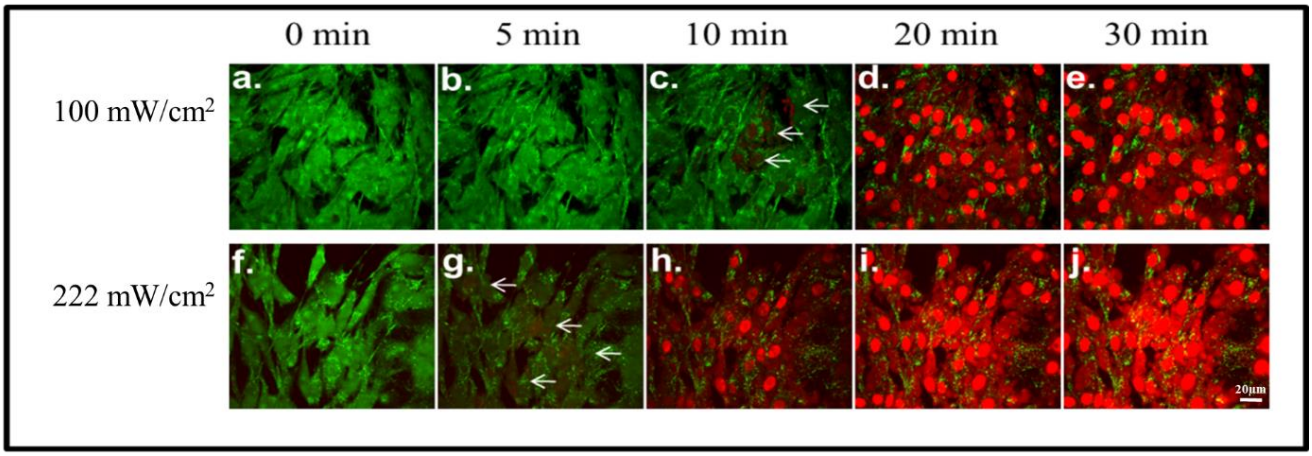

Figure 2.4: Confocal images of 9L cell lines treated with Methylene Blue-conjugated PAA nanoparticles. Intensity dependent cytotoxicity, induced by F3-targted Methylene Blue PAA nanoparticles and laser irradiation. The 9L gliosarcoma cells were incubated with Methylene Blue nanoparticles and irradiated with fluencies of 100 mW/cm^2 and 222 mW/cm^2. Images were taken (a) before light exposure; (b-e) over 30 min of light exposure at a dose of 100 mW/cm^2. Images were taken (f) before light exposure; (g-j) over 30 min light exposure at a dose of 222 mW/cm^2. Cytotoxicity was monitored by labeling the cells with Calcein-AM (green, for viable cells) and propidium iodide (red, for dead cells). Measurements taken on a confocal microscope.

Although the composite confocal images may seem to qualitatively display similar cytotoxic abilities for both experiments, a quantitative analysis displayed a more refined picture of cytotoxicity on the treated cells (Figure 2.5). This cell viability experiment indicates that a higher

fluence rate of laser light has the ability to achieve a faster rate of cellular cytotoxicity, however nearly all cells were killed after 15 min of irradiation with the above given dose.

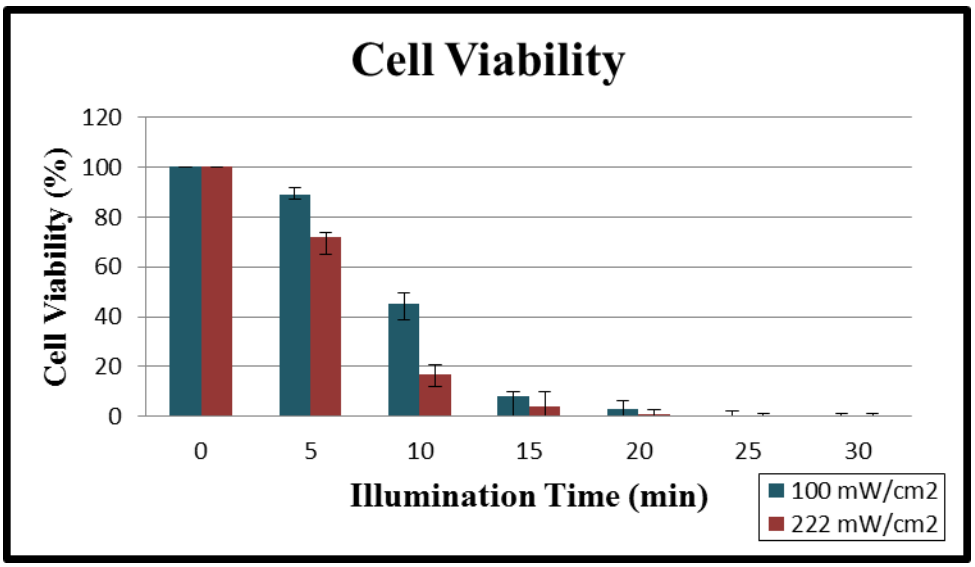

Figure 2.5: Cell viability assessment for the phototoxic effects of F3-targeted Methylene Blue polyacrylamide nanoparticles on a 9L cell line. Fluency dependent PDT efficiency at light doses of 100 mW/cm^2 and 222 mW/cm^2, over the course of 30 minutes of illumination. Cells exposed to a higher fluency responded with a more rapid cellular death than for a lower fluency.

From the above, one observes that cells exposed to a higher fluence rate display a significantly increased rate of cellular damage, which is induced within a shorter time frame, this was all signified by a rapid release of Calcein-AM (green) through the compromised cellular membrane allowing for the incorporation of PI (red) into the nucleus. These results demonstrate the light-dose dependency of PDT cytotoxicity, thus indicating that further optimization of the exposure time and fluence rate could better enhance the PDT efficacy.

Activation of the photosensitizer in the presence of oxygen is highly cytotoxic, however the short lifetimes (<0.04μs) and the short diffusion distances (<0.02μm) of the ROS allows the treatment

to be restricted to the nearby cells, tissue and vasculature where the illuminated photosensitizers are present [54]. To further demonstrate the localization and specificity achieved using this localized PDT therapy, a small section of the cells were irradiated using a 60X objective and then the images were captured post-irradiation, using a lower magnification objective, with the irradiated area on the right side of the image (Figures 2.6c, 2.6f). The focused illumination induced cell death only to the cells within proximity to the laser beam; whereas adjacent cells, containing methylene blue nanoparticles but not irradiated, display no detectable loss of membrane integrity, as indicated by their green fluorescence. In addition to these localization tests, cells not treated with Methylene Blue-linked polyacrylamide nanoparticle showed no detectable cytotoxicity when exposed to laser irradiation for 30 minutes, at varying fluence rates, suggesting that solely illuminating the cells is not cytotoxic to these cancer cells.

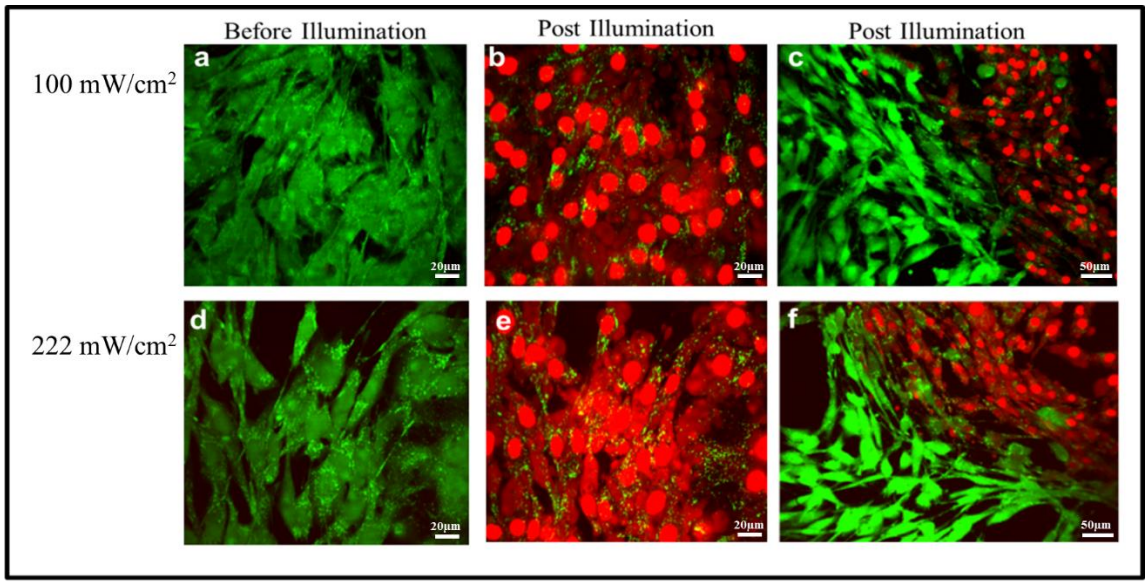

Figure 2.6: Confocal images of 9L cell lines treated with Methylene Blue-conjugated PAA nanoparticles, before and after laser illumination. Cell viability was monitored by labeling cells with Calcein-AM (green, viable cells) and propidium iodide (red, dead cells). Images were taken before illumination at 60X magnification. Post-illumination images were taken at a lower magnification to illustrate that cellular death merely occurred in the area exposed to laser irradiation.

When performing localized PDT *in vivo*, the efficacy of singlet oxygen generation and tumor eradication is directly proportional to the intratumoral concentration of the nanoparticle containing the photosensitizing agent. In order to improve therapeutic efficacy of this treatment it is imperative to understand the kinetics of the targeted nanoparticle, more specifically the incubation time needed to permit the highest concentration of NP at a specific site. Transvascular transport and accumulation of the nanoparticles within the glioma domain can be confirmed *in vivo* through delineation experiments. By performing intravital staining experiments using contrast dye containing nanoparticles for delineation of the implanted neoplasm, direct observation of color variations following the intravenous injection of dye enhanced polyacrylamide nanoparticles can be visualized through the rat cranial window model. Subsequently, this visualization will quantify of the optimal irradiation time, i.e. the incubation time with greatest accumulation of nanoparticles.

Brain tumor margins are poorly defined when looking through the BTW model. In previous studies, our group performed tumor delineation studies using Coomassie Brilliant Blue (CB) loaded polyacrylamide nanoparticles [55]. Coomassie Blue is an intensely blue colored dye agent and when covalently linked to the polyacrylamide nanoparticles it can be used as a color contrast agent to aid in intraoperative tumor margin delineation. After intravenous injection of the Coomassie Blue polyacrylamide nanoparticles into each rat's femoral vein, the amount of nanoparticles bound to the glioma tissue can be monitored *in vivo*, on a microscopic level, through the rat cranial window model. A quantitative evaluation of tumor delineation resulting from free Coomassie Blue dye, non-targeted CB-linked nanoparticles, and F3-targeted CB-linked nanoparticles was performed using a Coomassie Blue dose of 35mg/kg (NP dose was 500mg/kg). Each treatment resulted in rapid brain tumor delineation, with a more significant color contrast

resulting from the use of nanoparticles – a better defined tumor area and strong visual contrast over longer time durations.

This delineation study performed by the Kopelman group is applicable to determining the optimal times between the administration of the drug (Methylene Blue, in the form of free dye and encapsulated in nanoparticles) and the illumination time. Determining peak accumulation of Coomassie Blue nanoparticles within the brain tumor tissue will give insight as to the possible biodistribution of Methylene Blue nanoparticles in the tumor tissue when used for PDT treatment. The Coomassie Blue delineation study revealed peak accumulation of Coomassie Blue free dye at 30 minutes, *vs.* 120 minutes for non-targeted CB-linked NP-treated animals, while the color contrast for the F3-targeted Coomassie Blue nanoparticles continued to intensify throughout the end of the six-hour experiment. The contrast intensification over time induced by F3-targeted nanoparticles, compared to non-targeted NPs, may be due to the active targeting of the F3-peptide, i.e. their interactions with the nucleolin receptors which are highly expressed on 9L glioma cells and on the angiogenic vasculature [50-51]

When the brain tumor radius reached 3 mm in diameter, photosensitizers in the form of free dye and embedded within polyacrylamide nanoparticles were administered intravenously via the femoral vein. The Methylene Blue-conjugated nanoparticles were administered at a dose of 300 mg/kg, which corresponds to a dose of 0.86 mg MB/kg. This dose has proved to be safe in accordance with previous nanoparticle optimization and toxicology studies [50, 55]. The time interval between nanoparticle administration and light illumination was set at 105 minutes, based on previous incubation studies investigating nanoparticle accumulation at the treatment location and the light dose was fixed at 180 J/cm^2 [50]. To monitor tumor growth patterns, daily

photographs of the cortical surface through the BTW on the rat model, prior and post PDT treatments, were taken (Figure 2.7).

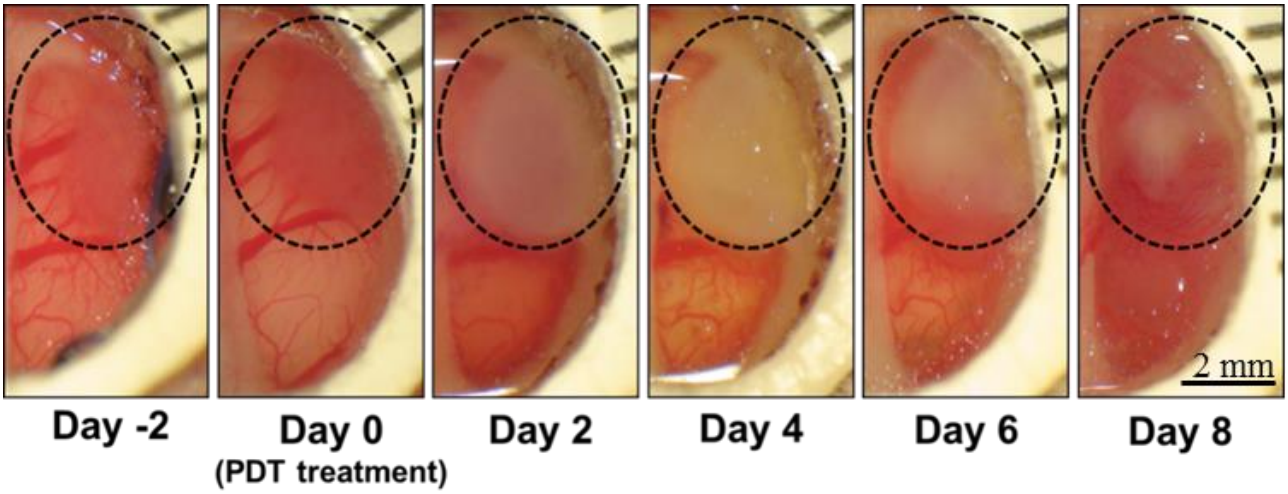

Figure 2.7: A series of cranial window pictures of a rat with an implanted 9L glioma, before and after the PDT, using F3-Methylene Blue polyacrylamide nanoparticles and a time interval of 105min between nanoparticle injection and light illumination. The dotted circle encloses the tumor area in each picture.

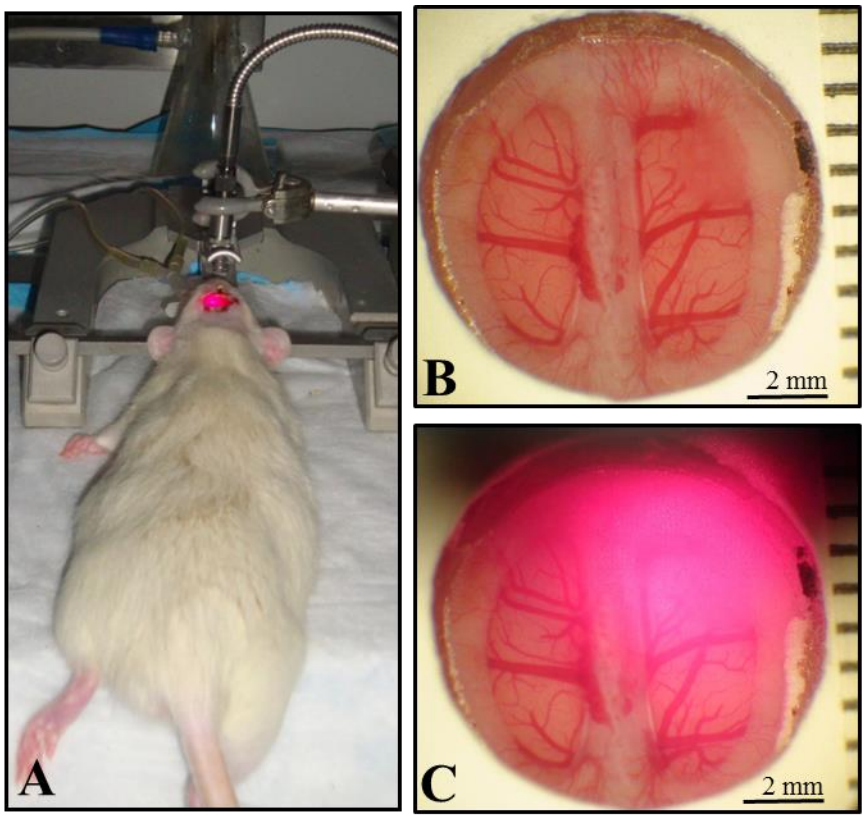

Figure 2.8: (A) Photograph displaying therapy setup. Rats with BTW are positioned in sterotactic frames with distance between cranial window and laser collimator fixed at 1 inch. Photographs of a tumor as seen through the BTW (B) before therapy and (C) during irradiation with a 671nm laser.

Systemic incubation times of 105 minutes and 24 hours were selected to further explore the consequence of incubation time on the PDT effects on tumor growth patterns. The goal of this work was to establish defined incubation conditions for use of future PDT experiments and optimize predictive functions of the treatment. Incubation times were chosen based on the Coomassie Blue delineation studies performed by the Sagher and Kopelman groups, concluding maximal accumulation of both targeted and non-targeted nanoparticles occurring at 120 minutes post-injection [50]. To guarantee light exposure during the greatest accumulation of nanoparticles within the brain tumor, laser illumination started at 105 minutes post-nanoparticle injection and

preceded for 30 minutes – ensuring irradiation occurred 15 minutes before and after the optimal irradiation window. The time interval of 24 hours between nanoparticle administration and light illumination was based on previous studies using HPPH post-loaded polyacrylamide nanoparticles on mice bearing Colon26 tumors [56].

The tumor growth curve (Figure 2.9) demonstrates that for equivalent protocols with varying incubation times, the PDT protocol with 105 minute incubation was more effective at inducing phototoxicity than the one with 24 hrs. Retardation in tumor growth was evident six days post-treatment and significantly noticeable differences in tumor size was seen through day ten. Thus, irradiation performed at 105 minute post-drug injection resulted in a more favorable treatment outcome when compared to the 24 hour incubation.

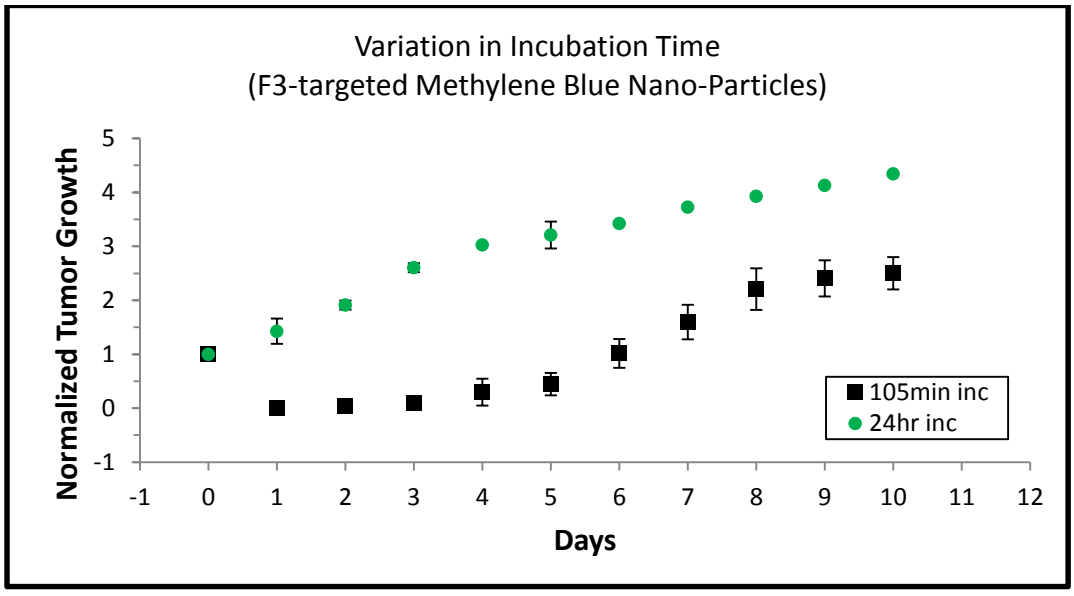

Figure 2.9: Incubation time dependent effects of photodynamic therapy treatment. F3-targeted Methylene Blue polyacrylamide nanoparticles were intravenously injected, and once completing 105 minutes or 24 hours of systemic incubation, the tumors were irradiated at 180 J/cm^2 through the BTW and observed daily.

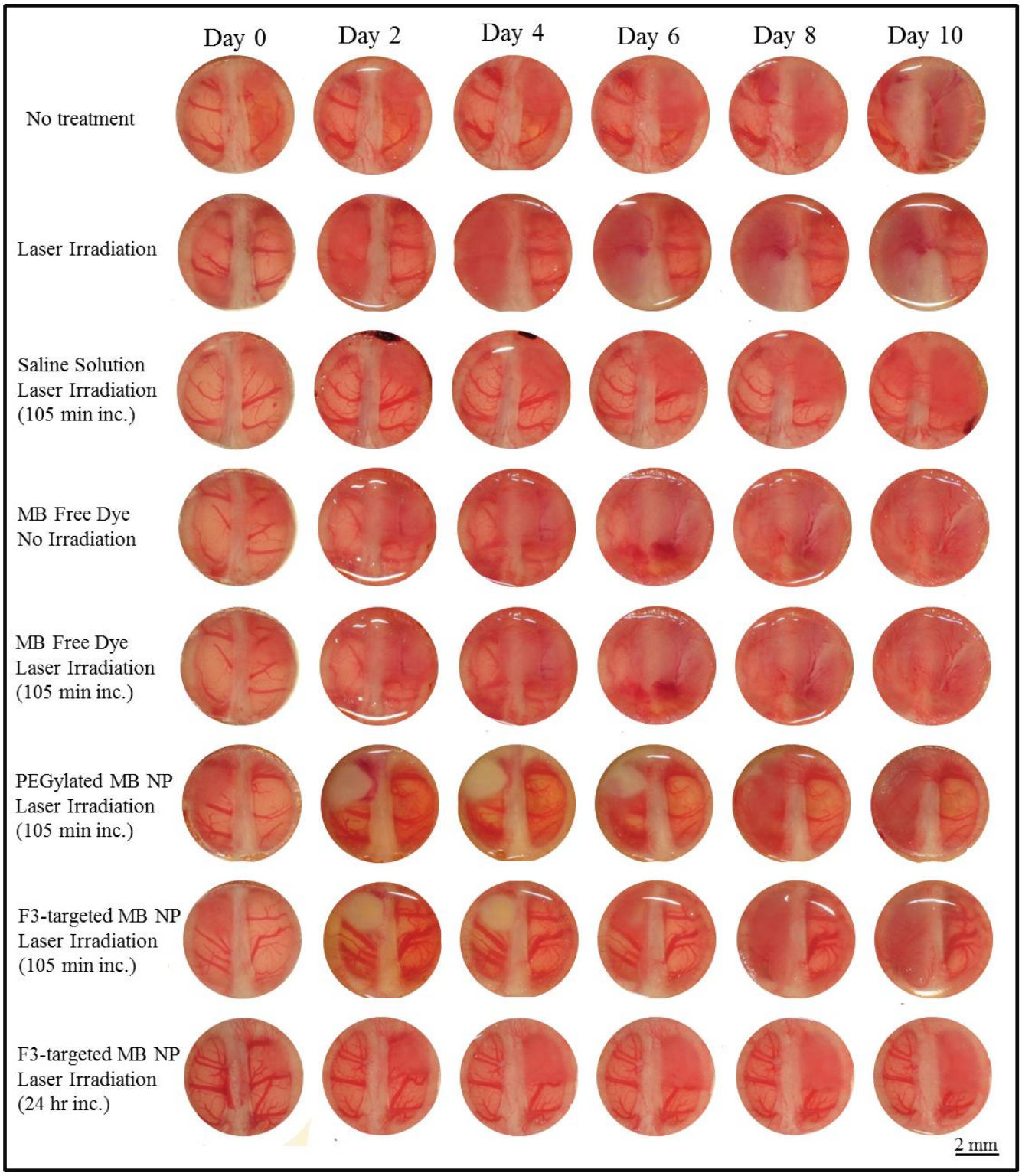

Figure 2.10: Daily photographs of the cortical surface depict tumor growth, images taken through brain tumor windows on rat models. Animals groups receiving irradiation experienced a fluence dose of 180 J/cm^2 using 671 nm laser.

Evaluation of the effects of each treatments group on the tumor growth patterns was accomplished and is presented in Figure 2.10. Control animals were not injected with photosensitizer, nor were they exposed to laser light; this group was purely acting as a control group for determining tumor growth patterns post tumor implantation surgery. Animals treated with laser illumination and free photosensitizer were dosed with 0.86 mg/kg of the Methylene Blue free dye and the effect on tumor tissue was assessed after 105 minutes of systemic incubation of the nanoparticles and irradiating animals with laser light (180 J/cm^2). The time course for incubation was empirically determined using tumor delineation results acquired by the Sagher and Kopelman groups and Figure 2.9 [50, 55].

As expected, the PDT treatment with Methylene Blue free dye did not affect the tumor growth when compared to the control group. This was probably due to the ability of enzymes to reduce free Methylene Blue to the photochemically-inactive form of Leuko-Methylene Blue, resulting in the loss of photodynamic activity. To study the difference in nanoparticle circulation and accumulation between targeted and non-targeted Methylene Blue nanoparticles, animals were injected with 0.86 mg/kg of the particles with dye loading of 0.37% wt/(NP wt). After the completion of nanoparticle administration, systemic incubation time of 105 minutes was followed by laser light irradiation with fluence rate of 180 J/cm^2.

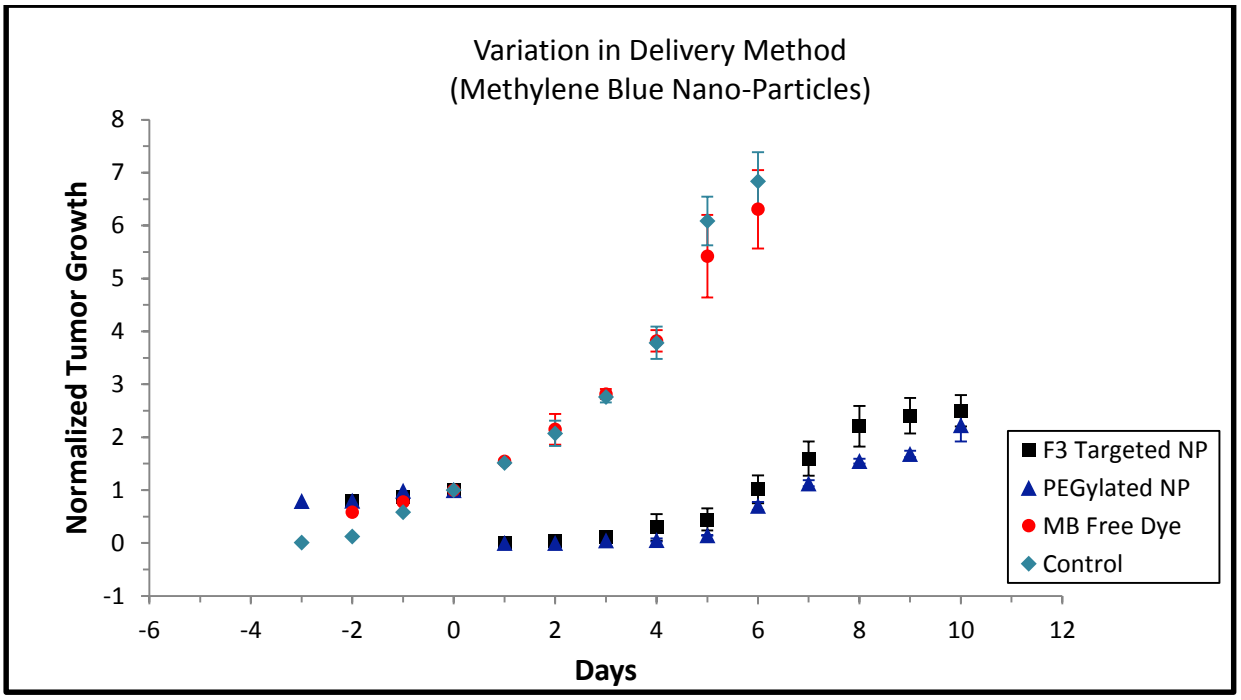

Figure 2.11: Effect of PDT treatment delivered 105 minutes after injection of Methylene Blue F3-targeted nanoparticles, Methylene Blue PEGylated nanoparticles and Methylene Blue free dye. The control animal was not administered with photosensitizer or exposed to the laser illumination. Another control animal group treated with light illumination showed the same tumor growth trend as the "no treatment" control animal group.

Overall there were significant statistical differences in median tumor size between the control and Methylene Blue free dye treatment, versus that by Methylene Blue polyacrylamide nanoparticles, whether F3-targeted or non-targeted. When treating the tumors with Methylene Blue polyacrylamide nanoparticles there is a significant arrest of tumor growth. However, the insignificant differences between the two delivery methods, F3-targeted and PEGylated verses PEGylated, signifies the use of F3-peptide did not significantly improve the PDT outcome. The similar growth trends of the targeted and non-targeted PEG polyacrylamide nanoparticles confirm that our particles effectively accumulated in the tumor sites via passive targeting of EPR as well. This clearly demonstrates the advantages of NP-based PDT agents. We also notice that the tumor growth was retarded for a period of time but continued to progress for all groups, including the

animals treated with PEGylated Methylene Blue polyacrylamide nanoparticles. This is probably because the tumor was illuminated from only one direction, i.e. through the cranial window, due to constraints imposed by the BTW. However in a clinical setting, where light can be directed at all angles for intra-operative PDT, we may expect a significantly higher efficacy.

Tumor growth patterns were calculated by measuring the surface area of the tumor tissue as seen through the BTW. Surface area dimensions were taken by quantifying tumor tissue remaining post-irradiation and normalizing to the tumor area measured on PDT-treatment day (day 0). Post-treatment areas of necrotic tissue were recorded, though not included in those data sets; however this subsequent outcome of treatment proves important in the evaluation of treatment success.

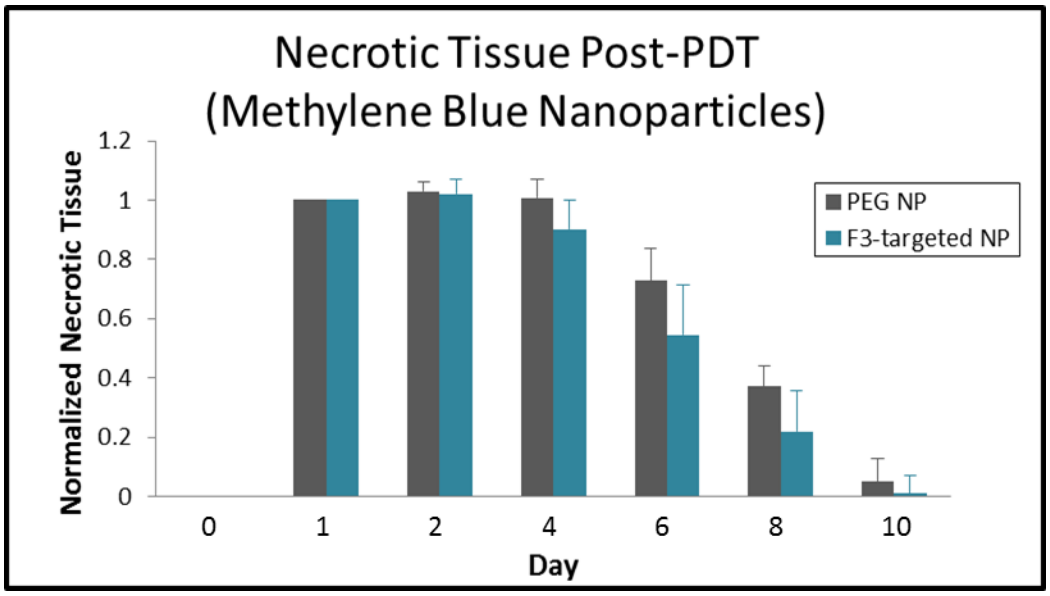

Figure 2.12: Post-PDT treatment necrotic tissue measurements for tumors treated with F3-targeted Methylene Blue polyacrylamide nanoparticles verses non-targeted (PEGylated) Methylene Blue nanoparticles. Both treatment groups express similar necrotic formation and regression patterns with a greater formation of necrotic tissue for non-targeted Methylene Blue nanoparticles.

Figure 2.12 compares the surface area measurements of necrotic tissue for F3-targeted and non-targeted Methylene Blue polyacrylamide nanoparticles. The day of treatment and one day post-

treatment showed no detectable traces of necrosis, however outstanding amounts of necrotic tissue appeared two days post-treatment and dissipated through day six as the necrotic tissue was no longer visible due to microglia and astrocytes (glial cells) removing the damaged tissue in addition to tumor tissue regrowth.

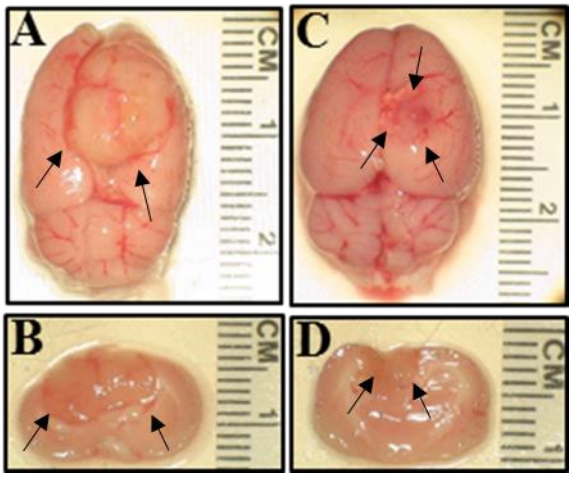

Figure 2.13: Gross specimen from animal model, excised 10 days post-PDT therapy. Representation of brain tumor for animal groups (A,B) without photosensitizer or laser illumination, and (C,D) animals receiving non-targeted Methylene Blue nanoparticles (105 minute incubation time) with irradiation fluence dose of 180 J/cm^2 using a 671 nm laser.

Optical penetration depth in tissue is the distance through which the radiant power decreases to 1/e or 37% of its initial value [57]. Beyond this depth, tissue is exposed to laser light of a lower intensity, which still may be adequate for PDT. Methylene Blue dye has a long absorption wavelength (λ_{max} = 670 nm) allowing for good penetration depth of laser light in live tissues, however the penetration of light through the tumor is dependent on the characteristics of the treated tissue. Laser light at 631 nm can achieve a penetration depth of 1.5 ± 0.43mm in brain tissue and 2.9 ± 1.5mm in brain tumor tissue [58]. The rat models used in these experiments contained tumor implants extending into the cortex – a depth which may exceed the penetration depth achievable by our 671 nm laser. This limitation resulted in incomplete eradication of the base of the tumor,

resulting in detectable growth patterns days after treatment. However, PDT is still expected to be effectively applied as a post-surgical adjunctive treatment because the microscopic residual tumor tissue is within effective range.

CONCLUSIONS

Our group demonstrated effective eradication of 9L glioma cells using both targeted and non-targeted nanoparticles. The nanoparticles encapsulated the Methylene Blue photosensitizer in a hydrogel matrix with an average size of 55 nm, containing approximately 0.27% dye by weight. These photosensitive nanoparticles proved suitable for the eradication of 9L glioma both *in vitro* and *in vivo*. Visual observations through the BTW model allowed for serial inspection and efficacy of various treatment protocols investigating photosensitizer delivery and incubation time between nanoparticle administration and laser treatment. Quantitative tumorigenic responses and growth patterns presented a more favorable treatment outcome for animals receiving treatment 105 minutes after nanoparticle administration, over the animals receiving a 24 hour incubation time. When investigating photosensitizer delivery methods, both the targeted and non-targeted Methylene Blue nanoparticles had comparable necrotic development and delays in tumor progression post-treatment. With substantial improvements in tumor response to treatment over control groups, advantages of nanoparticle-based PDT agents prove advantageous for the eradication of local tumors.

Such photoreactive nanoparticles have the potential to be used for photodynamic therapy as an aid to neurosurgery. The dye-loaded nanoparticle, administered just prior to surgery would help eradicate residual tumor after maximal resection, thereby minimizing the need for adjuvant

therapy. Such a novel approach has the potential to advance surgical and adjuvant therapy towards a major breakthrough in the treatment of brain tumors. We believe this method can efficiently and rapidly eradicate local tumors, lead to the eventual palliation of advanced disease or result in the cure of early disease [59].

(This chapter was written with the intent of future publication)

ACKNOWLEDGEMENTS

We thank Dr Hoe Jin Hah and Dr Gwangseong Kim for their informative discussions and assistance during nanoparticle synthesis and F3-peptide conjugation. Dr Oren Sagher, Dr Daniel Orringer, and Mr Dah-Luen Huang for the development of the BTW model and their theachings of animal behavior and protocol. Kristen A. Simmer acknowledges funding support from the University of Michigan Rackham Graduate School Merit Fellowship. The authors also acknowledge NIH grant R01EB007977 (RK) for research funding.

REFERENCES

[1] Sharman, Wesley M., Cynthia M. Allen, and Johan E. Van Lier. "Photodynamic therapeutics: basic principles and clinical applications." *Drug discovery today*4.11 (1999): 507-517.

[2] Pushpan, S. K., et al. "Porphyrins in photodynamic therapy-a search for ideal photosensitizers." *Current Medicinal Chemistry-Anti-Cancer Agents* 2.2 (2002): 187-207.

[3] Mellish, Kirste J., et al. "In Vitro Photodynamic Activity of a Series of Methylene Blue Analogues." *Photochemistry and photobiology* 75.4 (2002): 392-397.

[4] Orth, K., et al. "Intraluminal treatment of inoperable oesophageal tumours by intralesional photodynamic therapy with methylene blue." *The Lancet* 345.8948 (1995): 519-520.

[5] DeRosa, Maria C., and Robert J. Crutchley. "Photosensitized singlet oxygen and its applications." *Coordination Chemistry Reviews* 233 (2002): 351-371.

[6] Hopper, Colin. "Photodynamic therapy: a clinical reality in the treatment of cancer." *The lancet oncology* 1.4 (2000): 212-219.

[7] Redmond, Robert W., and Janet N. Gamlin. "A compilation of singlet oxygen yields from biologically relevant molecules." *Photochemistry and photobiology*70.4 (1999): 391-475.

[8] Severino, Divinomar, et al. "Influence of Negatively Charged Interfaces on the Ground and Excited State Properties of Methylene Blue." *Photochemistry and photobiology* 77.5 (2003): 459-468.

[9] Junqueira, Helena C., et al. "Modulation of methylene blue photochemical properties based on adsorption at aqueous micelle interfaces." *Physical Chemistry Chemical Physics* 4.11 (2002): 2320-2328.

[10] Tuite, Eimer M., and John M. Kelly. "New trends in photobiology: photochemical interactions of methylene blue and analogues with DNA and other biological substrates." *Journal of Photochemistry and Photobiology B: Biology* 21.2 (1993): 103-124.

[11] Ball, Denise J., et al. "The induction of apoptosis by a positively charged methylene blue derivative." *Journal of Photochemistry and Photobiology B: Biology* 42.2 (1998): 159-163.

[12] Wainwright, Mark, et al. "Increased cytotoxicity and phototoxicity in the methylene blue series via chromophore methylation." *Journal of Photochemistry and Photobiology B: Biology* 40.3 (1997): 233-239.

[13] Jockusch, Steffen, et al. "Photo-induced inactivation of viruses: adsorption of methylene blue, thionine, and thiopyronine on Qbeta bacteriophage."*Proceedings of the National Academy of Sciences* 93.15 (1996): 7446-7451.

[14] Wainwright, Mark. "Non-porphyrin photosensitizers in biomedicine." *Chem. Soc. Rev.* 25.5 (1996): 351-359.

[15] Wainwright, M., and K. B. Crossley. "Methylene blue-a therapeutic dye for all seasons?." *Journal of chemotherapy* 14.5 (2002): 431-443.

[16] Moldenhauer Brooks, Matilda. "Methylene blue as an antidote for cyanide and carbon monoxide poisoning." *The Scientific Monthly* 43 (1936): 585-586.

[17] Schirmer, R. Heiner, et al. "Methylene blue as an antimalarial agent." *Redox report* 8.5 (2003): 272-275.

[18] Guttmann, P. and P. Ehrlich. "Über die Wirkung des Methylenblaubei Malaria" (On the effect of methylene blue on malaria). *Berliner KlinischeWochenschrift,* 28 (1891): 953-956.

[19] Medina, David X., Antonella Caccamo, and Salvatore Oddo. "Methylene blue reduces Aβ levels and rescues early cognitive deficit by increasing proteasome activity." *Brain Pathology* 21.2 (2011): 140-149.

[20] Wischik, C. M., et al. "Selective inhibition of Alzheimer disease-like tau aggregation by phenothiazines." *Proceedings of the National Academy of Sciences* 93.20 (1996): 11213-11218.

[21] Bellin, Judith S., Steven C. Mohos, and Gerald Oster. "Dye-sensitized photoinactivation of tumor cells in vitro." *Cancer research* 21.10 (1961): 1365-1371.

[22] Orth, K., et al. "Methylene blue mediated photodynamic therapy in experimental colorectal tumors in mice." *Journal of Photochemistry and Photobiology B: Biology* 57.2 (2000): 186-192.

[23] Williams, J. L., et al. "Methylene blue and the photodynamic therapy of superficial bladder cancer." *Journal of Photochemistry and Photobiology B: Biology* 4.2 (1989): 229-232.

[24] Orth, K., et al. "Photochemotherapy of experimental colonic tumours with intra-tumorally applied methylene blue." *Langenbeck's Archives of Surgery* 383.3-4 (1998): 276-281.

[25] Dalla, Via L., and Magno S. Marciani. "Photochemotherapy in the treatment of cancer." *Current medicinal chemistry* 8.12 (2001): 1405-1418.

[26] Tardivo, J. P., et al. "Treatment of melanoma lesions using methylene blue and RL50 light source." *Photodiagnosis and Photodynamic Therapy* 1.4 (2004): 345-346.

[27] Tardivo, João P., et al. "New photodynamic therapy protocol to treat AIDS-related Kaposi's sarcoma." *Photomedicine and Laser Therapy* 24.4 (2006): 528-531.

[28] Photodynamic Therapy Associated with Full-mouth Ultrasonic Debridement in the Treatment of Severe Chronic Periodontitis. In *ClinicalTrials.gov [Internet]*. *Bethesda (MD): National Library of Medicine (US)*; EscolaBahiana de Medicina e SaudePublica. Available online: http://clinicaltrials.gov/show/NCT01535690 NLM Identifier: NCT01535690 (accessed on 3 January 2013).

[29] Gabrieli, D., et al. "Methylene blue aggregation in liver mouse mitochondria."*Photochem Photobiol* 79 (2004): 227-32.

[30] Leonard, Kristi A., et al. "Synthesis and evaluation of chalcogenopyrylium dyes as potential sensitizers for the photodynamic therapy of cancer." *Journal of medicinal chemistry* 42.19 (1999): 3953-3964.

[31] Yao, Junlan, and Guo-Jiang Zhang. "Loss of lysosomal integrity caused by the decrease of proton translocation in methylene blue-mediated photosensitization." *Biochimica et Biophysica Acta (BBA)-Biomembranes*1284.1 (1996): 35-40.

[32] Zhang, Lei Z., and Guo-Qing Tang. "The binding properties of photosensitizer methylene blue to herring sperm DNA: a spectroscopic study." *Journal of Photochemistry and Photobiology B: Biology* 74.2 (2004): 119-125.

[33] May, James M., Zhi-chao Qu, and Charles E. Cobb. "Reduction and uptake of methylene blue by human erythrocytes." *American Journal of Physiology-Cell Physiology* 286.6 (2004): C1390-C1398.

[34] Bongard, R. D., et al. "Reduction of thiazine dyes by bovine pulmonary arterial endothelial cells in culture." *American Journal of Physiology-Lung Cellular and Molecular Physiology* 269.1 (1995): L78-L84.

[35] Merker, MARILYN P., et al. "Pulmonary endothelial thiazine uptake: separation of cell surface reduction from intracellular reoxidation." *American Journal of Physiology-Lung Cellular and Molecular Physiology* 272.4 (1997): L673-L680.

[36] Hah, Hoe Jin, et al. "Methylene Blue-Conjugated Hydrogel Nanoparticles and Tumor-Cell Targeted Photodynamic Therapy." *Macromolecular bioscience* 11.1 (2011): 90-99.

[37] Moffat, Bradford A., et al. "A novel polyacrylamide magnetic nanoparticle contrast agent for molecular imaging using MRI." *Molecular imaging* 2.4 (2003).

[38] Weissleder, Ralph, et al. "MR lymphography: study of a high-efficiency lymphotrophic agent." *Radiology* 191.1 (1994): 225-230.

[39] Moghimi, S. Moein, A. Christy Hunter, and J. Clifford Murray. "Long-circulating and target-specific nanoparticles: theory to practice." *Pharmacological reviews*53.2 (2001): 283-318..

[40] Moghimi, S. M., and B. Bonnemain. "Subcutaneous and intravenous delivery of diagnostic agents to the lymphatic system: applications in lymphoscintigraphy and indirect lymphography." *Advanced drug delivery reviews* 37.1 (1999): 295-312.

[41] Maeda, H., et al. "Tumor vascular permeability and the EPR effect in macromolecular therapeutics: a review." *Journal of controlled release* 65.1 (2000): 271-284.

[42] Matsumura, Yasuhiro, and Hiroshi Maeda. "A new concept for macromolecular therapeutics in cancer chemotherapy: mechanism of tumoritropic accumulation of proteins and the antitumor agent smancs." *Cancer research* 46.12 Part 1 (1986): 6387-6392.

[43] Maeda, Hiroshi. "The enhanced permeability and retention (EPR) effect in tumor vasculature: the key role of tumor-selective macromolecular drug targeting."*Advances in enzyme regulation* 41.1 (2001): 189-207.

[44] Henderson, Barbara W., and Thomas J. Dougherty. "How does photodynamic therapy work?." *Photochemistry and photobiology* 55.1 (1992): 145-157.

[45] Koo, Yong-Eun Lee, et al. "Brain cancer diagnosis and therapy with nanoplatforms." *Advanced drug delivery reviews* 58.14 (2006): 1556-1577.

[46] Reddy, G. Ramachandra, et al. "Vascular targeted nanoparticles for imaging and treatment of brain tumors." *Clinical Cancer Research* 12.22 (2006): 6677-6686.

[47] Moreno, Maria João, et al. "Production of singlet oxygen by Ru(dpp(S03) & incorporated in polyacrylamide PEBBLES." *Sensors and Actuators B: Chemical* 90.1 (2003): 82-89.

[48] Yan, Fei, and Raoul Kopelman. "The Embedding of Meta-tetra (Hydroxyphenyl)-Chlorin into Silica Nanoparticle Platforms for Photodynamic Therapy and Their Singlet Oxygen Production and pH-dependent Optical Properties."*Photochemistry and photobiology* 78.6 (2003): 587-591.

[49] "Supporting Your Micro QC Requirements." *Endotoxin Detection and Microbial Identification*. N.p., n.d. Web, < http://www.criver.com>. , 7 Jan. 2014.

[50] Orringer, Daniel A., et al. "The brain tumor window model: a combined cranial window and implanted glioma model for evaluating intraoperative contrast agents." *Neurosurgery* 66.4 (2010): 736-743.

[51] Vinogradov, Serguei V., Tatiana K. Bronich, and Alexander V. Kabanov. "Nanosized cationic hydrogels for drug delivery: preparation, properties and interactions with cells." *Advanced drug delivery reviews* 54.1 (2002): 135-147.

[52] Davis, Mark E., and Dong M. Shin. "Nanoparticle therapeutics: an emerging treatment modality for cancer." *Nature Reviews Drug Discovery* 7.9 (2008): 771-782.

[53] Maeda, H., G. Y. Bharate, and J. Daruwalla. "Polymeric drugs for efficient tumor-targeted drug delivery based on EPR-effect." *European Journal of Pharmaceutics and Biopharmaceutics* 71.3 (2009): 409-419.

[54] Moan, Johan, and Kristian Berg. "The photodegradation of porphyrins in cells can be used to estimate the lifetime of singlet oxygen." *Photochemistry and photobiology* 53.4 (1991): 549-553.

[55] Nie, Guochao, et al. "Hydrogel nanoparticles with covalently linked coomassie blue for brain tumor delineation visible to the surgeon." *Small* 8.6 (2012): 884-891.

[56] Wang, Shouyan, et al. "Novel methods to incorporate photosensitizers into nanocarriers for cancer treatment by photodynamic therapy." *Lasers in surgery and medicine* 43.7 (2011): 686-695.

[57] Dougherty, T. J., KR, and Weishaupt, and D. G. Boyle. "Photodynamic sensitizers." *Cancer: principles and practice of oncology* 2 (1985): 2272-2279.

[58] Muller, Paul J., and Brian C. Wilson. "Photodynamic therapy of malignant primary brain tumours: clinical effects, postoperative ICP, and light penetration of the brain." *Photochemistry and photobiology* 46.5 (1987): 929-935.

[59] Dougherty, Thomas J., et al. "Photodynamic therapy." *Journal of the National Cancer Institute* 90.12 (1998): 889-905.

CHAPTER 3

Evaluating the Effect of HPPH Mediated Photodynamic Therapy for Arresting Glioma

INTRODUCTION

While the disease is well-localized and neoplastic growths are small, highly localized therapies have the potential advantage of reduced adverse side-effects and nominal damage to surrounding tissue, nerves, and major blood vessels – not a routine feature of systematic chemotherapy or invasive surgery [1-3]. An example of a localized therapy harnessing these benefits is photodynamic therapy (PDT). PDT is a minimally invasive treatment that involves the activation of a photosensitizer by light of a specific wavelength that generates cytotoxic reactive oxygen species, ensuing in direct destruction of tumor cells [4]. It has been proven to be an effective localized treatment for a range of solid tumors and has demonstrated anti-tumor responses [5-9].

Depending on the region in which one is performing PDT, photosensistizers can be administered topically, intraperitoneally, or intravenously – the latter being required for the treatment of tumors situated in the brain [10-11]. Following the localization of nanoparticles in the treatment region, irradiation at wavelengths specific to the photosensitizer generates reactive oxygen species, which are cytotoxic to surrounding tumor cells [4]. In addition to dependence on the local level of molecular oxygen, the biological effects of PDT are directly correlated to the dynamic interaction between the laser light and the photosensitizer. A requirement for an ideal photosensitizer intended

for the treatment of cerebral tumors is that it should exhibit strong absorption in the therapeutic window (600-900 nm). Light at this wavelength can effectively penetrate tumor tissue in order to eradicate dysplastic cells undergoing therapy [12]. The photosensitizer should also have the following characteristics: systemically non-toxic in the dark, chemical purity, maximal efficiency of tumor selectivity, high photochemical ability, and being rapidly excreted from systemic tissue to avoid post-treatment photosensitivity [13-16].

The first FDA approved photosensitizing agent for treatment of cancer belongs to the poryphrin family, porfimir sodium (Photofrin). Photofrin is known as a first-generation photosensitizer and has been used for the treatment of papillary bladder cancer, cervical cancer, endobronchial cancer, esophageal cancer, lung cancer, and Barrett's esophagus before 2003 [12, 17-21]. However, Photofrin has numerous intrinsic limitations, making it less desirable for clinical applications, specifically its low molar absorption coefficient (1,170 M^{-1} cm^{-1}) as well as cutaneous photosensitivity resulting from retention of residual photosensitizer [22-23].

These limitations have been the major impetus behind the synthesis of a second-generation photosensitizer developed at the Rosewell Park Cancer Institute (RPCI), 2-devinyl-2-(1-hexyloxyethyl) pyropheophorbide (HPPH). HPPH has a peak absorbance in the red region of the visible spectrum, at 665 nm, with a large molar extinction coefficient (ε_{max}) ~ 47,000 M^{-1} cm^{-1} [24] and a high quantum yield of singlet oxygen generation (Φ_{Δ}~0.48) [8, 25-26]. These chemical properties make HPPH a promising photosensitizer for *in vivo* PDT treatment. In contrast to most porphyrin-based agents, such as Photofrin, an absorbance at 665 nm enhances tissue penetration and did not show any significant prolonged skin photosensitivity in the patients [25]. HPPH had been approved for use in several clinical trials and has undergone Phase I trials involving basal cell skin cancer, head and neck cancer, and for treating dysplasia, carcinoma of the oral cavity,

and carcinoma of the oropharynx [27-29]. HPPH is currently in Phase II trials for lung cancer and Phase I/II trials for esophageal cancer, both showing effective anti-tumor responses [3, 19, 24, 30].

Localization and distribution of the photosensitizers in dysplastic cells is highly dependent on the photosensitizer's solubility and lipophilicity. Diffusion through lipid barriers of the cellular membrane and crossing into endocellular sites, like the nucleus, of the cell, requires that the drug be lipophilic in its free form [31]. HPPH is an extremely hydrophobic photosensitizer, consequently it requires a 1% Tween 80 / 5% dextrose formula to be used under physiologic conditions [32]. Systemic administration of such photosensitizers has been enabled through advancements in nanotechnology. Inherent solubility limitations require that HPPH be incorporated into a nanoparticle composed of a hydrogel matrix such as polyacrylamide (PAA). Biocompatible, polyacrylamide nanoparticles have previously been reported as promising vehicles for therapeutic photosensitizer delivery to tumor tissues [33-40]. The narrow hydrogel pores of the polyacrylamide matrix protect the active form of the photosensitizer from enzymatic degradation, but do not hinder the free flow of molecular oxygen – an important element required for the photochemical reaction of PDT. This loading method allows stable delivery of the hydrophobic photosensitizer under physiologic conditions and avoids systemic solubility limitations [41].

Nanoparticle (NP) surface modifications allow enhanced and active targeting by attachment of a tumor specific homing moiety, e.g. the F3-peptide, and coating the NP with polyethylene glycol (PEG) for longer plasma circulation (~24 hrs) [42]. Further selective uptake of the nanoparticles by tumor tissue ensues by the "enhanced permeability and retention effect" (EPR), allowing tissue retention of macromolecules by way of leaky microvasculature and poor lymphatic drainage [4, 43-44]. Designing nanoparticles between 10-100 nm in diameter is advantageous in order to utilize EPR. Molecules larger than 10 nm have the ability to bypass renal elimination, allowing for a

prolonged circulatory levels, and molecules smaller than 100 nm go unrecognized by phagocytes [45-47].

EXPERIMENTAL

Nanoparticle synthesis

Materials

The 2-devinyl-2-(1-hexyloxyethyl) pyropheophorbide (HPPH) was supplied by Roswell Park Cancer Institute (Buffalo, NY). Sodium dioctyl sulfosuccinate (AOT), Brij 30, Acrylamide (AA), ammonium persulfate (APS), N,N,N',N'-tetramethyl ethylenediamine (TEMED), and glycercol dimethacrylate (GDMA) were all acquired from Sigma-Aldrich (St Louis, MO). The 3-(aminopropyl) methacrylamide hydrochloride salt (APMA) was purchased from Polysciences Inc. (Warrington, PA). Ethanol (95%) and hexane were purchased from Fisher Scientific. Phosphate-buffered solution (PBS) was made using a phosphate-buffered saline tablet from Sigma-Aldrich. F3-Cys peptide (KDEPQRRSARLSAKPAPPKPEPKPKKAPAKKC) was purchased from SynBioSci. The heterobifunctional PEG (MAL-PEG-NHS, 2k) was purchased from Creative PEG Works. All chemicals were used as purchased without further purification.

Preparation of HPPH nanoparticles

HPPH post-loaded polyacrylamide nanoparticles were prepared by a reverse microemulsion polymerization method [18]. Then, HPPH (20 mg/ml in DMSO) was added to blank polyacrylamide nanoparticles suspended in 1% Tween 80 solution. The mixture was then stirred

under inert atmosphere, at room temperature, for 2 hours. Excess photosensitizer and DMSO were removed from the remnant mixture by washing the particles with ethanol and distilled water, followed by a 1% Tween 80 washing, using an Amicon Ultra-Filtration Cell (Millipore Corp., Bedford, MA), with a 500 kDa filter membrane, under pressure (10–20 psi).

F3-peptide conjugation to polyacrylamide nanoparticles

F3-peptides were conjugated to the surface of the nanoparticles for specific targeting of the nucleolin receptors overexpressed on the glioma cells. The freeze-dried PAA nanoparticles (50 mg) were dissolved in PBS (2.5 mL, pH 7.4), and bifunctional PEG (4 mg) was conjugated to the NP surface by amine-succinimidyl ester. This mixture was allowed to react under stirring conditions for 30 min, at room temperature, before undergoing thorough washings using an Amicon centrifugal filter (Millipore, 100 kDa), thus eliminating any unreacted ligands, and the final concentrated to ~20 mg/mL. Cystein tagged F3-peptide, F3-Cys peptides (0.06 μmol), were added to the concentrated nanoparticle solution and gently stirred overnight (>6 hours), at room temperature. L-Cysteine aqueous solution was added to the mixture and stirred for 2 hours in order to deactivate the terminal site of the unreacted PEG. The resultant F3-targeted HPPH-conjugated polyacrylamide nanoparticle solution was thoroughly washed with PBS and distilled water, in an Amicon ultra-filtration cell (Millipore Corp., Bedford, MA), and then freeze-dried with a 5L ModulyoD freeze dryer (ThermoFisher Scientific), until re-hydrated for experimental use.

Surface modification of non-targeted nanoparticles

Dye-conjugated polyacrylamide nanoparticles (50 mg) were dissolved in PBS (2.5 mL, pH 7.4). Bifunctional PEG (4 mg), was added to the nanoparticles solution and then the mixture was stirred for 30 min, at room temperature. A rinsing procedure was carried out using an Amicon centrifugal filter (Millipore, 100 kDa), removing any unreacted ligands, and concentrated to ~20 mg/mL. Following the addition of PEG, an aqueous solution of L-Cysteine was added to the mixture and stirred for 2 hours, in order to deactivate the terminal site of PEG. The resultant non-targeted HPPH-conjugated PAA nanoparticle solution was thoroughly washed with PBS and distilled water, in an Amicon ultra-filtration cell (Millipore Corp., Bedford, MA), and then freeze-dried with a 5L ModulyoD freeze dryer (ThermoFisher Scientific) until re-hydrated for experimental use.

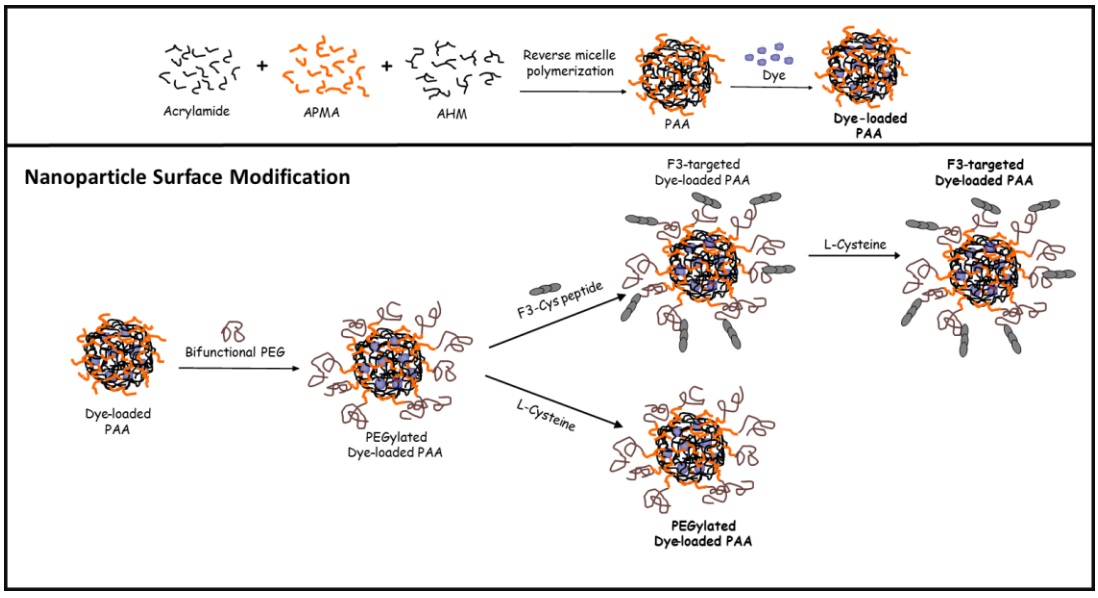

Figure 3.1: Surface modification and conjugation of HPPH post-loaded PAA nanoparticles.

Nanoparticle characterization

Dynamic light scattering measurements

The size distribution of the HPPH-conjugated PAA nanoparticles in an aqueous solution was measured by dynamic light scattering (DLS, DelsaNano, Beckman Coulter, Inc., Brea, CA, USA). The surface charge of the HPPH-conjugated polyacrylamide nanoparticles in water was measured by zeta potential measurements, using the above instrument.

Quantification of dye loading

The amount of HPPH dye encapsulated in the nanoparticles was evaluated by absorption measurements using an UV-Vis spectrometer (UV-1601, Shimadzu, Scientific Instruments Inc., Columbia, MD, USA). The amount of photosensitizer loaded was calculated based on a calibration curve of free HPPH in 1% Tween-80/water, developed using the Beer-Lambert law.

Reactive oxygen species detection

Reactive oxygen species (ROS) production from the HPPH-encapsulated polyacrylamide nanoparticles was measured by using Anthracene-9,10-dipropionic acid disodium salt (ADPA) as a ROS ($^1O_2$) detection probe [48-49]. HPPH post-loaded nanoparticles were suspended in PBS and mixed with ADPA in a cuvette. While under constant stirring the solution was irradiated at the excitation wavelength to determine the ROS production rate, with the ADPA photobleaching rate constant, measured using fluorescence spectroscopy (FluoroMax-3, Jobin Yvon/SPEX Division, Instruments S.A. Inc., Edison, NJ, USA).

Toxicity analysis

MTT assay

For cytotoxicity studies, 9L glioma cells were plated on 96-well plates, at a density of 5000 cells per well, and incubated at 37^{o}C overnight. For comparison, the cells were incubated with blank PAA, PEGylated PAA, and F3-targeted PAA nanoparticles, at various concentrations (0.1, 0.2, 0.5, 1.0 mg/ml), and left at 37^{o}C, with slow intermittent rocking using a 55S single platform shaker (Reliable Scientific, Inc). After incubation, to remove any unbound nanoparticles, the treated cells were carefully washed 3 times with fresh cell medium. The cells were further prepared using the MTT assay kit; 25 μl of 5.0 mg/ml 3-(4,5-dimethylthiazol-2-yl)-2,5-diphenyltetrazolium bromide (MTT) in PBS was added to each well and left to incubate for 4 hours while slowly rocking. After 4 hours the medium solution was removed and 200 μl of DMSO was added to each well, so as to solubilize the water-insoluble formazan crystals produced by the MTT cellular dehydrogenase activity in viable cells. The 96-well plate was covered with foil and left to steadily rock on a rocking table (Reliable Scientific, Inc) overnight. To quantify the cell viability of the treated cells, the absorbance spectra were analyzed, using a microplate reader (SpectraMAX Plus 384, Molecular Devices LLC, Sunnyvale, CA) at 550nm, and compared to untreated cells. The experiment was performed using 12 wells per condition, so as to assure statistically meaningful results.

Endotoxin detection

Enodotoxin levels were measured using an Endosafe-PTS (Charles River) and following the LAL Assay [50]. A portable endotoxin meter has sterile cartridges for detecting endotoxin in aqueous

samples. Within the device, a reaction between horseshoe crab blood extract, limulus amebocyte lysate (LAL), and bacterial endotoxin, or with a membrane component of Gram negative bacteria, can quantify bacterial endotoxins. All nanoparticle batches and samples were tested prior to injecting the nanoparticle solution into the animal model during PDT treatment.

Based on our experience with testing endotoxin levels for the nanoparticle samples, endotoxin growth rates are highly sensitive to both time and temperature – longer exposure to solutions, after hydration, and warm temperatures can exacerbate bacteria growth. To avoid this growth and contamination, our nanoparticle samples are rehydrated within minimal time intervals between hydration and injection; in addition, the sample is refrigerated at all times post rehydration, with the exception of when the sample is warmed to physiological temperature prior to injection.

Cell culture

Cell culture

Rat 9L gliosarcoma cells (Brain Tumor Research Center, University of California, San Francisco, CA) were routinely maintained in Rosewell Park Memorial Institute (RSPI), with 400mg/L $_{D}$-glucose and 292 mg/ml $_{L}$-gluamine supplemented with 10% fetal bovine serum, 100U/ml (3%) penicillin, 1mM sodium pyruvate, and 100 μg/ml streptomycin sulfate. Cells were grown at a 37ºC, 5% CO_2 , 95% air and 100 % humidity environment.

Cells were plated on the 96 well plates for the MTT assay and 35 mm culture dishes with coverslip bottom, for the *in vitro* PDT.

In vitro set-up

Fluence dependent PDT

To investigate the effects of PDT phototoxicity, a series of *in vitro* experiments were performed on rat 9L gliosarcoma cells. Glass cover slips were incubated with 1 mg/mL HPPH-loaded polyacrylamide nanoparticles (containing F3-peptide) for 15 minutes, rinsed with appropriate cell media and placed in a temperature-controlled sample chamber at 37^{o}C. Methylene blue-mediated cytotoxicity was then monitored, before and after illumination, by labeling the cells with 5 μL Calcein-AM and 10 μL propidium iodide (PI) fluorescent stains. Fluorescence observations of Calcein-AM (excitation: 490nm, emission: 515nm) and PI (excitation: 536nm, emission: 617nm) were monitored for 30 minutes, using a Perkin Elmer Ultra View Confocal microscope system equipped with an argon-krypton laser. Irradiating with the microscope laser, illumination was performed at 647 nm, with 80 μW of power, for 1 minute intervals and stopped. The live/dead assay allows for obvious distinctions of viable/cytotoxic cells. In living cells, intracellular esterase converts the non-fluorescent Calcein-AM into a green fluorescent Calcein, indicating viable cell metabolism. PI is barred by viable cells but can invade cells with damaged membranes. Upon irradiation, in a time-dependent manner, compromised cells release the green fluorescence of the Calcein-AM through damaged membranes and permit the binding of PI to their nucleic acids – consequently emitting a red fluorescence. Upon completion of treatment, the optical lens was switched to a lower magnification so as to show that the treatment was localized to the illumination area – showing there red stained, dead cells, which are surrounded by viable, green stained cells, just outside the illuminated area.

Furthermore, fluency-dependent PDT studies were performed at illumination fluence rates of 180 J/cm^2 and 400 J/cm^2. Pre-exposure images were taken using a 60X optical lens. The cells were

exposed for a total of 30 minutes, using a 671 nm red diode laser (model 671RLMH1W, Changchun Dragon Lasers Co., Ltd) with power densities of 100 mW/cm^2 and 222 mW/cm^2. Post-exposure images were taken using a 20X lens, to observe the localized cellular damage.

In vivo set-up

Cranial window model

The animal research protocol was reviewed and approved by the University Committee on Use and Care of Animals (UCUCA) at the University of Michigan, Ann Arbor. Biparietal craniectomies were performed on 8-week old Sprague-Dawley male rats (Charles River Laboratory, Wilmington, MA). Rats weighing between 250 to 350 g were anesthetized and placed into a stereotactic frame. Rat 9L gliosarcoma cells were harvested in monolayers and, following a full craniectomy, suspended in media, and then the cells (10^5) were injected, using a syringe micro-injector (Medfusion 3500 syringe pump). The 9L cells were implanted in the forebrain, at a depth of 1.5 mm, through a burr hole extending 1mm below the injection location, so as to create a pocket for growth. To allow for serial inspection, a thin, round microscope cover slip was bonded to the cranial opening, with cyanoacrylate glue, creating a brain tumor window (BTW) model [51].

HPPH nanoparticle administration

Nanoparticles were synthesized and formulated according to the previously described methods. The nanoparticles had a dye loading dose of HPPH dye of 0.3 mg HPPH/(kg of the rat), with dye loading of 1% wt/(NP wt). The stock solution was determined to have nominal endotoxin levels, as determined by the LAL assay. Once the tumor radius reached 2-3 mm in diameter,

photosensitizers in the form of free dye, or dye embedded polyacrylamide nanoparticles, were administered intravenously through the right femoral vein, using a programmable micro-injector (Medfusion 3500 syringe pump). After injection, rats were kept in the dark during nanoparticle systemic incubation (105 minutes, 6 hours, or 10 hours) until undergoing irradiation therapy.

Laser set-up

Tumors in the BTW model were irradiated, from outside the glass window, in a cross sectional manner, via the exposed tumor surface immediately beneath the window. *In vivo* light illumination was performed using a 671 nm red diode laser (model 671RLMH1W, Changchun Dragon Lasers Co., Ltd) with tunable output power (0 – 1 W), so as to precisely expose with various fluency rates.

The size of the laser beam was controlled with the use of a collimator (CSMA-8-B collimator, Newport Corp) so as to accurately control the light fluence for PDT. For all of our experiments, a constant beam diameter of 4 mm was used, while the distance between the cranial window and the collimator was fixed at 1 inch.

Calibration of the laser was performed; the laser was tuned to the desired power, set to warm for 30 minutes, and then checked again using a power meter to assure light fluency stability. After observing for a complete hour of consistent power output, the laser was cleared for PDT illumination. It was not typical to find fluctuations in power; and so it was important to assure ourselves that the laser was working at the desired standard before treatment.

Tumor size measurement

Damage to sensitized tumor and brain parenchyma by photo-irradiation was observed using a Sony digital camera. Daily photographs of the cortical surface were taken as seen through the BTW, giving an evident depiction of the tumor growth patterns prior and post PDT treatments. Tumor growth patterns were then evaluated by delineating the tumor boundaries, based on the variations of pixelated coloration and measuring the total pixelated surface area of the tumor. The *in vivo* PDT efficiency was determined by tumor surface area measurements, as seen through the BTW model, of individual animals and animal groups.

RESULTS AND DISCUSSION

HPPH was loaded into nanoparticles by way of post-loading. Post-loading the photosensitizer into the polyacrylamide matrix of the nanoparticle causes no chemical change to the photosensitizer and results in a high drug loading efficiency. This loading method allows for a stable delivery of the hydrophobic photosensitizer under physiological conditions. The hydrogel PAA nanoparticle matrix protects the active form of the photosensitizer from enzymatic degradation, but allows for free flow of molecular oxygen, which is imperative for PDT [48, 52].

The DLS measurements in aqueous solution showed the size of the nanoparticles to have a diameter of 39 ± 5 nm, with a fairly uniform size distribution. The surface charge of the F3-modified nanoparticles was measured to be +13.2 (± 0.2) mV, whereas the non-targeted (surface PEGylated) nanoparticles have a charge of +1.9 (± 0.1) mV. The unmodified nanoparticles, having free amine groups on the nanoparticle matrix, have a surface charge of +14 (± 3). Addition of the

highly positive charge from the F3-peptide results in a positively charged nanoparticle, while the non-targeted nanoparticle has a nearly neutral surface charge due to the presence of the neutral PEG molecules.

Absorption spectra of HPPH nanoparticles show a strong absorbance peak at 662 nm. Dye loading was measured by comparison of the 1 mg/ml nanoparticle concentration to the absorption peak values and the extinction coefficient of HPPH in a 1% Tween 80 solution. Florescence and absorbance measurements show that the post-loaded HPPH nanoparticles have a 95% loading efficiency, with a dye concentration of 1% by weight [32].

To ensure that the reactive oxygen species was generated as a response to light activating the dye encapsulated in the nanoparticle matrix, dye leaching needed to be examined. It is imperative to test dye leaching because photosensitizers outside the nanoparticle can interact with cellular surface proteins and organelles *in vitro*; furthermore, enzymatic degradation of the leached out HPPH dye might alter the optical properties of the dye during intraoperative *in vivo* applications. In order to survey the dye leaching, the HPPH content in the filtrate separated from the nanoparticles by centrifugation filtration was measured, using UV-VIS absorbance spectra.

Dye leaching experiments of the HPPH post-loaded nanoparticle in a 1% Tween 80 water filtrate solution showed untraceable amounts of HPPH when testing absorbance at 665 nm [32]. This ensures that dye-leaching complications will be avoided during systemic *in vivo* circulation and ensures the delivery of the full pay-load of photosensitizer to cells *in vitro* or to tumor sites *in vivo*. These dye loading and leaching experiments confirm that the reaction between the photosensitizing dye and the singlet oxygen must occur within the nanoparticle.

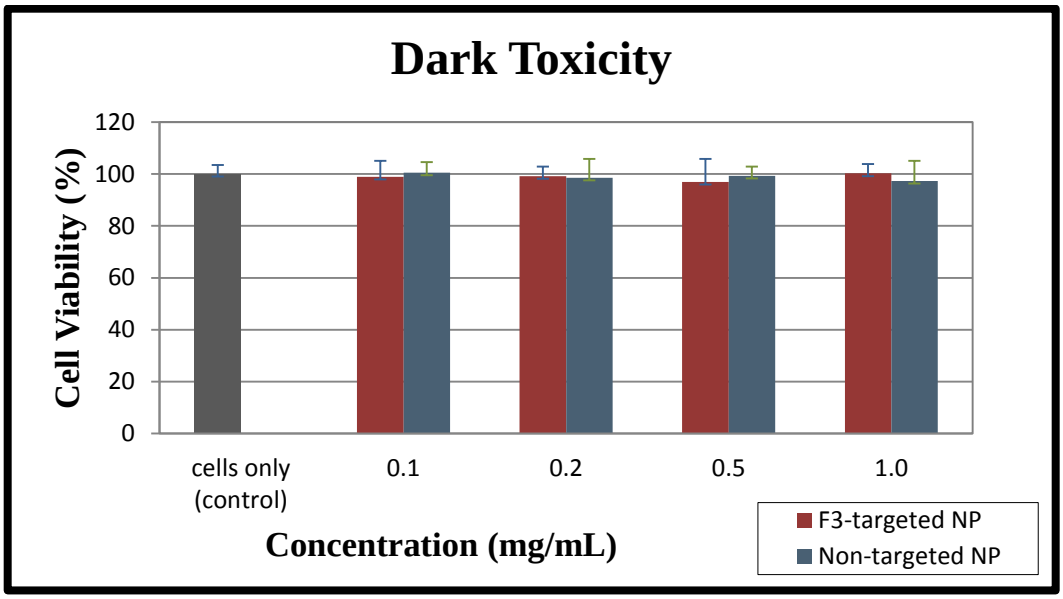

Figure 3.2: Cytotoxicity test using the MTT assay. Cell viability of 9L gliosarcoma, evaluated after 24 hours incubation, with varying concentrations of F3-targted and non-targeted HPPH polyacrylamide nanoparticles. Cell survival rates indicated no measurable differences among nanoparticle concentrations (0.1, 0.2, 0.5, and 1.0 mg/mL), including the cell only control group (not treated with nanoparticles).

Dark toxicity of the nanoparticles was investigated by performing MTT assays, using various concentrations of nanoparticles. F3-targted and non-targeted nanoparticles were added to 9L glioma cells, with increasing concentrations, for survival assessment, as determined by the assay. These toxicity assays show that the HPPH polyacrylamide nanoparticles are non-toxic to cells, and exhibit a higher than 97% cell viability, up to the nanoparticle concentration of 1 mg/ml (Figure 3.2). This dark toxicity test ensures that viability differences during PDT experiments will not be attributed to the use of the nanoparticles alone, but rather represent the cytotoxicity as a result of treatment.

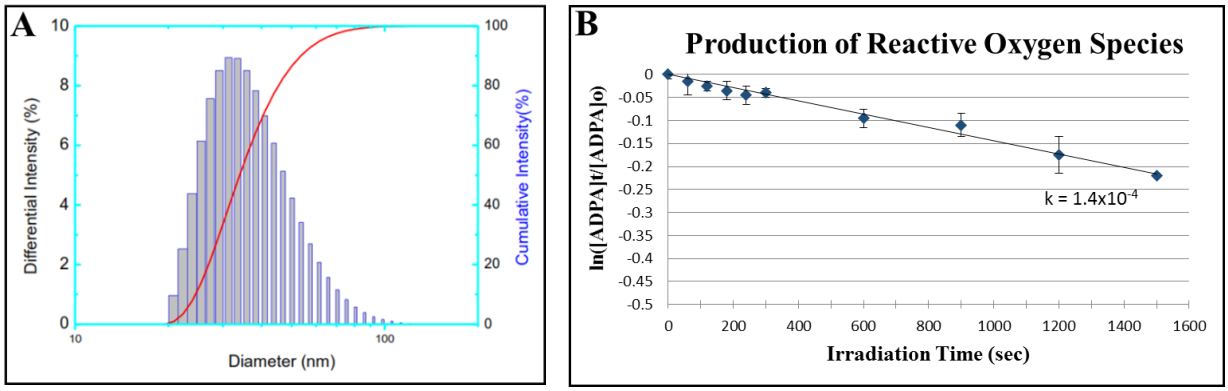

Figure 3.3: (A) Size distribution of polyacrylamide nanoparticles in solution as measured by DLS. (B) ROS production measurement of HPPH post-loaded polyacrylamide nanoparticles in DI water, with excitation peak for HPPH at 665nm: Linear fitted plot of fluorescence change of ADPA as a function of irradiation time, irradiation performed at 378nm.

The ROS production from HPPH post-loaded polyacrylamide nanoparticles was tested using ADPA photobleaching [48-49]. Figure 3.3 shows the fluorescence spectra of HPPH polyacrylamide nanoparticles with 1% wt/(NP wt) dye loading and nanoparticle concentration of 0.068 mg/ml. The conjugated nanoparticles show very strong fluorescence at 665nm [32]. The ADPA oxidation rate (k-value) is calculated to be $1.4x10^{-4}$/s for post-loaded HPPH polyacrylamide nanoparticles.

To confirm that cell death in response to light activating ROS, dye leaching needed to be examined. Performing dye leaching tests proves important because photosensitizers outside the nanoparticle can interact with cellular surface proteins and organelles, resulting in unwanted cytotoxicity. In order to assess the dye leaching, the filtrate from washing HPPH nanoparticles was separated from the nanoparticles by centrifugation filtration and measured using UV-Vis absorbance spectra. There was no detectable absorbance at 665 nm, verifying negligible dye leaching of HPPH out of the HPPH post-loaded polyacrylamide nanoparticles. This verifies that the detected reaction between the HPPH dye and the ROS must occur within the nanoparticle. It also verified that post-

loading the HPPH dye to the nanoparticle matrix completely eliminates dye leaching, thus ensuring the delivery of the full pay-load of photosensitizer to cells *in vitro* or to tumor sites *in vivo*.

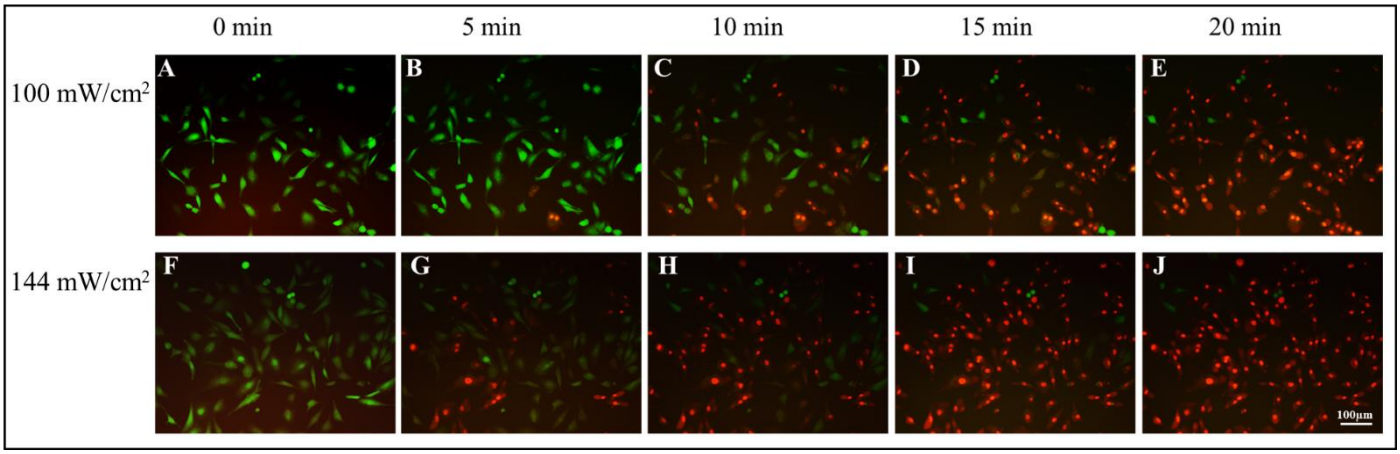

Figure 3.4: Confocal images of 9L cell lines treated with F3-targeted HPPH post-loaded PAA nanoparticles. Intensity dependent cytotoxicity, induced by F3-targted HPPH PAA nanoparticles and laser irradiation at 671 nm. The 9L gliosarcoma cells were incubated with HPPH nanoparticles and irradiated with fluencies of 100 J/cm^2 and 144 J/cm^2. Images were taken (A) before light exposure; (B-E) over 30 min of light exposure at a dose of 100 mW/cm^2. Images were taken (F) before light exposure; (G-J) over 30 min light exposure at a dose of 144 mW/cm^2. Cytotoxicity was monitored by labeling the cells with Calcein-AM (green, for viable cells) and propidium iodide (red, for dead cells). Measurements taken on a confocal microscope.

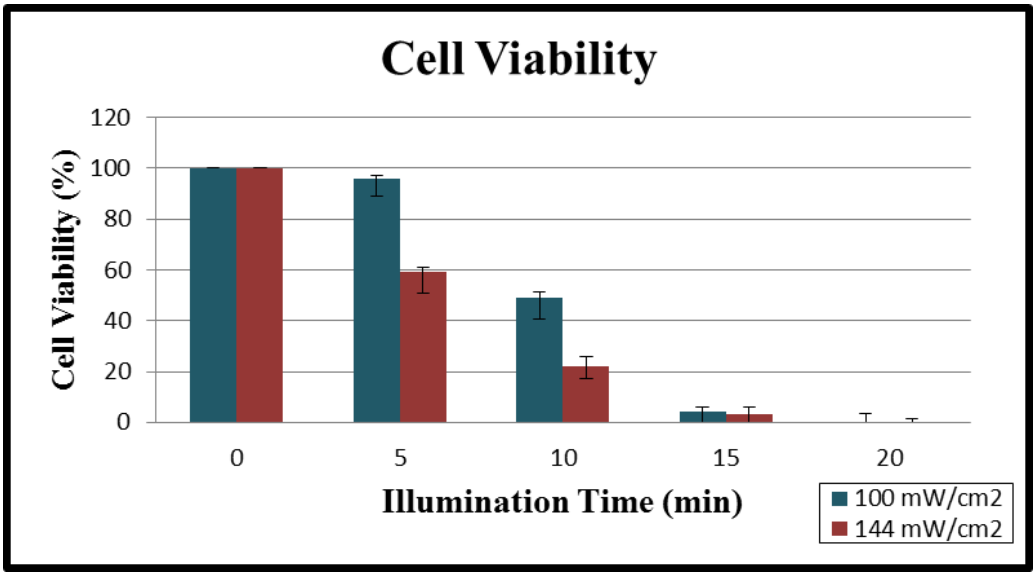

Figure 3.5: Cell viability assessment for the phototoxic effects of F3-targeted HPPH post-loaded polyacrylamide nanoparticles on a 9L cell line. Fluency dependent PDT efficiency at light doses of 100 mW/cm^2 and 144 mW/cm^2, over the course of 20 minutes of illumination. Cells exposed to a higher fluency responded with a more rapid cellular death than for a lower fluency.

To investigate the fluence rate dependence of PDT phototoxicity, a series of *in vitro* experiments were performed on rat 9L gliosarcoma cells. Using the protocols for the live/dead assay, 9L cells were irradiated at two separate light intensities, 100 mW/cm^2 and 144 mW/cm^2, using an excitation wavelength of 671 nm. A series of images of the cells were sequentially taken over 20 minutes, in 1 minute intervals, using an Ultra-View confocal microscope (Figure 3.4).

In order to examine the effect of irradiating the 9L cells at different laser fluencies; cells were exposed to two laser fluencies and the confocal images are displayed side-by-side (100 mW/cm^2: Figure 3.4 A-E; 144 mW/cm^2: Figure 2.4 F-J). In preparation for light irradiation, all cells were stained by Calcein-AM, showing green fluorescence, verifying cell viability for both experiments (Figures 3.4A, 3.4F). After 5 minutes of irradiation, the cells exposed to the greater fluence rate showed initial signs of cell death, by the presence of PI-stained red nuclei (Figure 3.4G) while the lesser fluence rate shows no sign of cellular death (Figure 3.4B). After completing 10 minutes of

illumination, the cells exposed to the higher illumination fluence show a convincing display of cellular death (Figure 3.4H) and continuously improve in displaying cytotoxic effects with total cellular death 15 minutes into the experiment. The lower fluence rate displayed primary signs of cell death at 10 minutes and the cellular cytotoxicity increased through 15 and 20 minutes of illumination (Figures 3.4D, 3.4E).

These cell viability experiments show that photosensitizers exposed to a higher fluence rate result in a significantly increased rate of cellular cytotoxicity. Complete cellular death was achieved in a shorter time frame, this was all signified by a rapid release of Calcein-AM (green) through the compromised cellular membrane allowing for the incorporation of PI (red) into the nucleus. These results demonstrate the light- dose dependency of PDT cytotoxicity, which would enhanced the PDT efficieny by better understanding cell death rates as exposed to various light dose.

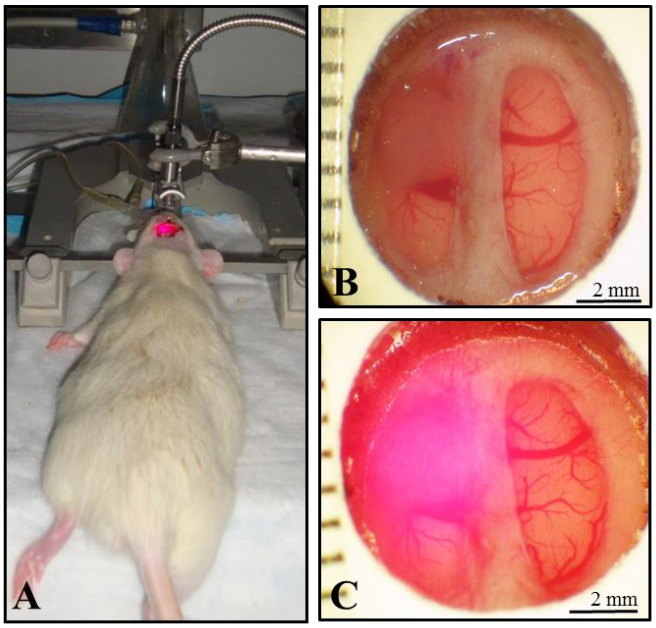

Figure 3.6: (A) Photograph displaying photodynamic therapy setup. Rats with BTW are placed in sterotactic frames with distance between cranial window and laser collimator fixed at 1 inch. Photographs of a tumor as seen through the BTW (B) before laser therapy and (C) during irradiation with a 671nm laser.

The *in vivo* efficacy of HPPH mediated photodynamic therapy was evaluated by tumor growth experiments performed on rat bearing intracranial 9L glioma. When the brain tumor radius reached 3 mm in diameter, the HPPH photosensitizers, in the form of free dye, or of dye loaded polyacrylamide nanoparticles, were administered intravenously, via the femoral vein. The HPPH PAA nanoparticles were administered at a dose of 60 mg/kg, which corresponds to 1% wt/(NP wt) dye loading. This dose has proved to be safe, in accordance with our previous nanoparticle optimization and toxicology studies [51, 53]. In line with previous incubation studies, 105 minutes after intravenous injection of HPPH, interstitial PDT treatment at 671 nm was administered, using a fixed light dose of 180 J/cm^2 [35]. Daily photographs of the cortical surface were taken, prior and post PDT treatments, to quantify tumor growth patterns (Figure 3.7).

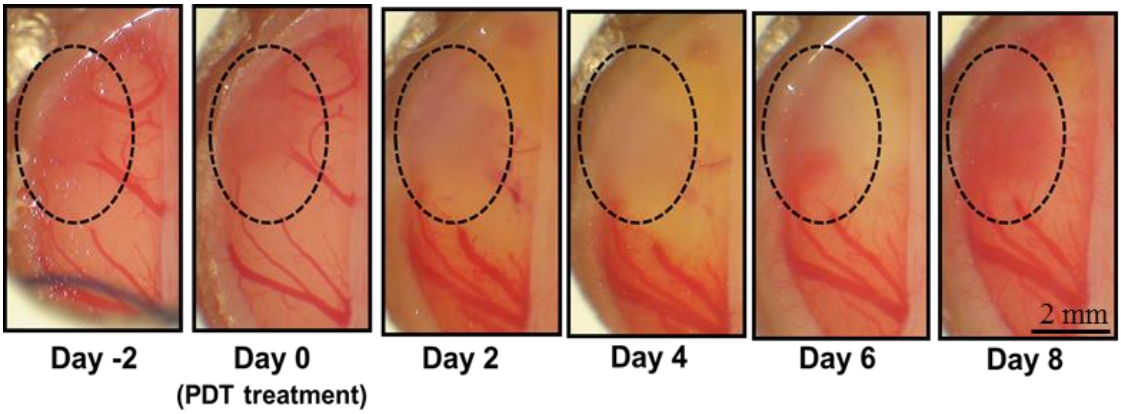

Figure 3.7: A series of cranial window pictures of an implanted 9L glioma, before and after the PDT, using non-targeted HPPH polyacrylamide nanoparticles and a time interval of 6 hours between nanoparticle injection and light illumination. The dotted circle encloses the tumor area in each picture.

Figure 6 shows images of glioma development, as seen through the brain tumor window, for untreated animals (withheld laser illumination and NP administration), and animals treated with HPPH free dye, F3-targeted HPPH polyacrylamide nanoparticles, and non-targeted PEGylated

HPPH polyacrylamide nanoparticles. The untreated gliomas grew continuously throughout the observation period. Animals treated with HPPH free dye and laser illumination show a slight regression in tumor surface area, accompanied by a period of necrotic tissue post-PDT treatment. Among the animal groups tested, those administered with HPPH post-loaded in PAA nanoparticles showed the most effective treatment in inducing phototoxicity, in response to PDT. Gliomas treated with HPPH containing nanoparticles and irradiated with laser light resulted in a significant decrease in tumor surface area and produced necrosis localized to the treatment regions, demonstrated by the opaque tissue, as seen through the brain tumor window. Tumor growth patterns of the F3-targted HPPH NPs and non-targeted HPPH PEGylated NPs showed analogous regression and regrowth patterns over the ten day observation period, post-treatment (Figure 3.8).

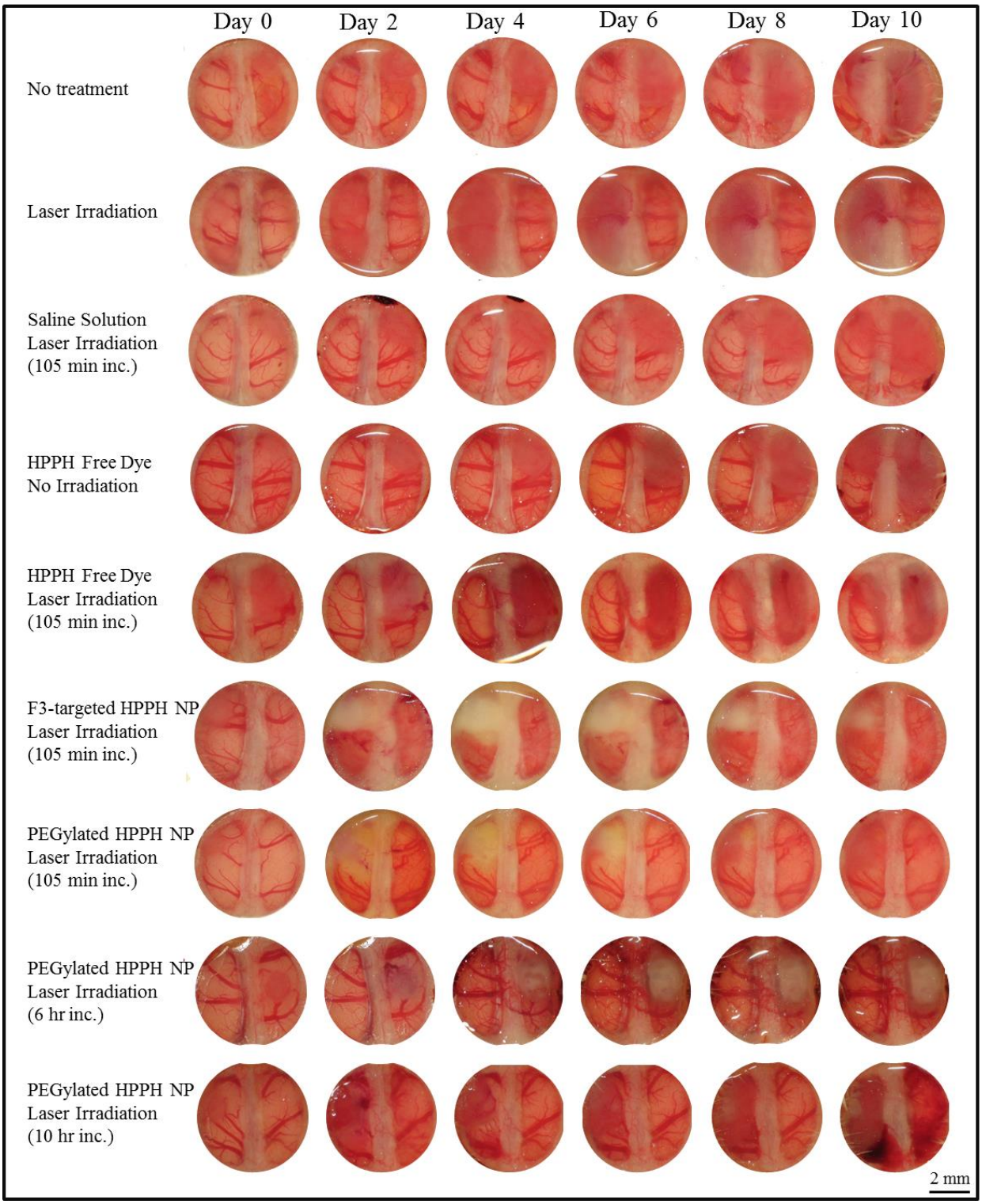

Figure 3.8: BTW view of the brain on the day of photodynamic therapy (Day 0), showing tumor growth of approximate size of 3mm. Days following PDT treatment, extensive necrosis was seen in the treatment area for those animals administered HPPH nanoparticles and irradiated with the laser light.

The differences in treatment response between HPPH administered in the form of free dye and post-loaded in nanoparticles can be explained to some extent by the pharmacokinetic behavior of these two delivery methods. The extreme hydrophobic, lipophilic photosensitizer, in the form of a free dye, shows a decline in activity, possibly due to drug aggregation and drug accumulation variations within the treatment area. This limited efficacy of the hydrophobic photosensitizer suggests the need for a drug delivery system for enhanced PDT efficiency.

In contrast to the HPPH free dye treated animal group, the similar PDT efficacy and tumor response between active targeting (F3-targeted NPs) and passive targeting (PEGylated NPs) nanoparticles indicate equivalent sensitizer exposure within the localized region during the 30 minute irradiation. As seen *in vitro*, complete cellular death was experienced between 15 and 20 minutes into the treatment, with fluency rates identical to that of the *in vivo* studies. *In vivo* phototoxicity using active targeting is achieved through the continuous systemic circulation of nanoparticles, even after the nucleolin bound, F3-targeted nanoparticles have been completely irradiated - damaging the entirety of the exposed epithelial surface receptors. Passive targeted PEGylated nanoparticles accumulate in the tumor region by the EPR effect, in addition to the uninterrupted distribution of nanoparticles throughout the treatment area by way of systemic circulation. Figure 3.9 and Figure 3.10 detail tumor growth response and necrotic tissue development post-PDT for these delivery methods. These figures affirm that the cytotoxic efficiency achieved by F3-targeted nanoparticles parallel that of PEGylated nanoparticles. These identical PDT effects between active and passive targeting were the result of a complex interplay of the amount of HPPH in the treatment region and its replenishment after local photobleaching due to systemic distribution.

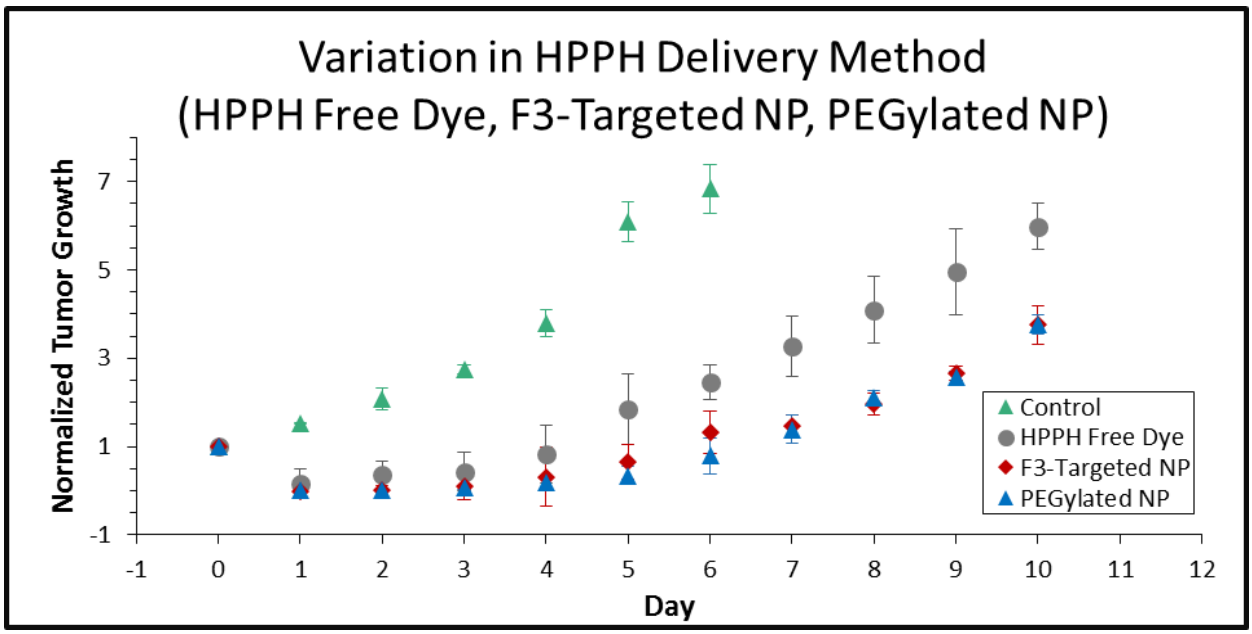

Figure 3.9: Tumor response as a result of delivery dependent photodynamic therapy. HPPH in the form of free dye and post-loaded in nanoparticles, F3-targeted or non-targeted polyacrylamide nanoparticles, were intravenously injected. Following nanoparticle incubation time of 105 minutes tumors were irradiated at 180 J/cm^2 using 671 nm laser light through the BTW and observed daily.

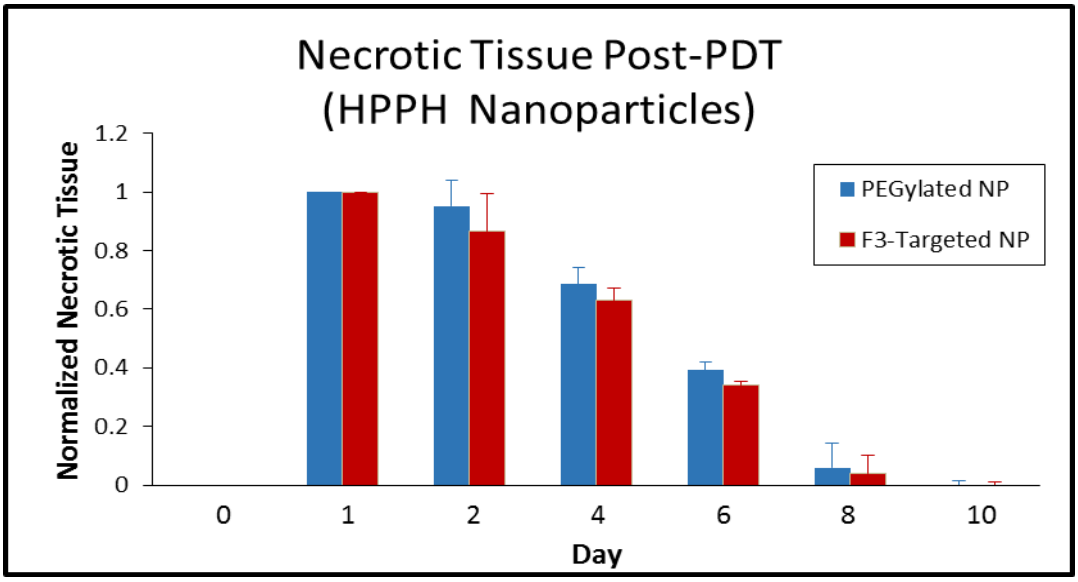

Figure 3.10: Tumor necrosis measurements. Following nanoparticle incubation time of 105 minutes tumors were irradiated at 180 J/cm^2, for 30 minutes, using 671 nm laser light. Measurements were taken for animal groups treated with non-targeted HPPH PEGylated polyacrylamide nanoparticles and F3-targted HPPH polyacrylamide nanoparticles. Both treatment groups demonstrate irradiation induced tumor necrosis.

Figure 3.11 shows the tumor growth patterns post-PDT as a result of varying incubation times, the time between nanoparticle administration and laser illumination. Irradiation of the tumor site were performed 105 minutes, 6 hours, and 10 hours following the administration of HPPH PEGylated nanoparticles. The animal group receiving PDT treatment 10 hours post-injection of HPPH nanoparticles experienced a retarded tumor growth post-treatment through day four followed by an aggressive development of tumor growth and nominal necrotic tissue. PDT treatment following 6 hours incubation of the HPPH nanoparticles resulted in complete eradication of the tumor, indicated by the appearance of opaque necrotic tumor as seen through the BTW model (Figure 3.8 and 3.12). Tumor regrowth patterns for this animal group display equivalent/similar tumor area measurements eight days post-treatment as seen on treatment day (Figure 3.11 and 3.12). Laser irradiation performed 6 hours after injection displayed maximal tumor regression and necrotic tissue development over other treatment groups. Animals incubated with HPPH nanoparticles for 105 minutes experienced similar effects from treatment with the exception of distinct tumor re-growth patterns following the eight day of observation. This suggests HPPH PEGylated nanoparticle retention and circulation provided greatest photosensitizer exposure in the treatment region when irradiation was performed at 6 hours post-administration of nanoparticles.

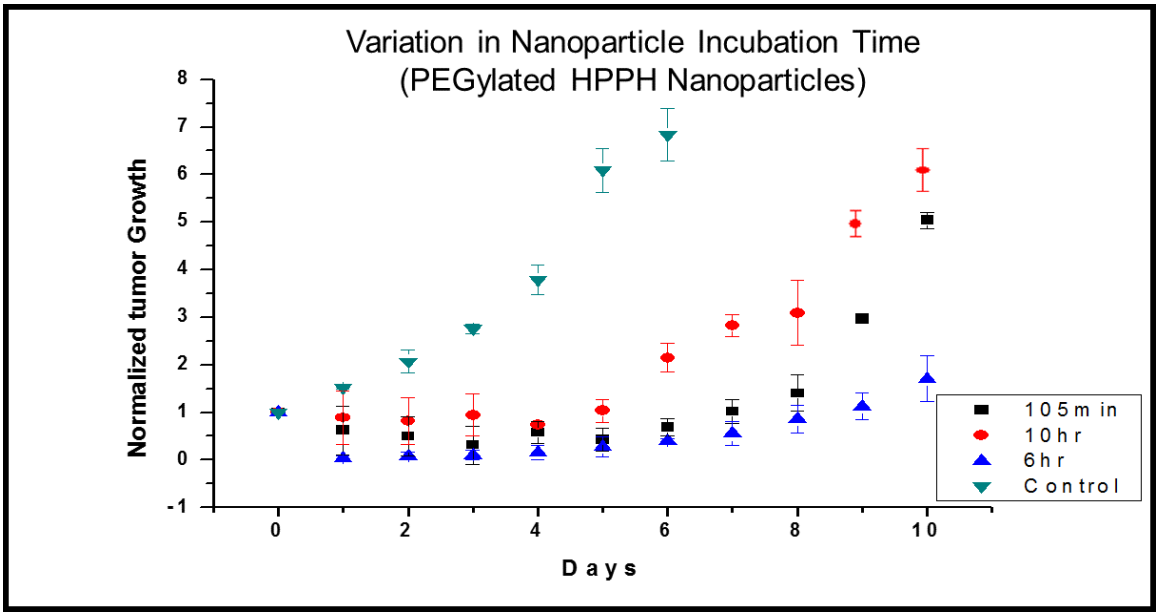

Figure 3.11: Tumor response for variations in incubation times of non-targeted HPPH PEGylated polyacrylamide nanoparticles. Following nanoparticle incubation time of 105 minutes, , 6 hours, and 10 hours tumors were irradiated at 180 J/cm^2 using 671 nm laser light through the BTW and observed daily.

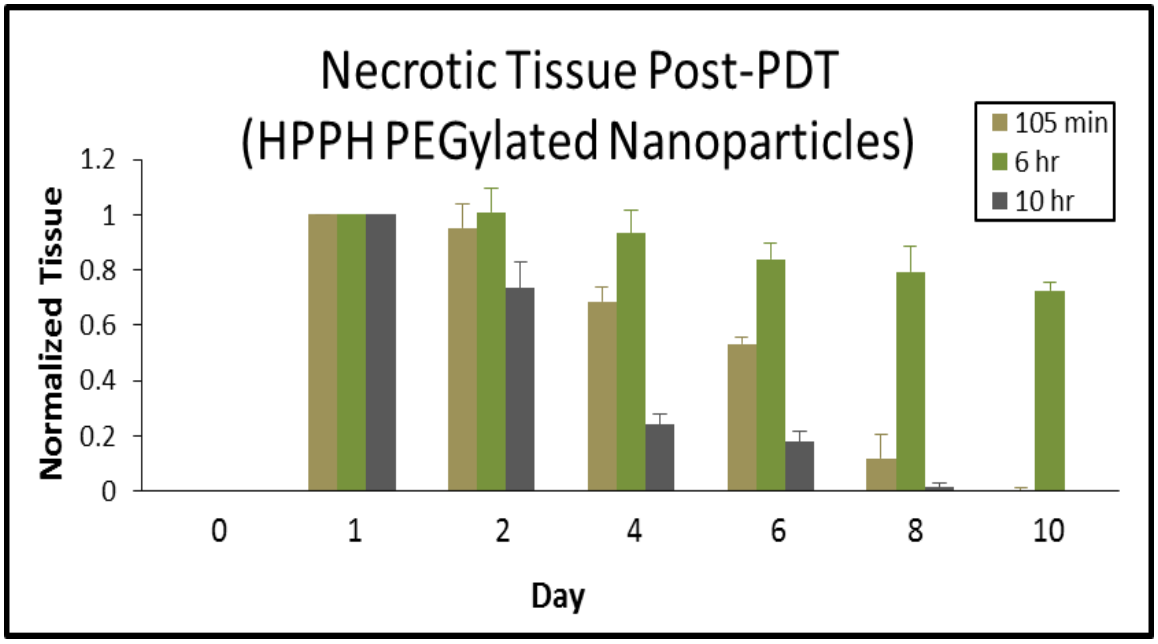

Figure 3.12: Tumor necrosis measurements for variations in incubation times of non-targeted HPPH PEGylated polyacrylamide nanoparticles. Following nanoparticle incubation time of 105 minutes, 6 hours, and 10 hours tumors were irradiated at 180 J/cm^2 using 671 nm laser light. Prolonged duration of tumor necrosis found in treatment groups receiving irradiation following 6 hour incubation.

Response of glioma treated with HPPH post-loaded PEGylated polyacrylamide sensitized at 671 nm, using varying irradiation regimens: power density of 100 mW/cm^2 at incident fluence of 180 J/cm^2, power density of 100 mW/cm^2 at incident fluence of 260 J/cm^2, power density of 144 mW/cm^2 at incident fluence of 260 J/cm^2 (Figure 3.11 and 3.12). Comparing two conditionally different animal groups that have been exposed to the same fluence rates will demonstrate clear relationships between incident irradiation fluence rate and therapeutic outcome. This approach investigates the effective delivery of higher light intensities with minimal prolongation of treatment time (144 mW/cm^2, 30 minute exposure time) and lower light intensities with a broader range of treatment times (100 mW/cm^2, 45 minute exposure time).

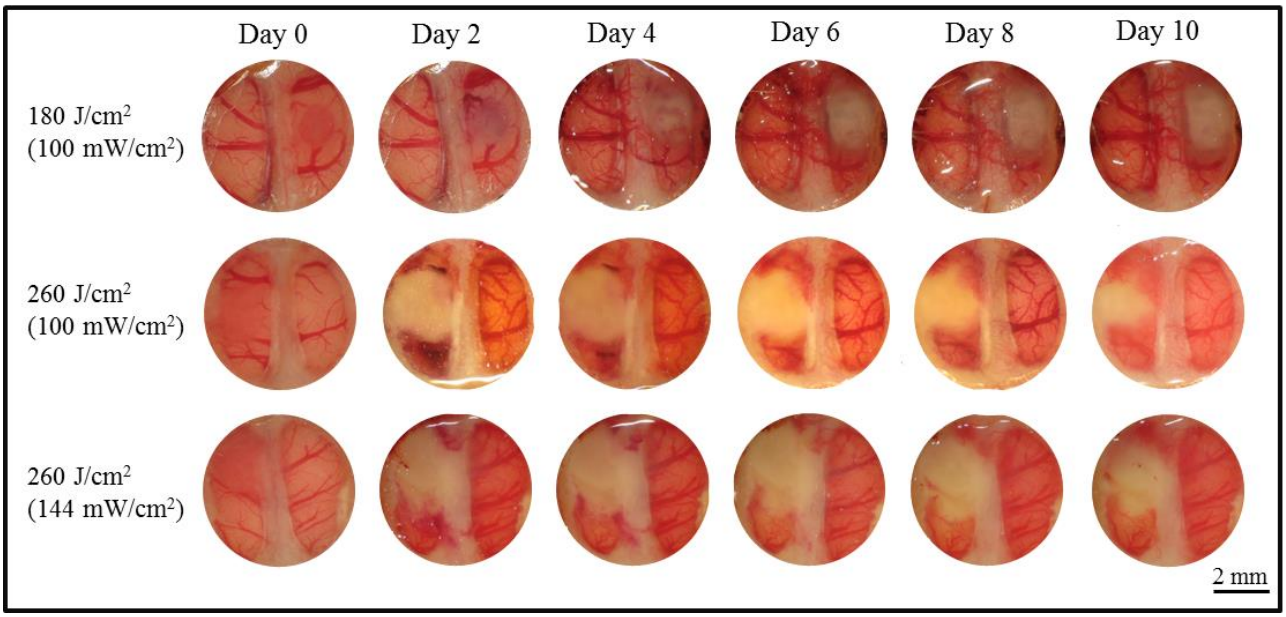

Figure 3.13: Representation of animal groups receiving PEGylated HPPH polyacrylamide nanoparticles with systemic incubation time of 6 hours between nanoparticle administration and laser illumination. Photographs depict the brain as seen through the BTW on the day of photodynamic therapy (Day 0), showing tumor growth of approximate size of 3 mm, and the days post-treatment. Days following PDT treatment, significant necrosis was seen in the treatment area for all animal groups following PDT treatment.

All of the fluency treatment procedures produced delays in tumor surface area growth as seen through the BTW model (Figure 3.13). Comparison between the various fluency treatment groups revealed that glioma response to power density of 100 mW/cm^2 at an incident fluence of 260 J/cm^2 treatment was more desirable out of the three treatment protocols. Tumor regrowth following 100 mW/cm^2 (260 J/cm^2) irradiation was delayed significantly longer than it was for treatment groups exposed to a power density of 144 mW/cm^2 (260 J/cm^2). For the animal group receiving a larger power density and higher fluency rate, the tumor doubling time was extended to 10 days, with tumor necrosis remaining at 70% of the original tumor area (Figure 3.14 and 3.15). While regrowth following 100 mW/cm^2 (260 J/cm^2) irradiation took 10 days to return to the original tumor size pre-treatment and tumor necrosis was at 83% of the size of the original tumor area. The discovery that using an increased fluency rate over longer period of illumination results in more effective PDT treatments proves consistent with previously reported results observed using photofrin [54-56]. These improved outcomes could be attributed to the improved restoration of tissue oxygenation within the treatment area during the time of irradiation exposure [57-59].

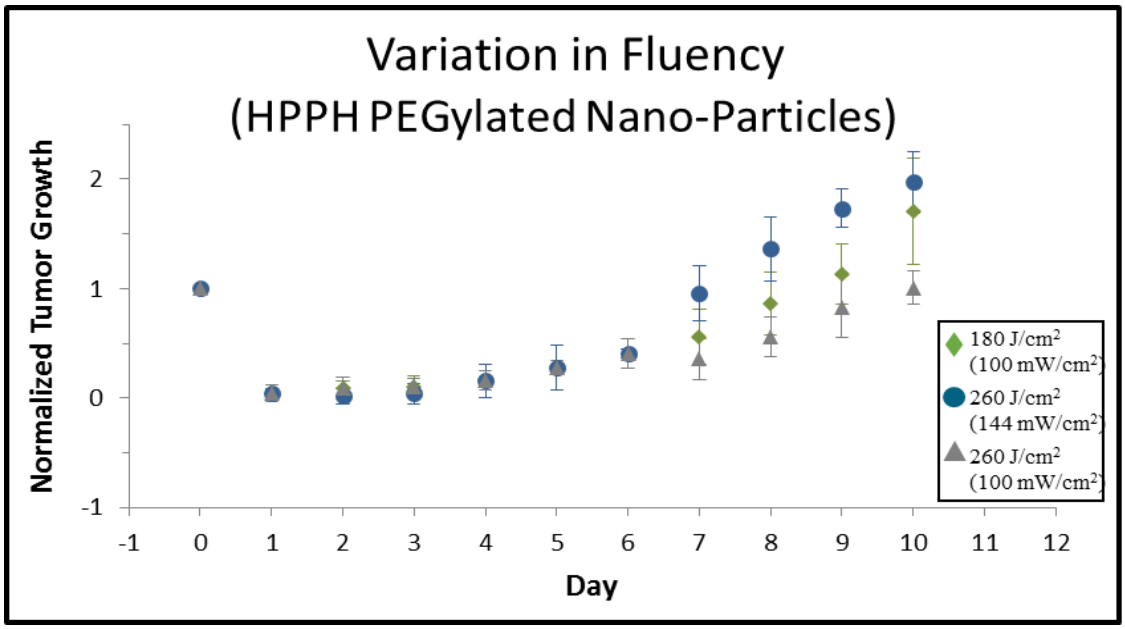

Figure 3.14: Response of glioma treated with HPPH post-loaded PEGylated polyacrylamide sensitized at 671 nm using varying irradiation regimens. Following nanoparticle incubation time of 6 hours tumors were irradiated at 180 J/cm^2 (100 mW/cm^2) – 30 minute illumination, 260 J/cm^2 (100 W/cm^2) – 45 minute illumination, and 260 J/cm^2 (144 mW/cm^2) – 30 minute illumination.

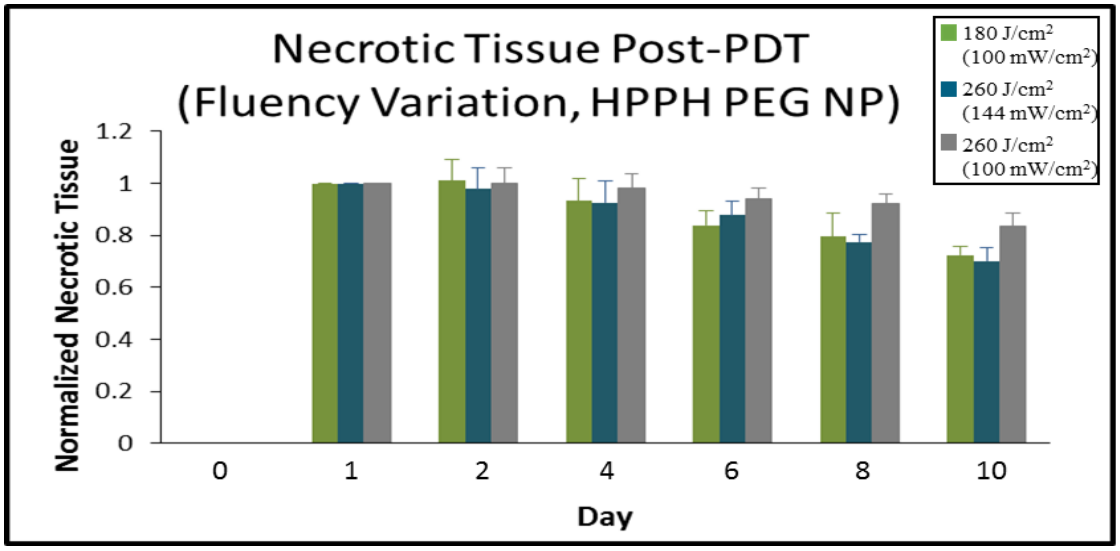

Figure 3.15: Tumor necrosis measurements for variations in fluence rates of exposed non-targeted HPPH PEGylated polyacrylamide nanoparticles. Following nanoparticle incubation time of 6 hours tumors were irradiated at 180 J/cm^2 (100 mW/cm^2) – 30 minute illumination, 260 J/cm^2 (100 W/cm^2) – 45 minute illumination, and 260 J/cm^2 (144 mW/cm^2) – 30 minute illumination using 671 nm laser light. Tumor necrosis as seen through the BTW, observed daily.

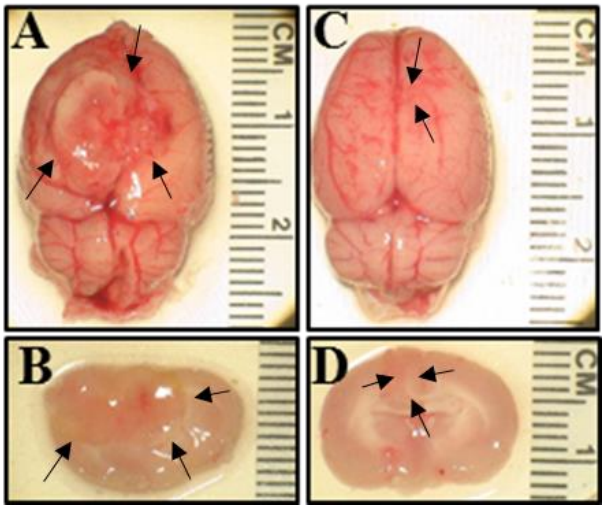

Figure 3.16: Gross specimen from animal model, excised 10 days post-PDT therapy. Representation of brain tumor for animal groups (A,B) without photosensitizer or laser illumination, and (C,D) animals receiving non-targeted HPPH nanoparticles (6 hour incubation time) with irradiation fluence dose of 260 J/cm^2 (144 mW/cm^2) using a 671 nm laser.

Optical penetration depth is the tissue thickness which results in the radiant power of light to decreases to 1/e or 37% of its initial value [60]. Beyond this depth, tissue is exposed to laser light of a lower intensity, which still may be adequate for PDT. HPPH dye has a long absorption wavelength (λ_{max} = 665 nm) allowing for deep penetration depth of laser light in live tissues, however the penetration depth varies depending on the optical properties of the treated tissue. It has been measured that laser light at 631nm can achieve a penetration depth of 1.5 ± 0.43mm in brain tissue and 2.9 ± 1.5mm in brain tumor tissue [61]. The rat models used in these experiments have tumors implanted into the cortex – a depth which may surpass the penetration depth achievable by our 671 nm laser. This limitation resulted in incomplete eradication of the base of the tumor, resulting in detectable growth patterns days after treatment. The utility of PDT in this application is restricted mainly due to the large size of the implanted tumor as compared to the post-surgical size of the residual tumor. However, the depth of the microscopic residual tumor

tissue post-surgical debulking is at a depth within treatment range, allowing PDT to be an effective post-surgery adjuvant therapy.

CONCLUSIONS

In vivo photodynamic therapy experiments led to more clearly defined treatments conditions for intra-operative glioma photodynamic therapy. We have successfully demonstrated the progress towards more optimal treatment conditions for glioma intra-operative PDT using HPPH nanoparticles. The hydrophobic photosensitizer HPPH was post-loaded into hydrogel nanoparticles with an average size of 39 nm, containing approximately 1% dye by weight. Advancements and considerable attention to nanoparticle characteristics, incubation time, and photosensitizer delivery are allowing for the quantification of PDT efficacy. The F3-targeted and PEGylated nanoparticles displayed homing and passive targeting efficiency towards the implanted 9L glioma. Both delivery methods displayed similar capacities of delivering the photosensitizer within the irradiation field which was evident through the phototoxic effect, killing the tumor cells – resulting in necrotic tissue, and ultimately retarding tumor growth in the treatment area of the BTW model. PDT treatments with HPPH polyacrylamide nanoparticles, F3-targeted or PEGylated, produced significant arrest of tumor growth over control groups, which demonstrates the potential advantages of nanoparticle-based PDT agents for the intra-operative eradication of residual brain tumors.

While all of these irradiation protocols produced delays in tumor regrowth and expressed significant amounts of tumor necrosis, investigating incident irradiation fluence rate is imperative in optimizing *in vivo* therapeutic outcomes. Photodynamic dose derives from photosensitizer exposure to photons and not simply by the total optical energy density irradiating a tissue sample.

Meaning that phototoxic success rests on the interplay of the light dose and the amount of photosensitizer circulating within the treatment field. Although this study was not designed to observe the pharmacological properties of our HPPH nanoparticles, determining photosensitizer concentrations in serum, tumor, and brain parenchyma within the treatment region, over the irradiation time, would be useful in gauging photosensitizer exposure and efficiency. This would quantify serum and tissue kinetics and the half-life of HPPH polyacrylamide over the therapeutic window. Exploring the chemical properties of the therapeutic window during treatment and the hours following treatment could quantify immediate PDT outcomes and give insight for the therapeutic index required for tumor regression. Chemical sensors detecting relative traces of O_2 along with the resulting ROS within the tumor tissue and exposed vasculature would indicate optimal fluency rates and the extent to which ROS generation is necessary to create sufficient cytotoxic effects on the localize treatment region. This knowledge could facilitate the effective delivery light doses with minimal prolongation of treatment time and laser exposure.

(This chapter was written with the intent of future publication)

ACKNOWLEDGEMENTS

We thank Dr Shouyan Wang and Dr Qinghong Yao for their useful discourse and aid in nanoparticle synthesis. Dr Oren Sagher, Dr Daniel Orringer, and Mr Dah-Luen Huang for the development of the BTW model and for animal assistance during therapy sessions. Kristen A. Simmer acknowledges funding support from the University of Michigan Rackham Graduate

School Merit Fellowship. The authors also acknowledge NIH grant R33CA125297 (RK) for research funding.

REFERENCES

[1] Biel, M. "Advances in photodynamic therapy for the treatment of head and neck cancers." *Lasers in surgery and medicine* 38.5 (2006): 349-355.

[2] Lou, P. J., et al. "Interstitial photodynamic therapy as salvage treatment for recurrent head and neck cancer." *British journal of cancer* 91.3 (2004): 441-446.

[3] Rigual, Nestor R., et al. "Adjuvant intraoperative photodynamic therapy in head and neck cancer." *JAMA Otolaryngology–Head & Neck Surgery* 139.7 (2013): 706-711.

[4] Henderson, Barbara W., and Thomas J. Dougherty. "How does photodynamic therapy work?." *Photochemistry and photobiology* 55.1 (1992): 145-157.

[5] Agostinis, Patrizia, et al. "Photodynamic therapy of cancer: an update." *CA: a cancer journal for clinicians* 61.4 (2011): 250-281.

[6] Bellnier, D. A., et al. "Murine pharmacokinetics and antitumor efficacy of the photodynamic sensitizer 2-[1-hexyloxyethyl]-2-devinyl pyropheophorbide-a."*Journal of Photochemistry and Photobiology B: Biology* 20.1 (1993): 55-61.

[7] Brasseur, Nicole, et al. "PHOTODYNAMIC ACTIVITIES and SKIN PHOTOSENSITIVITY OF THE bis (DIMETHYLTHEXYLSILOXY) SILICON 2, 3-NAPHTHALOCYANINE IN MICE." *Photochemistry and photobiology* 62.6 (1995): 1058-1065.

[8] Furukawa, Kinya, et al. "Localization and treatment of transformed tissues using the photodynamic sensitizer 2-[1-hexyloxyethyl]-2-devinyl pyropheophorbide-a." *Lasers in surgery and medicine* 18.2 (1996): 157-166.

[9] Magne, Michael L., et al. "Photodynamic therapy of facial squamous cell carcinoma in cats using a new photosensitizer." *Lasers in surgery and medicine*20.2 (1997): 202-209.

[10] Van Dongen, G. A. M. S., G. W. M. Visser, and M. B. Vrouenraets. "Photosensitizer-antibody conjugates for detection and therapy of cancer."*Advanced drug delivery reviews* 56.1 (2004): 31-52.

[11] Moan, J., and Q. Peng. "An outline of the history of PDT." *Photodynamic therapy* 2 (2003): 1-18.

[12] Pushpan, S. K., et al. "Porphyrins in photodynamic therapy-a search for ideal photosensitizers." *Current Medicinal Chemistry-Anti-Cancer Agents* 2.2 (2002): 187-207.

[13] Sharman, Wesley M., Cynthia M. Allen, and Johan E. Van Lier. "Photodynamic therapeutics: basic principles and clinical applications." *Drug discovery today*4.11 (1999): 507-517.

[14] Mellish, Kirste J., et al. "In Vitro Photodynamic Activity of a Series of Methylene Blue Analogues." *Photochemistry and photobiology* 75.4 (2002): 392-397.

[15] Orth, K., et al. "Intraluminal treatment of inoperable oesophageal tumours by intralesional photodynamic therapy with methylene blue." *The Lancet* 345.8948 (1995): 519-520.

[16] DeRosa, Maria C., and Robert J. Crutchley. "Photosensitized singlet oxygen and its applications." *Coordination Chemistry Reviews* 233 (2002): 351-371.

[17] Nseyo, Unyime O., et al. "Photodynamic therapy (PDT) in the treatment of patients with resistant superficial bladder cancer: a long term experience."*Journal of clinical laser medicine & surgery* 16.1 (1998): 61-68.

[18] Yamaguchi, Satoshi, et al. "Photodynamic therapy for cervical intraepithelial neoplasia." *Oncology* 69.2 (2005): 110-116.

[19] Loewen, Gregory M., et al. "Endobronchial photodynamic therapy for lung cancer." *Lasers in surgery and medicine* 38.5 (2006): 364-370.

[20] Overholt, Bergein F., et al. "Five-year efficacy and safety of photodynamic therapy with Photofrin in Barrett's high-grade dysplasia." *Gastrointestinal endoscopy* 66.3 (2007): 460-468.

[21] Usuda, Jitsuo, et al. "Photodynamic therapy (PDT) for lung cancers." *Journal of Thoracic Oncology* 1.5 (2006): 489-493.

[22] Dolmans, Dennis EJGJ, Dai Fukumura, and Rakesh K. Jain. "Photodynamic therapy for cancer." *Nature Reviews Cancer* 3.5 (2003): 380-387.

[23] Sibata CH, Colussi VC, Oleinick NL, and TJ Kinsella. "Photodynamic therapy in oncology". *Expert Opin Pharmacother* 2.6 (2001): 917–927.

[24] Lobel, Jeffrey, et al. "2-[1-hexyloxyethyl]-2-devinyl pyropheophorbide-a (HPPH) in a nude rat glioma model: Implications for photodynamic therapy." *Lasers in surgery and medicine* 29.5 (2001): 397-405.

[25] Bellnier, David A., et al. "Population pharmacokinetics of the photodynamic therapy agent 2-[1-hexyloxyethyl]-2-devinyl pyropheophorbide-a in cancer patients." *Cancer research* 63.8 (2003): 1806-1813. [26] Pandey, Ravindra K., et al. "Alkyl Ether Analogs of Chlorophyll-a Derivatives: Part 1. Synthesis, Photophysical Properties and Photodynamic Efficacy. "*Photochemistry and photobiology* 64.1 (1996): 194-204.

[27] Roswell Park Cancer Institute. Photodynamic Therapy in Treating Patients with Basal Cell Skin Cancer. In *ClinicalTrials.gov [Internet]. Bethesda (MD): National Library of Medicine (US)*;

Available online: http://clinicaltrials.gov/show/NCT00017485 NLM Identifier: NCT00017485 (accessed on 8 January 2014).

[28] Roswell Park Cancer Institute. Photodynamic Therapy using HPPH in Treating Patients with Recurrent Dysplasia, Carcinoma in Situ, or Stage I Oral Cavity Cancer. In *ClinicalTrials.gov [Internet]*. *Bethesda (MD): National Library of Medicine (US)*; Available online: http://clinicaltrials.gov/show/NCT00670397 NLM Identifier: NCT00670397 (accessed on 8 January 2014).

[29] Roswell Park Cancer Institute. A Trial of Photodynamic Therapy with HPPH for Treatment of Dysplasia, Carcinoma in Situ and T1 Carcinoma of the Oral Cavity and/or Oropharynx. In *ClinicalTrials.gov [Internet]*. *Bethesda (MD): National Library of Medicine (US)*; Available online: http://clinicaltrials.gov/show/NCT01140178 NLM Identifier: NCT01140178 (accessed on 8 January 2014).

[30] Roswell Park Cancer Institute. Photodynamic Therapy using HPPH in Treating Patients with Advanced Non-Small Cell Lung Cancer That Blocks the Air Passages. In *ClinicalTrials.gov [Internet]*. *Bethesda (MD): National Library of Medicine (US)*; Available online: http://clinicaltrials.gov/show/NCT00528775 NLM Identifier: NCT00528775 (accessed on 8 January 2014).

[31] Jori, Giulio. "Tumour photosensitizers: approaches to enhance the selectivity and efficiency of photodynamic therapy." *Journal of Photochemistry and photobiology B: Biology* 36.2 (1996): 87-93.

[32] Wang, Shouyan, et al. "Novel methods to incorporate photosensitizers into nanocarriers for cancer treatment by photodynamic therapy." *Lasers in surgery and medicine* 43.7 (2011): 686-695.

[33] Koo, Yong-Eun Lee, et al. "Brain cancer diagnosis and therapy with nanoplatforms." *Advanced drug delivery reviews* 58.14 (2006): 1556-1577.

[34] Koo, Yong-Eun Lee, et al. "Photonic explorers based on multifunctional nanoplatforms for biosensing and photodynamic therapy." *Applied optics* 46.10 (2007): 1924-1930.

[35] Herrmann, Kristen, et al. "Photodynamic characterization and optimization using multifunctional nanoparticles for brain cancer treatment." *SPIE BiOS*. International Society for Optics and Photonics, 2013.

[36] Reddy, G. Ramachandra, et al. "Vascular targeted nanoparticles for imaging and treatment of brain tumors." *Clinical Cancer Research* 12.22 (2006): 6677-6686.

[37] Kopelman, Raoul, et al. "Multifunctional nanoparticle platforms for in vivo MRI enhancement and photodynamic therapy of a rat brain cancer." *Journal of Magnetism and Magnetic Materials* 293.1 (2005): 404-410.

[38] Baba, Koichi, et al. "New method for delivering a hydrophobic drug for photodynamic therapy using pure nanocrystal form of the drug." *Molecular pharmaceutics* 4.2 (2007): 289-297.

[39] Wong, Joseph, et al. "Suspensions for intravenous (IV) injection: a review of development, preclinical and clinical aspects." *Advanced drug delivery reviews*60.8 (2008): 939-954.

[40] Cinteza, Ludmila O., et al. "Diacyllipid micelle-based nanocarrier for magnetically guided delivery of drugs in photodynamic therapy." *Molecular pharmaceutics* 3.4 (2006): 415-423.

[41] Hah, Hoe Jin, et al. "Methylene Blue-Conjugated Hydrogel Nanoparticles and Tumor-Cell Targeted Photodynamic Therapy." *Macromolecular bioscience* 11.1 (2011): 90-99.

[42] Moffat, Bradford A., et al. "A novel polyacrylamide magnetic nanoparticle contrast agent for molecular imaging using MRI." *Molecular imaging* 2.4 (2003).

[43] Matsumura, Yasuhiro, and Hiroshi Maeda. "A new concept for macromolecular therapeutics in cancer chemotherapy: mechanism of tumoritropic accumulation of proteins and the antitumor agent smancs." *Cancer research* 46.12 Part 1 (1986): 6387-6392.

[44] Maeda, Hiroshi. "The enhanced permeability and retention (EPR) effect in tumor vasculature: the key role of tumor-selective macromolecular drug targeting."*Advances in enzyme regulation* 41.1 (2001): 189-207.

[45] Weissleder, Ralph, et al. "MR lymphography: study of a high-efficiency lymphotrophic agent." *Radiology* 191.1 (1994): 225-230.

[46] Moghimi, S. Moein, A. Christy Hunter, and J. Clifford Murray. "Long-circulating and target-specific nanoparticles: theory to practice." *Pharmacological reviews*53.2 (2001): 283-318.

[47] Moghimi, S. M., and B. Bonnemain. "Subcutaneous and intravenous delivery of diagnostic agents to the lymphatic system: applications in lymphoscintigraphy and indirect lymphography." *Advanced drug delivery reviews* 37.1 (1999): 295-312.

[48] Moreno, Maria João, et al. "Production of singlet oxygen by Ru(dpp(S03) & incorporated in polyacrylamide PEBBLES." *Sensors and Actuators B: Chemical* 90.1 (2003): 82-89.

[49] Yan, Fei, and Raoul Kopelman. "The Embedding of Meta-tetra (Hydroxyphenyl)-Chlorin into Silica Nanoparticle Platforms for Photodynamic Therapy and Their Singlet Oxygen Production and pH-dependent Optical Properties."*Photochemistry and photobiology* 78.6 (2003): 587-591.

[50] "Supporting Your Micro QC Requirements." *Endotoxin Detection and Microbial Identification*. N.p., n.d. Web, < http://www.criver.com>. , 7 Jan. 2014.

[51] Orringer, Daniel A., et al. "The brain tumor window model: a combined cranial window and implanted glioma model for evaluating intraoperative contrast agents." *Neurosurgery* 66.4 (2010): 736-743.

[52] Kim, Sehoon, et al. "Organically modified silica nanoparticles co-encapsulating photosensitizing drug and aggregation-enhanced two-photon absorbing fluorescent dye aggregates for two-photon photodynamic therapy." *Journal of the American Chemical Society* 129.9 (2007): 2669-2675.

[53] Nie, Guochao, et al. "Hydrogel nanoparticles with covalently linked coomassie blue for brain tumor delineation visible to the surgeon." *Small* 8.6 (2012): 884-891.

[54] Sitnik, Theresa M., and Barbara W. Henderson. "The effect of fluence rate on tumor and normal tissue responses to photodynamic therapy." *Photochemistry and photobiology* 67.4 (1998): 462-466.

[55] Foster, T. H., S. L. Gibson, and R. F. Raubertas. "Response of Photofrin-sensitised mesothelioma xenografts to photodynamic therapy with 514 nm light." *British journal of cancer* 73.8 (1996): 933.

[56] Gibson, S. L., et al. "Effects of photodynamic therapy on xenografts of human mesothelioma and rat mammary carcinoma in nude mice." *British journal of cancer* 69.3 (1994): 473.

[57] Henderson, Barbara W., et al. "Photofrin photodynamic therapy can significantly deplete or preserve oxygenation in human basal cell carcinomas during treatment, depending on fluence rate." *Cancer research* 60.3 (2000): 525-529.

[58] Sitnik, T. M., J. A. Hampton, and B. W. Henderson. "Reduction of tumour oxygenation during and after photodynamic therapy in vivo: effects of fluence rate." *British journal of cancer* 77.9 (1998): 1386.

[59] Foster, Thomas H., et al. "Analysis of photochemical oxygen consumption effects in photodynamic therapy." *OE/LASE'92*. International Society for Optics and Photonics, 1992.

[60] Dougherty, T. J., KR, and Weishaupt, and D. G. Boyle. "Photodynamic sensitizers." *Cancer: principles and practice of oncology* 2 (1985): 2272-2279.

[61] Muller, Paul J., and Brian C. Wilson. "Photodynamic therapy of malignant primary brain tumours: clinical effects, postoperative ICP, and light penetration of the brain." *Photochemistry and photobiology* 46.5 (1987): 929-935.

CHAPTER 4

Efficacy of Reactive Oxygen Species Production for Methylene Blue and Coomassie Blue Mixture: For Possible Combined Tumor Delineation and Therapy

INTRODUCTION

For most patients diagnosed with brain tumors, surgical resectioning is an essential treatment modality. However, visually determining tumor margins at the microscopic level when performing the operation proves difficult for surgeons. Measureable differences in quality of life and survival rates have been directly correlated to the extent of surgical resectioning, which in turn is limited by the ability to distinguish tumor boundaries [1-2]. In the current clinical setting, resectioning of the tumor is mostly aided by preoperative imaging acquired by ultrasound, X-Ray CT, or intraoperative MRI (magnetic resonance imaging). Tumor structural shifts and interval growth, not detected by preoperative image guided surgery, can lead to significant resectioning inaccuracy, because tumor margins detected by low resolution imaging cannot be easily translated to tumor margins in the operative field. Intra-operative real time imaging aided by MRI would allow for the surgeon to detect residual tumor tissue in the operating room. However, operative delays for comparative imaging, limited signal distinctions between tumor resectioning and retraction injury, and significant cost make intraoperative MRI an infrequently implemented method for surgical imaging.

Various attempts to visually delineate tumor margins on the operative field have been made using fluorescent and visible reagents: Coomassie Blue, Bromophenol Blue, fluorescein, Indocyanine Green, 5-aminolevulinic acid (5-ALA), and fluorescent porphyrins [3-11]. Fenestrations in the vasculature wall of the blood brain barrier allow these dyes to preferentially accumulate and stain malignant glioma for delineation of neoplastic tissue within the operative field. However, the use of delineating dyes has various restrictions. For instance, fluorescence based dye delineation requires the use of special lighting conditions under dark operative settings, posing higher surgical risks. Attempting adequate visual delineation between tumor and non-neoplastic tissue, required the use of high concentrations of intravenous contrast dyes – which can be associated with systemic toxicity [5]. As a result of this drawback, it is important to maintain low therapeutic doses of contrast dyes while sustaining delineation potential, a fiat that has proven difficult.

The Kopelman group has investigated Coomassie Blue dye and nanoparticle delineated glioma, proving that this method is effective in enhancing visualization of the tumor brain interface in rat models while maintaining optimal operative conditions [3, 12-13]. The deep blue color of Coomassie Blue offers brilliant contrasts against non-neoplastic tissue, blood, and other crucial structures near the tumor.

The Coomassie Blue dye has been covalently linked to the polyacrylamide matrix of a nanoparticle with surface modifications by conjugation of F3-peptides, for active tumor targeting, and polyethylene glycol (PEG), for longer plasma circulation (~24 hrs) [14]. Selective targeting and retention within the tumor tissue is a limiting factor for the use of free dye molecules as a delineating agent, which may be overcome by utilizing nanoparticles. Additional accumulation of the nanoparticles within tumor tissue and vasculature is abetted by the “enhanced permeability and

retention effect" (EPR), allowing tissue retention of macromolecules by way of leaky microvasculature and poor lymphatic drainage [15-17].

Though surgery is the most effective treatments for patients with glioblastoma, residual tumor cells left behind during surgical resectioning could cultivate recurring tumors. Adjuvant therapy such as photodynamic therapy could aid in the removal of residual tissue left behind by surgeons, enhancing the chances of palliating the disease and increase patient survival rates.

The Methylene Blue dye has been reported for numerous medical applications and therapies including photodynamic therapy [18-22]. Similar to delineation dyes, Methylene Blue has the potential to accumulate in tumor tissue, however enzymatic degradation of the dye produces a colorless form of the dye - failing to pigment tumor tissue [23]. Its incorporation into a nanoparticle composed of polyacrylamide (PAA) matrix serves to embed the active form of the Methylene Blue photosensitizer, protecting it against enzymatic degradation into the colorless and photochemically inactive form of Leuko-Methylene Blue (LMB). Thus, incorporating the photosensitizing dye into the same polyacrylamide nanoparticle designed for delineating dyes, might serve to guard the active form of Methylene Blue [23].

It has previously been shown, that polyacrylamide nanoparticles can be utilized as a vehicle to transport for multiple types of molecules such as delineating/imaging agents and drugs to tumors [24-31]. Thus, collectively incorporating Coomassie Blue and Methylene Blue dyes in polyacrylamide nanoparticles can potentially produce a biofunctional agent that can be used for both delineation purposes during intraoperative surgery and as a photosensitizing drug in the adjuvant treatment of PDT.

Here we investigate the possibility of combining Methylene Blue and Coomassie Blue for potential dual application of diagnostics and therapy and quantify its ability to efficiently produce reactive oxygen species. A mixture of Methylene Blue and Coomassie Blue dye, at different ratios, was used and the amount of reactive oxygen species produced 'k-value' was monitored as a function of this ratio. We observe a steady decrease in the k-value with increasing concentration of Coomassie Blue dye. This may be attributed to the quenching of the ROS due to incorporation of Coomassie Blue dye into the Methylene Blue mixture. These results suggests that introducing Coomassie Blue and Methylene Blue dye in the nanoparticle will reduce the PDT efficiency and ultimately might not be the best choice for this dual application.

EXPERIMENTAL

Materials

Methylene Blue succinimidyl ester (MB-SE) was purchased from Emp. Biotech. Phosphate-buffered solution (PBS) was made using a phosphate-buffered saline tablet from Sigma-Aldrich. 9,10-dipropionic acid disodium salt (ADPA) was purchased from Invitrogen. A stock solution of 100 μM ADPA was made in water and kept in the dark until use. The water used throughout the experiments was purified by Millipore Milli-Q Advantage A10 water purification system by Millipore. All chemicals were used as purchased without further purification.

Reactive oxygen species detection

ADPA was used to detect the rate of production of ROS from Meythelene Blue when combined with Coomassie Blue dye, compared to Methylene Blue free dye. ADPA is an anthracene based dye which becomes oxidized by ROS, producing non-fluorescent ADPA endoperoxide, leading to a reduction in detectable fluorescence intensity [32]. A stock solution of ADPA in PBS (100 µM) was prepared and stored in the refrigerator, under dark conditions (wrapped in foil covering), between uses. However, fresh solutions of ADPA were prepared for every experiment to avoid inaccuracies as a result of oxidation/photobleaching during storage. Solutions of 80 µL ADPA was mixed into 2 mL of 1 µM Methylene Blue free dye in PBS solution. Coomassie Blue dye was added to the 2 mL solution at varying concentrations (1, 2, 2.5, 3, 3.5, 5, 8, 10 µM). The oxidation of the ADPA, due to the ROS produced, was monitored by measuring the fluorescence intensity for 25 minutes (measuring time points of 0 sec, 1 min, 2 min, 3 min, 4 min, 5 min, 10 min, 15 min, 20 min, and 25 min), while the solution was irradiated using 660 nm excitation beam (slit width of 10 nm) under constant stirring to ensure solution homogeneity and to replenish oxygen diffusion within the sample. The fluorescence spectrum of ADPA was evaluated and measured using a fluorimeter (FluoroMax-3, Jobin Yvon/SPEX Division, Instruments S.A. Inc., Edison, NJ, USA).

RESULTS AND DISCUSSION

The production of reactive oxygen species from Methylene Blue free dye was tested by monitoring the fluorescence emission from ADPA. Figure 4.2A shows the fluorescence emission spectra of ADPA in a mixture of 1.0 µM Methylene Blue dye in PBS, after irradiation at the excitation wavelength at different time points. The spectra shows a gradual decrease in the fluorescence

emission intensity of ADPA with the increase in irradiation time. The slope of the linear curve obtained by plotting the logarithm of the ratio of ADPA fluorescence intensity at 431 nm, at time 't' vs the initial intensity, provides the rate constant, as shown in Figure 4.2A. ADPA in a mixture of 1.0 µM Methylene Blue dye in PBS expresses a very strong fluorescence at 431 nm, with first-order decay rate constant (k-value), calculated as $\ln([ADPA]_t/[ADPA]_o) = -kt$, to be $5.5x10^{-4}$/s [32].

Mixtures of Methylene Blue and Coomassie Blue dye, at different ratios, were used to determine the effectiveness of ROS production from each mixture and obtain an optimal ratio. This optimized ratio can then be used for preparation of the dual-functional nanoparticles. The sensitivity of Methylene Blue ROS generation was tested to evaluate the effect of co-loading a delineating dye, Coomassie Blue, along with the photosensitizing dye Methylene Blue into polyacrylamide nanoparticles.

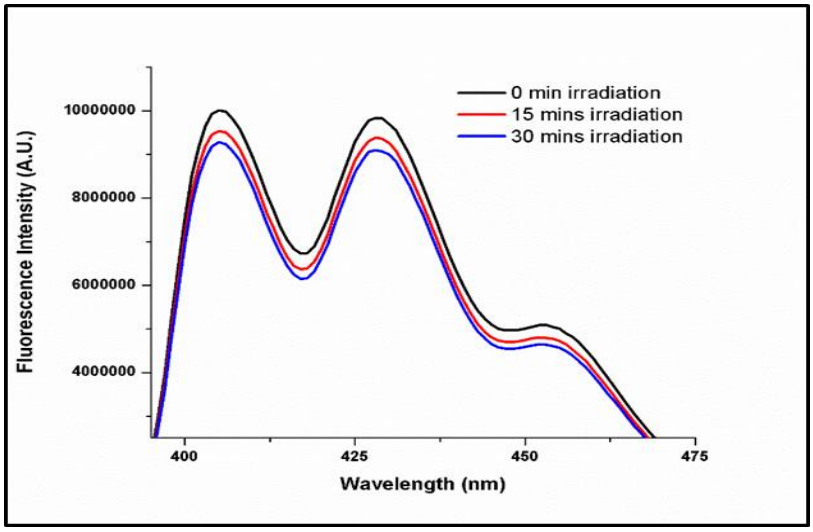

Figure 4.1: Fluorescence spectra of ADPA over a time course of 30 minutes.

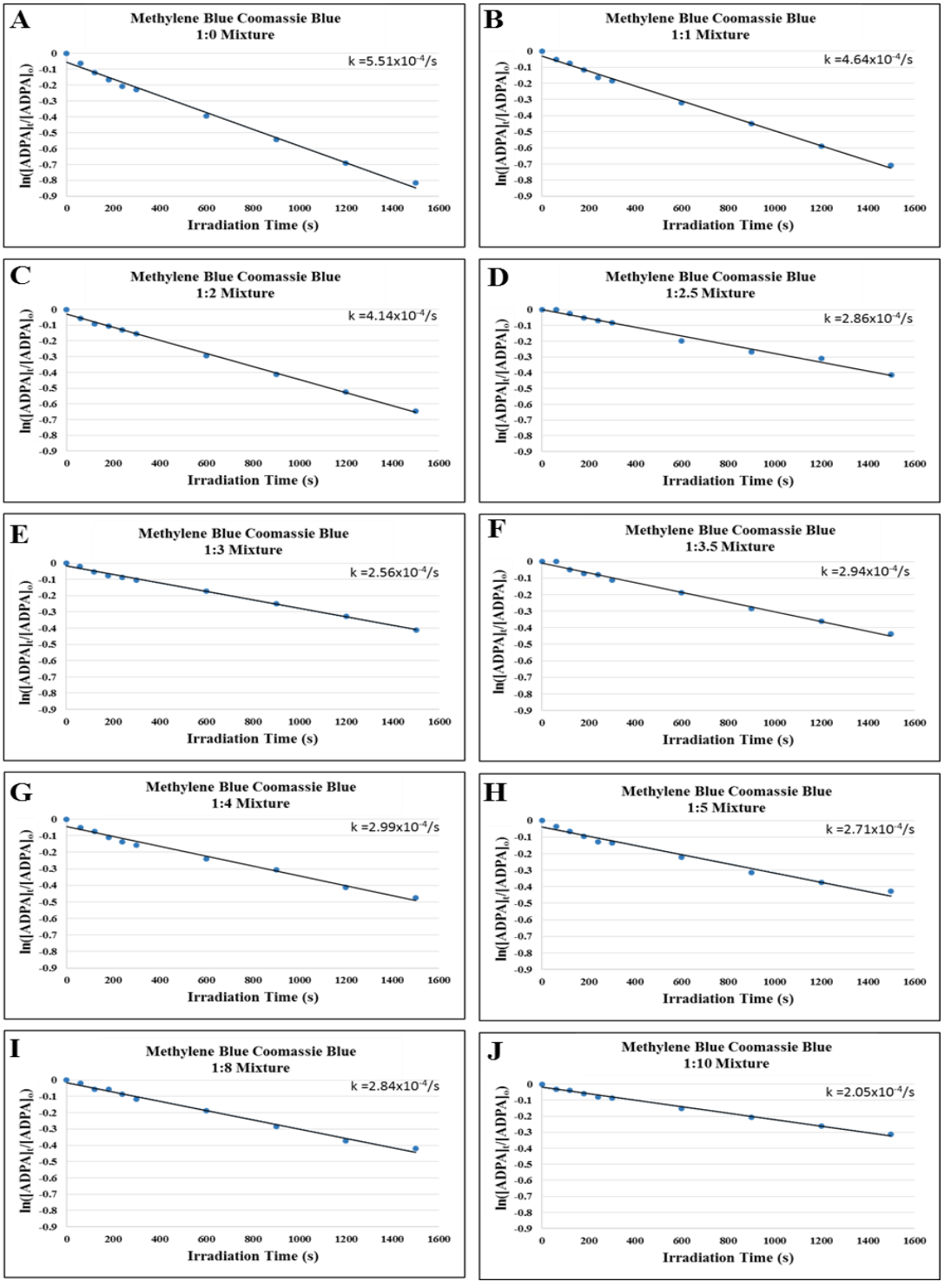

Figure 4.2: ADPA was used to detect the ROS production from Methylene Blue when combined with Coomassie Blue dye. The logarithm of the ratio of ADPA fluorescence intensity at 431nm provides the first order decay rate constant, or k-value. A) Calculation of the rate of ROS production from MB free dye using ADPA. (B-J) ROS production of various MB:CB mixtures.

Solutions of various concentrations of Methylene Blue to Coomassie Blue were examined under identical conditions of irradiation, using 1.0 µM MB free dye in PBS, with 660 nm excitation for 25 minutes. The decay rates of ADPA fluorescence, for each Methylene Blue – Coomassie Blue concentration ratio, were examined using fluorescence spectroscopy and plotted in Figure 4.3 so as to compare the ROS production rates using increased amounts of Coomassie Blue delineation dye. Methylene Blue dye solution or Methylene Blue - Coomassie Blue mixture solution of various concentrations in PBS was mixed with ROS detecting probe, ADPA, in a cuvette.

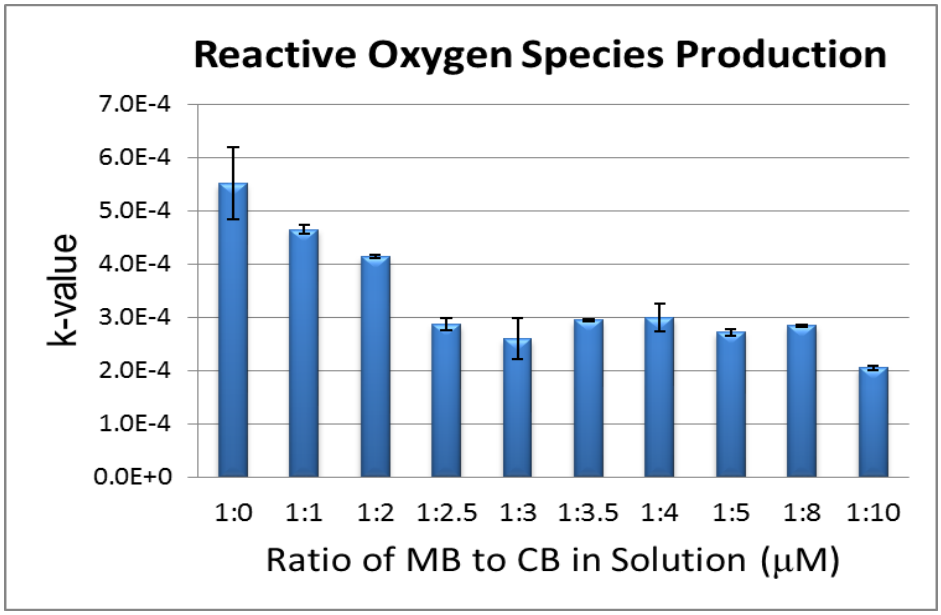

Figure 4.3: Comparison of ROS generation from the various compositions of Methylene Blue and Coomassie Blue mixtures.

Methylene Blue free dye exhibited a significantly faster fluorescence decay compared to Methylene Blue – Coomassie Blue mixtures, clearly indicating Methylene Blue dye alone has better ROS production ability. Among all formulations, the lowest concentration Coomassie Blue

mixture showed the highest reactive oxygen production. ROS production from 1:2 Methylene Blue and Coomassie Blue was reduced by 25%, compared to Methylene Blue alone, due to the presence of Coomassie Blue.

After a sudden decrease, the k-value begins to plateau for the dye ratios between 1:2.5 and 1:8 Methylene Blue to Coomassie Blue (Figure 4.3). This range showed equivalent intensities, with k-value of about $3x10^{-4}$, approximately a 50% reduction in ROS production as compared to Methylene Blue dye solution. The ROS generation of various dye compositions was significantly less than that of Methylene Blue dye only, and continued to decrease as the Coomassie Blue content in the solution increased.

ROS production, in the form of singlet oxygen, superoxide, peroxides, etc., is generated from the excited Methylene Blue molecule, with the nature of the mix depending on the ratio of monomeric to dimeric state [33]. The primary component of the generated ROS, singlet oxygen, has a short lifetime (0.04 μs) and an average diffusion distance of 0.02 μm in media [27]. This limitation gets worse with a highly concentrated media sample, and also when increasing the amount of Coomassie Blue molecules in the sample, because the proximity of excited photosensitizer to other quencher/dye molecules could result in significant quenching of the radicals produced. As displayed in Figure 1, using Coomassie Blue dye contents greater than 2.5 μM, the k-values are observed to plateau, or in some cases decrease, with the increased addition of Coomassie Blue dye. This can be attributed to saturation and the quenching of ROS production. Additionally the presence of Coomassie Blue dye can lead to dimerization or aggregation of the Methylene Blue dye, which has lower quantum yield, or even formation of complexes between the two, which could potentially quench the Methylene Blue dye. All or some of the above mentioned factors leads to a reduction in ROS production.

Irradiation of brain tumors, for PDT, in Chapter 2 utilized Methylene Blue polyacrylamide nanoparticles with 0.37% wt/(NP wt) dye loading. In comparison, the Coomassie Blue polyacrylamide nanoparticle used for tumor differentiation studies required 7% wt/(NP wt) Coomassie Blue dye loading for obtaining a sufficient color delineation effects in a rat BTW model [13]. Among all preparations, only the Methylene Blue and Coomassie Blue in 1:8 and 1:10 ratio would allow for a Coomassie Blue dose effective for delineation, however with ROS production efficiency of 51% and 37%, such mixtures fail to generate effective cytotoxic destruction capable to elicit a long-term damage to the tissue.

While dye loading contrast agents at such high doses allows for visual differentiation of tumor tissue from adjacent brain tissue, consequently the high dye loading reduces the PDT efficacy due to decrease in ROS production. Meanwhile, dye loading contrast agents in low concentrations would permit sufficient ROS production, insignificant amounts of delineating dye would result in undetected demarcation between healthy and tumor tissue for *in vivo* delineation purposes.

CONCLUSIONS

Here we investigate the combination Methylene Blue and Coomassie Blue dyes for potential dual application of diagnostics and therapy and quantify its ability to efficiently produce reactive oxygen species. A mixture of Methylene Blue and Coomassie Blue dye, at different ratios, was used and the amount of ROS produced 'k-value' was monitored as a function of this ratio. We observe a decrease in the k-value with increasing concentration of Coomassie Blue dye, e.g., a 50% reduction in ROS production at 1:2.5 and only 37% efficacy at 1:10 Methylene Blue:Coomassie Blue, as compared to a pure Methylene Blue solution . This is attributed to the

quenching of ROS due to the incorporation of Coomassie Blue dye into the Methylene Blue mixture. These results suggests that introducing Coomassie Blue in addition to Methylene Blue dye in the nanoparticle will reduce the PDT efficiency and ultimately might not be optimal for this dual application.

The results of combining PDT and visual delineation emphasizes the need for an alternate strategy to achieve the goal of tumor delineation and therapy. Therefore, it is necessary to investigate the relationship between two separate nanoparticles, one for delineation purposes and the second dedicated for therapeutic treatment. Systemic interplay and accumulation in the treatment field would need to be investigated to ensure concentrations of both the delineating nanoparticle and photosensitive nanoparticle to serve their individual purpose.

ACKNOWLEDGEMENTS

The authors would like to thank Dr Yong-Eun Lee Koo for her advice and assistance. This research has been funded by NIH grant R01EB007977 (RK).

REFERENCES

[1] Sanai, Nader, and Mitchel S. Berger. "Glioma extent of resection and its impact on patient outcome." *Neurosurgery* 62.4 (2008): 753-766.

[2] Lo, Simon S., et al. "Single dose versus fractionated stereotactic radiotherapy for meningiomas." *The Canadian Journal of Neurological Sciences* 29.3 (2002): 240-248.

[3] Orringer, Daniel A., et al. "The brain tumor window model: a combined cranial window and implanted glioma model for evaluating intraoperative contrast agents." *Neurosurgery* 66.4 (2010): 736-743.

[4] Britz, Gavin W., et al. "Intracarotid RMP-7 enhanced indocyanine green staining of tumors in a rat glioma model." *Journal of neuro-oncology* 56.3 (2002): 227-232.

[5] Hansen, Douglas A., et al. "Indocyanine green (ICG) staining and demarcation of tumor margins in a rat glioma model." *Surgical neurology* 40.6 (1993): 451-456.

[6] Moore, George E. "Fluorescein as an agent in the differentiation of normal and malignant tissues." *Science* 106.2745 (1947): 130-131.

[7] Moore, George E., et al. "The Clinical Use of Fluorescein in Neurosurgery: The localization of brain tumors." *Journal of neurosurgery* 5.4 (1948): 392-398.

[8] Ozawa, Tomoko, et al. "Bromophenol blue staining of tumors in a rat glioma model." *Neurosurgery* 57.5 (2005): 1041-1047.

[9] Stummer, Walter, et al. "Fluorescence-guided surgery with 5-aminolevulinic acid for resection of malignant glioma: a randomised controlled multicentre phase III trial." *The lancet oncology* 7.5 (2006): 392-401.

[10] Veiseh, Mandana, et al. "Tumor paint: a chlorotoxin: Cy5. 5 bioconjugate for intraoperative visualization of cancer foci." *Cancer research* 67.14 (2007): 6882-6888.

[11] Shinoda, Jun, et al. "Fluorescence-guided resection of glioblastoma multiforme by using high-dose fluorescein sodium: technical note." *Journal of neurosurgery*99.3 (2003): 597-603.

[12] Orringer, Daniel, et al. "Dye-loaded nanoparticle." U.S. Patent Application 12/565,583.

[13] Nie, Guochao, et al. "Hydrogel nanoparticles with covalently linked coomassie blue for brain tumor delineation visible to the surgeon." *Small* 8.6 (2012): 884-891.

[14] Moffat, Bradford A., et al. "A novel polyacrylamide magnetic nanoparticle contrast agent for molecular imaging using MRI." *Molecular imaging* 2.4 (2003).

[15] Matsumura, Yasuhiro, and Hiroshi Maeda. "A new concept for macromolecular therapeutics in cancer chemotherapy: mechanism of tumoritropic accumulation of proteins and the antitumor agent smancs." *Cancer research* 46.12 Part 1 (1986): 6387-6392.

[16] Maeda, Hiroshi. "The enhanced permeability and retention (EPR) effect in tumor vasculature: the key role of tumor-selective macromolecular drug targeting."*Advances in enzyme regulation* 41.1 (2001): 189-207.

[17] Henderson, Barbara W., and Thomas J. Dougherty. "How does photodynamic therapy work?." *Photochemistry and photobiology* 55.1 (1992): 145-157.

[18] Wainwright, Mark. "Non-porphyrin photosensitizers in biomedicine." *Chem. Soc. Rev.* 25.5 (1996): 351-359.

[19] Orth, K., et al. "Photochemotherapy of experimental colonic tumours with intra-tumorally applied methylene blue." *Langenbeck's Archives of Surgery* 383.3-4 (1998): 276-281.

[20] Dalla, Via L., and Magno S. Marciani. "Photochemotherapy in the treatment of cancer." *Current medicinal chemistry* 8.12 (2001): 1405-1418.

[21] Williams, J. L., et al. "Methylene blue and the photodynamic therapy of superficial bladder cancer." *Journal of Photochemistry and Photobiology B: Biology* 4.2 (1989): 229-232.

[22] Tardivo, J. P., et al. "Treatment of melanoma lesions using methylene blue and RL50 light source." *Photodiagnosis and Photodynamic Therapy* 1.4 (2004): 345-346.

[23] Hah, Hoe Jin, et al. "Methylene Blue-Conjugated Hydrogel Nanoparticles and Tumor-Cell Targeted Photodynamic Therapy." *Macromolecular bioscience* 11.1 (2011): 90-99.

[24] Herrmann, Kristen, et al. "Photodynamic characterization and optimization using multifunctional nanoparticles for brain cancer treatment." *SPIE BiOS*. International Society for Optics and Photonics, 2013.

[25] Koo, Yong-Eun Lee, et al. "Brain cancer diagnosis and therapy with nanoplatforms." *Advanced drug delivery reviews* 58.14 (2006): 1556-1577.

[26] Koo, Yong-Eun Lee, et al. "Photonic explorers based on multifunctional nanoplatforms for biosensing and photodynamic therapy." *Applied optics* 46.10 (2007): 1924-1930.

[27] Reddy, G. Ramachandra, et al. "Vascular targeted nanoparticles for imaging and treatment of brain tumors." *Clinical Cancer Research* 12.22 (2006): 6677-6686.

[28] Kopelman, Raoul, et al. "Multifunctional nanoparticle platforms for in vivo MRI enhancement and photodynamic therapy of a rat brain cancer." *Journal of Magnetism and Magnetic Materials* 293.1 (2005): 404-410.

[29] Wong, Joseph, et al. "Suspensions for intravenous (IV) injection: a review of development, preclinical and clinical aspects." *Advanced drug delivery reviews*60.8 (2008): 939-954.

[30] Cinteza, Ludmila O., et al. "Diacyllipid micelle-based nanocarrier for magnetically guided delivery of drugs in photodynamic therapy." *Molecular pharmaceutics* 3.4 (2006): 415-423.

[31] Baba, Koichi, et al. "New method for delivering a hydrophobic drug for photodynamic therapy using pure nanocrystal form of the drug." *Molecular pharmaceutics* 4.2 (2007): 289-297.

[32] Moreno, Maria João, et al. "Production of singlet oxygen by Ru(dpp(S03) & incorporated in polyacrylamide PEBBLES." *Sensors and Actuators B: Chemical* 90.1 (2003): 82-89.

[33] Yoon, Hyung Ki, et al. "Nano-photosensitizers Engineered to Generate a Tunable Mix of Re-active Oxygen Species, for Optimizing Photodynamic Therapy, Using a Microfluidic Device." *Chemistry of Materials* (2013).

CHAPTER 5

FUTURE DIRECTIONS

1. Nanoparticles for therapy and tumor delineation: This thesis focuses on development of nanoparticles as a PDT agent and their application to glioma as an adjuvant therapy to surgery. Thus, as mentioned in chapter 4, using the same nanoparticle for therapy as well as for delineating the tumor boundary is an attractive proposition. However there lies a delicate balance between the ratio of photosensitizer and the contrast agent that can be incorporated into the nanoparticle. A high loading of contrast agents would be needed to provide a clear visual demarcation, however this in turn would reduce the efficacy of PDT by quenching the amount of ROS produced. Additionally some photosensitizers, such as Methylene Blue, have a drawback that at high local concentration they tend to form molecular dimers, which reduces the ROS production efficiency. A few alternate approaches that might enable this dual mode are listed below:

(i). Utilizing Indocyanine Green (ICG) as a multifunctional molecule for therapy and providing visual contrast agent: ICG is a tri-carbocyanine dye that has been approved by the FDA for several applications [1]. Although it has a relatively low yield of ROS production, as compared to Methylene Blue or HPPH, it has been successfully utilized for treatment of tumors in the past [2-4]. The photo-toxicity of the ICG comes from two mechanisms: 1) the production of ROS that results in PDT, 2) Localized heating which is known as photothermal therapy [2-4]. Additionally, ICG can be used as visual contrast as well as a fluorescent contrast agent. The deep green color

can provide a strong visual contrast, and has been previously used to demarcate rat glioma with a high degree of success [5]. ICG also has excellent fluorescence properties that have been exploited for imaging tumors [6]. The main advantage of using ICG over other commonly used photosensitizers is that its absorption peak (780 nm), as well as its fluorescence emission peak (~800 nm) lies in the infrared region of the spectrum, making it extremely efficient for *in vivo* applications due to the larger penetration depth of light at this wavelength, compared to the visible region. With ICG nanoparticles it may be possible to achieve this aim of using the same nanoparticle as contrast agent as well as for therapeutic applications. Incorporating ICG into a nanoparticle will also improve other undesirable properties seen in other photosensitive dyes, such as 1) tendency to dimerize, 2) fast photobleaching, 3) molecular degradation as well as cell specific targeting abilities [7]. The challenge lies in designing the appropriate nanoparticle as the carrier for ICG and optimizing its loading.

(ii). Utilizing core shell nanoparticles containing photosensitizers and noble metals: Using a noble metal core it is possible to enhance the efficiency of the photosensitizer to produce ROS [8-9]. This enhancement is due to the presence of surface plasmon resonance, which is the act of oscillating electrons present on the surface of noble metals by the activation of light. Surface plasmons can be excited by illuminating the metal surface at an appropriate wavelength [10]. By maintaining the photosensitizers at appropriate distance from the metal surface, typically on the order of 10 nm, it is possible to enhance the dye's characteristics - fluorescence and generation of ROS. Other properties such as resonance energy transfer and surface non-linearity can also provide the desirable effects [11]. Light illumination in the presence of the metal core will not only irradiate the cells, but also significantly heat the adjacent tissue and thus contribute towards cellular death due to photothermal effects. This will lead to a synergistic effect, thereby improving the cell killing

efficiency of the nanoparticle. Additionally, the scattering from metal surface may also enhance the visual contrast provided by the photosensitizer. These nanoparticles containing a metal core also have the potential to lend excellent contrast enhancements for imaging modalities such as X-Ray CT and photoacoustics, which are popular diagnostic tools.

2. Dynamic monitoring of oxygen levels in tissue before, during, and after therapy: Oxygen plays a key role in PDT. The photosensitizers, when irradiated with an appropriate wavelength of light, becomes excited and this energy is transferred to oxygen, so as to create ROS [12]. Thus monitoring the tissue oxygen level before treatment can be extremely critical, to predict and evaluate the success of this therapy. Additionally, continuous monitoring of oxygen levels during light irradiation will enable a better fundamental understanding of the dynamics of this process *in vivo* (oxygen consumption and replenishment at different tissue depth). Several different types of nanosensors have been utilized in the Kopelman lab for quantitative measurement of molecular oxygen in cells and *in vivo* using fluorescence and photoacoustics [13-14]. These nanosensors can be used along with the photosensitizer loaded nanoparticle for monitoring the oxygen level in tumors. By having the same polymer matrix as well as physical and chemical properties, the nanoparticle mixture is expected to have a similar distribution throughout the tumor after injection into the animals. Alternately, the photosensitizer itself can be used as a reporter of the local oxygen level in addition to therapeutic use [15-16].

3. Monitoring the dynamics of therapy and determining the therapeutic index: Clinically PDT has been performed using the photosensitizer in its free molecular form. The use of nanoparticles for this application has recently gained prominence, and to maximize the effect of nanoparticle

aided PDT, it is essential to study the dynamics of cell killing and changes in tissue properties during the therapeutic window, as well as monitor the local nanoparticle distribution. This necessitates the quantification of nanoparticles inside the tumor tissue, right before and during the light irradiation process. Dynamic quantification of the three dimensional concentration of the nanoparticle in animal models can be achieved using imaging techniques, such as MRI, X-Ray, optical imaging, etc., and by loading an appropriate contrast agent into the nanoparticle [17]. The damage to tumor tissue, and the effective cellular death, at different depths, can be monitored by staining the cells with different markers (e.g., propidium iodide) and performing *in vivo* optical microscopy [18]. Staining the different cellular components will enable us to monitor the dynamics of tissue damage at the subcellular level. Alternately, assessment of this information can be achieved using histopathology, although this would require sacrificing a large number of animals to obtain temporal information.

Another important parameter is the determination of the therapeutic index of this type of nanoparticle. This is an essential factor that would give an indication regarding the suitability of these nanoparticles as drugs and possible applications on humans.

4. Investigating adverse effects and treatment response: Our study demonstrated tumor growth response to the use of nanoparticle mediated photodynamic therapy, however patient pain assessment and visual impairments have not been examined for these treatment parameters. The side effects may be mild, moderate, or severe but these are not yet known. While treating the animals with various treatment regimens, no adverse effects of the treatment were apparent.

(i). Abating treatment induced pain in patients: Light illumination and fluency rates are key factors in refining neoplastic response to therapy. Although various illumination protocols may allow for

the eradication of residual cells, the therapy protocol may induce intolerable discomfort for patients. Animals were stabilized in stereotactic head holders and anesthetized with inhaled isoflurane during irradiation. These conditions made it difficult to assess pain tolerance during therapy sessions as a result of warmth generated during irradiation treatments. Pain can be controlled by cooling off the tumor site location, however this method would have extended investigations associated with vasodilation *versus* vasoconstriction and variations in nanoparticle delivery to the tumor site. This retrospective analysis between irradiance and pain could assist in fixing maximal power doses and fluency rates.

(ii). Assessing laser effects on visual performance: In addition to pain evaluation, routine eye examinations pre- and post-therapy are necessary for detecting retinal damage. Long periods of laser exposure to the brain may cause histological changes to the eye [19-20]. Systemic circulation of photosensitizers inherently passes through the choroid, vascular layer located between the sclera and retinal walls, and, if irradiated, iatrogenic phototoxicity to nerve cells in the retina and macula would occur. The macula covers about five degrees of the visual field, however it is the only part of the eye that enables precise vision and detection of colors. If extensive damage occurs in the retinal periphery, impairments to normal vision may cause nearsightedness [21]. Furthermore, disruptions of membrane pumps responsible for regulating hydration of the eye can result in pressure changes within the eye causing temporary visual disturbances. These potential hazardous destructions of the eye could limit patients from resuming normal activity or function as a result of thermal and scattering effects of lasers [22]. Optimal PDT condition that involve pain reduction and treatment efficiency with better defined properties within the therapeutic index to decrease treatment time would be the principal goals in the continuation of nanoparticle mediated PDT.

5. Combination of surgery and PDT: The primary focus of this thesis is utilizing nanoparticle containing photosensitizers for PDT, as an adjuvant therapy to surgery. The results presented here show that the nanoparticles efficiently halt the tumor growth and a large amount of necrosis is observed on the tumor surface. However the halting of the tumor growth is temporary, indicating that the effectiveness of this therapy is mostly superficial. Monitoring the tissue damage as a function of depth, by performing experiments proposed in the previous section, will help in optimizing this specific therapeutic process. Additionally, the efficacy of this process can be improved by optimizing the light dose and the different associated parameters, such as the photon flux, illumination process, etc. Modeling the light propagation through the brain/tumor tissue containing nanoparticles will give an insight into the intensity of light at different depths. This can be achieved by using different simulation techniques, with the Monte Carlo approach being the most commonly used method [23]. Most simulations are performed on tissue matrix, however the addition of nanoparticles, which have excellent scattering properties, may cause significant deviations from a tissue only matrix and affect the depth of light penetration.

The actual effectiveness of this proposed approach can truly be evaluated by first performing surgery followed by PDT. Surgically removing the brain tumor will eliminate the bulk of the tissue, leaving behind minute traces of tumor residue that, based on the current results presented here, could be successfully eradicated using PDT.

6. Considering the biological and molecular responses to PDT: Destruction to the vascular network surrounding the treated tumor tissue, either angiogenic or healthy, after the completion of PDT treatment greatly affects the degree of tumor curability.

Vessel constriction and leaky vasculature endothelium can result in post-PDT tumor hypoxia, inhibiting possible tumor regeneration [24-25]. Monitoring these vasculature responses to PDT treatment can be achieved using imaging techniques such as intrinsic fluorescence or photoacoustic imaging. The endothelial and microvasculature damage in response to PDT can be monitored using fluorescent microscopic imaging in live animals, pre- and post-treatment, without destroying the imaged cells and tissue. Similarly, employing photoacoustic imaging of blood, we can monitor destruction of microvasculature, resulting in leaky vasculature, and vascular repair following therapy. Blood has a light optical absorption peak of 532 nm, generating a strong photoacoustic signal making it an advantageous method for monitoring the effects of PDT on vasculature surrounding the tumor [26].

Ensuring maximal destruction of angiogenic vasculature post-PDT may enhance the long-term tumor control. Endothelium-derived nitric oxide (NO) has vasodilatory properties and is a mediator of angiogenesis, and when stimulated by vascular endothelium growth factor (VEGF) it upregulates the expression of nitric oxide synthase (NOS) [27-28]. Designing our nanoparticle to incorporate agents inhibiting nitric oxide synthase or scavenging nitric oxide could assist with tumor regression patterns post-therapy. The release of such drugs within the treatment location and reducing the NO bioactivity would allow for vasoconstriction and attenuate angiogenesis.

Photodynamic therapy of tumors results in the rapid induction of inflammatory response that is crucial for the suppression of tumor growth post-treatment. This response is activated by signal transduction pathways that lead to the infiltration of leukocytes, predominately neutrophils, into the treatment area [29]. After infiltration, neutrophils undergo apoptosis followed by macrophages, and other phagocytes, consuming the apoptotic neutrophils – resolving the inflammatory response. Regulating the activation of neutrophils, macrophages enhance the clearance of treated tissue and

activate antitumor immunity. To ensure the patient's inflammatory response is not prolonged, we can utilize the idea of incorporating NO inhibitors in the treatment region. It has been discovered that the production of small amounts of NO can enhance the recruitment of neutrophils [29]. This, along with a potential decrease in angiogenesis, can possibly leading to a condensed inflammatory response and a suppression of tumor regrowth. Therefore measuring and regulating the NO levels within the treatment region may facilitate the understanding of the effects of NO levels post *in vivo* PDT and limit the duration of the PDT-induced inflammation.

REFERENCES

[1] Saxena, Vishal, Mostafa Sadoqi, and Jun Shao. "Degradation kinetics of indocyanine green in aqueous solution." *Journal of pharmaceutical sciences*92.10 (2003): 2090-2097.

[2] Tseng, William W., et al. "Infrared laser activation of indocyanine green inhibits growth in human pancreatic cancer." *Pancreas* 27.3 (2003): e42-e45.

[3] Shafirstein, Gal, et al. "Indocyanine green enhanced near-infrared laser treatment of murine mammary carcinoma." *International Journal of Cancer*130.5 (2012): 1208-1215.

[4] Chen, Wei R., et al. "Photothermal effects on murine mammary tumors using indocyanine green and an 808-nm diode laser: an in vivo efficacy study." *Cancer letters* 98.2 (1996): 169-173.

[5] Britz, Gavin W., et al. "Intracarotid RMP-7 enhanced indocyanine green staining of tumors in a rat glioma model." *Journal of neuro-oncology* 56.3 (2002): 227-232.

[6] Kitai, Toshiyuki, et al. "Fluorescence navigation with indocyanine green for detecting sentinel lymph nodes in breast cancer." *Breast cancer* 12.3 (2005): 211-215.

[7] Yoon, Hyung Ki, et al. "Nano-photosensitizers Engineered to Generate a Tunable Mix of Reactive Oxygen Species, for Optimizing Photodynamic Therapy, Using a Microfluidic Device." *Che*mistry of Materials* (2013).

[8] Lin, Jing, et al. "Photosensitizer-loaded gold vesicles with strong plasmonic coupling effect for imaging-guided photothermal/photodynamic therapy." *ACS nano* 7.6 (2013): 5320-5329.

[9] Huang, Peng, et al. "Photosensitizer-conjugated silica-coated gold nanoclusters for fluorescence imaging-guided photodynamic therapy." *Biomaterials* 34.19 (2013): 4643-4654.

[10] Barnes, William L., Alain Dereux, and Thomas W. Ebbesen. "Surface plasmon subwavelength optics." *Nature* 424.6950 (2003): 824-830.

[11] Ray, Aniruddha, et al. "Two-Photon Fluorescence Imaging Super-Enhanced by Multishell Nanophotonic Particles, with Application to Subcellular pH." *small*8.14 (2012): 2213-2221.

[12] Dolmans, Dennis EJGJ, Dai Fukumura, and Rakesh K. Jain. "Photodynamic therapy for cancer." *Nature Reviews Cancer* 3.5 (2003): 380-387.

[13] Koo Lee, Yong-Eun, et al. "Near infrared luminescent oxygen nanosensors with nanoparticle matrix tailored sensitivity." *Analytical chemistry* 82.20 (2010): 8446-8455.

[14] Ray, Aniruddha, et al. "Lifetime-based photoacoustic oxygen sensing in vivo."*Journal of biomedical optics* 17.5 (2012): 0570041-0570044.

[15] Ashkenazi, Shai, et al. "Photoacoustic probing of fluorophore excited state lifetime with application to oxygen sensing." *Journal of biomedical optics* 13.3 (2008): 034023-034023.

[16] Ashkenazi, Shai. "Photoacoustic lifetime imaging of dissolved oxygen using methylene blue." *Journal of biomedical optics* 15.4 (2010): 040501-040501.

[17] Kopelman, Raoul, et al. "Multifunctional nanoparticle platforms for in vivo MRI enhancement and photodynamic therapy of a rat brain cancer." *Journal of Magnetism and Magnetic Materials* 293.1 (2005): 404-410.

[18] Cevik, I. Unal, and T. Dalkara. "Intravenously administered propidium iodide labels necrotic cells in the intact mouse brain after injury." *Cell Death & Differentiation* 10.8 (2003): 928-929.

[19] Marshall, W. And D. Sliney (editors): Laser Safety Guide. Orlando, FL: Laser Institute of America, 2000.

[20] Kanagasabay, S. "Safety with Lasers and Other Optical Sources—A Comprehensive Handbook." *British journal of industrial medicine* 38.3 (1981): 307.

[21] Youssef, P. N., N. Sheibani, and D. M. Albert. "Retinal light toxicity." *Eye* 25.1 (2011): 1-14.

[22] Cvetkovic, Mario, Dragan Poljak, and Andres Peratta. "Thermal modelling of the human eye exposed to laser radiation." *Software, Telecommunications and Computer Networks, 2008. SoftCOM 2008. 16th International Conference on*. IEEE, 2008.

[23] Valentine, R. M., et al. "Monte Carlo simulations for optimal light delivery in photodynamic therapy of non-melanoma skin cancer." *Physics in medicine and biology* 57.20 (2012): 6327.

[24] Henderson, Barbara W., and Victor H. Fingar. "Relationship of tumor hypoxia and response to photodynamic treatment in an experimental mouse tumor."*Cancer research* 47.12 (1987): 3110-3114.

[25] Chen, Q., H. Chen, and F. W. Hetzel. "Tumor Oxygenation Changes Post-Photodynamic Therapy." *Photochemistry and photobiology* 63.1 (1996): 128-131.

[26] Hoelen, C. G. A., et al. "Three-dimensional photoacoustic imaging of blood vessels in tissue." *Optics letters* 23.8 (1998): 648-650.

[27] Hood, John D., et al. "VEGF upregulates ecNOS message, protein, and NO production in human endothelial cells." *American Journal of Physiology-Heart and Circulatory Physiology* 274.3 (1998): H1054-H1058.

[28] van der Zee, Rien, et al. "Vascular endothelial growth factor/vascular permeability factor augments nitric oxide release from quiescent rabbit and human vascular endothelium." *Circulation* 95.4 (1997): 1030-1037.

[29] Kobayashi, Yoshiro. "The regulatory role of nitric oxide in proinflammatory cytokine expression during the induction and resolution of inflammation."*Journal of leukocyte biology* 88.6 (2010): 1157-1162.